A STUDY OF NEGATIVE PION PHOTOPRODUCTION IN COMPLEX NUCLEI BY THE ANALYSIS OF ACTIVATION PRODUCTS.

by

GIAS UDDIN AHMAD.

OCTOBER 1966.

ProQuest LLC.
789 East Eisenhower Parkway
P.O. Box 1346
Ann Arbor, MI 48106 – 1346

PREFACE

This thesis describes the work carried out by the author from October, 1962 to September, 1966 in the Department of Natural Philosophy in candidature for the degree of Doctor of Philosophy.

The cross-sections for the reactions Cu^{63} (γ, π^-) Zn^{63} and Cu^{63} $(\gamma, \pi^- n)$ Zn^{62} have been measured as a function of photon energy by exposing a copper target and suitable "monitoring" elements to the X-ray beam of the Glasgow University Electron Synchrotron. Chapter 1 gives a review of the relevant theoretical and experimental works in this field. The cross-sections were measured by detecting the 0.511 MeV annihilation γ-rays resulting from the positron activities of Zn^{63} and Zn^{62}. For this purpose a 5" x 5" NaI (Tl) crystal was set up as a γ-ray spectrometer which is described in Chapter 2. As the success of this experiment depended heavily on an efficient radio-chemical separation, a technique which successfully isolated a small amount of zinc from a large amount of copper and other interfering metals has been developed and is described in Chapter 3. Chapter 4 describes the experimental arrangement for the synchrotron runs.

An "unexplained activity" below the meson threshold has been reported in previous works. An important intention when undertaking this experiment was to investigate this activity. It is believed that as a result of experiments described in Chapter 5 the origin and nature of this activity have been definitely established.

Chapter 6 describes the method of cross-section analysis. The results are presented and discussed in Chapter 7. Reasonable agreement between the results and current theories was obtained.

The last part of this thesis describes the relative yields of some photonucleon reactions on zinc, copper and carbon in an energy range of 100 - 320 MeV.

The setting up of the γ-ray spectrometer described in Chapter 2 was carried out by the author who was also responsible for the development of the method of separation of the Zn isotopes.

The synchrotron runs and experimental observations were carried out in collaboration with Mr. A. L. Cockroft.

The interpretation of results presented in Chapter 7 is the work of the author.

The author is grateful to his supervisor Mr. A. L. Cockroft for continued help, guidance and the long useful discussions throughout this experiment and also for sustained inspiration without which this thesis would not have been possible. The author wishes to thank gratefully Professor P. I. Dee, F.R.S. for his keen interest and encouragement and extending to the author the privilege of working in his laboratory. The author expresses his gratitude to Dr. W. McFarlane and his team of assistants for providing many hours of synchrotron beam and keeping the intensity of the beam at the high level needed for the experiment. Thanks are also due to Dr. S. J. Thomson of the Chemistry Department for helpful discussions and to

Professor H. W. Wilson, Director of the Scottish Universities Research Reactor Centre, for the provision of radio-active tracers. Much is owed to the assistance given by members of the technical staff of this department, and in this connection the author wants to thank specially Mr. D. A. Seath, who spent many hours in drawing the diagram reproduced in this thesis.

The author gratefully acknowledges the award of a Scholarship by the Govt. of East Pakistan for the first three years and three months of this research, and the award of a Research Studentship by the University Court of the University of Glasgow for the final nine months.

CONTENTS

LIST OF FIGURES

Part of the Ph.D. Thesis of G.A. Ahmad (Oct. 1966)

APPENDIX B

This Thesis describes the measurement of the yields of 38 m Zn^{63} and 9 h Zn^{62} produced by the irradiation of natural copper in a high energy X-ray beam. There are two stable isotopes of copper, Cu^{63} (69.09%) and Cu^{65} (30.91%). Both radioactive isotopes could be produced from each of these by the following reactions:

$Cu^{63}(\gamma, \pi^-)Zn^{63}$ $\quad$ $Cu^{63}(\gamma, \pi^- n)\ Zn^{62}$

$Cu^{65}(\gamma, \pi^- 2n)Zn^{63}$ $\quad$ $Cu^{65}(\gamma, \pi^- 3n)\ Zn^{62}$

The results of the experimental work could therefore best be summarized in graphs showing:

(1) The cross section (per atom of natural copper) for the production of 38 m Zn^{63}.

(2) The cross section (per atom of natural copper) for the production of 9 h Zn^{62}.

Figs. (7.1 & 7.3) may be modified to show the results in this form by multiplying the "σ" scales by the isotopic abundance ratio of Cu^{63} (69.09/100). Further analysis to suggest separate cross sections for the processes involved is a matter of theoretical interpretation in the light of an assumed model. The method by which this analysis was attempted is described below.

As discussed in the Thesis, γ, π^- reactions may be supposed to take place by the following processes:

(1) A photon interacts with an essentially free surface neutron producing a π^- which is emitted without collision and a

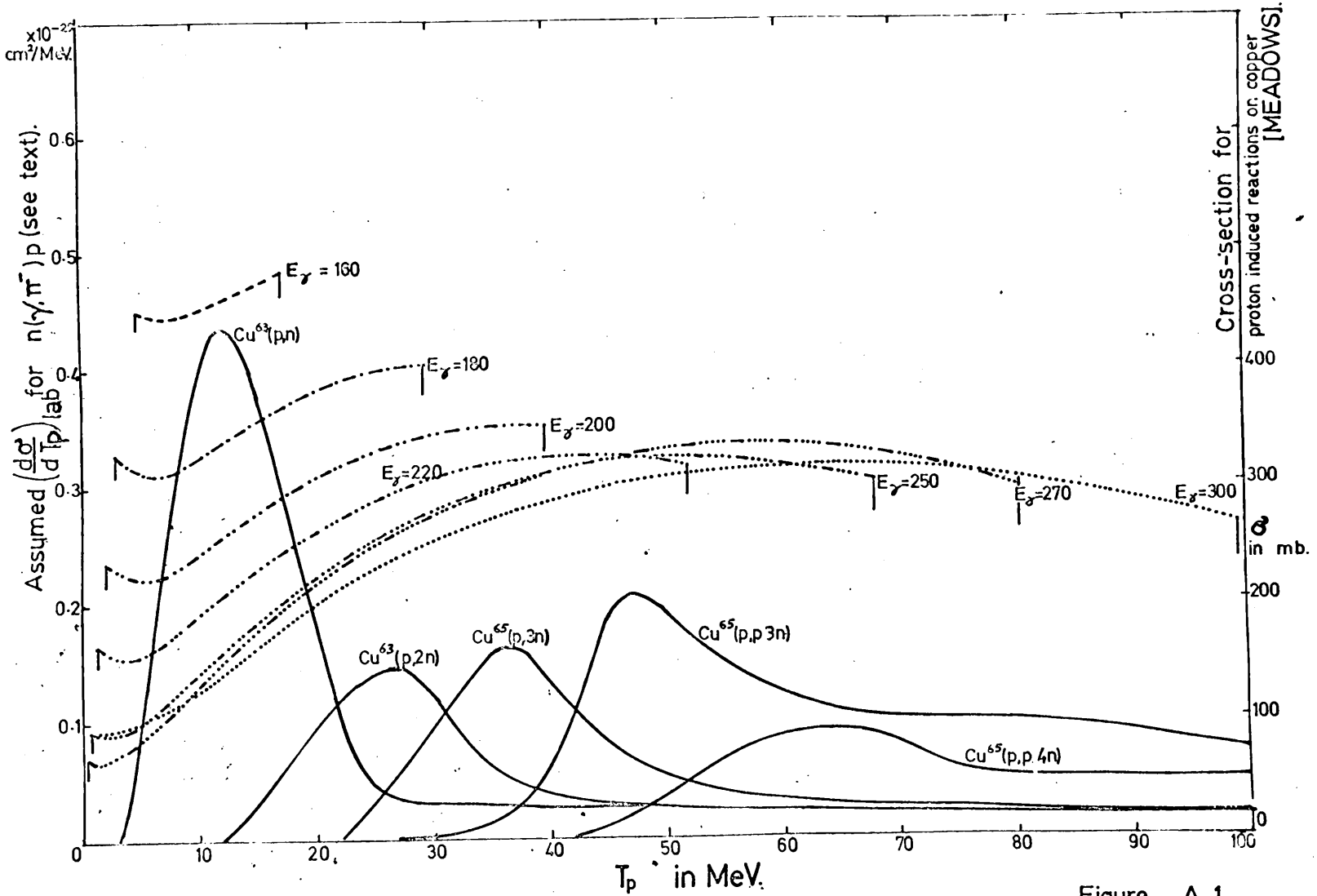
Assumed $\left(\frac{d\sigma}{d T_p}\right)_{lab}$ for $n(\gamma,\pi^-)p$ (see text).
$\times 10^{-28}$ cm²/MeV.
Cross-section for proton induced reactions on copper [MEADOWS].
σ in mb.
T_p in MeV.
E_γ = 160
E_γ=180
E_γ=200
E_γ=220
E_γ=250
E_γ=270
E_γ=300
$Cu^{63}(p,n)$
$Cu^{63}(p,2n)$
$Cu^{65}(p,3n)$
$Cu^{65}(p,p\,3n)$
$Cu^{65}(p,p\,4n)$

Figure A 1.

proton.

(2) The recoil proton may escape the nucleus or may form a compound nucleus perhaps after the emission of one or more "cascade" nucleons.

(3) The de-excitation of the compound nucleus may result in the "evaporation" of further nucleons.

It may therefore be possible to estimate the shapes and relative magnitudes of the cross sections for, in particular, $(\gamma, \pi^- xn)$ reactions by combining a proton energy distribution with cross sections for the appropriate (p, xn) reactions.

It has been assumed that the energy distribution of recoil protons from photopion reactions at surface neutrons may be represented sufficiently well by the energy distribution of neutrons produced at a free proton by the $p(\gamma, \pi^+)n$ reaction. This distribution $(\frac{d\sigma}{dT_n})_{lab.}$ where T_n is the kinetic energy of the neutron, which has been computed for a series of photon energies using the tabulated values of Robinson[A1] for the differential cross section $(\frac{d\sigma}{d\Omega})_{C.M.}$. The results of these calculations are shown in Fig. A1 where strictly $\frac{d\sigma}{dT_n}(E\gamma)$ for $p(\gamma, \pi^+)n$ is plotted against T_n. As stated above, it is assumed that they also represent approximately the variation of $\frac{d\sigma}{dT_p}(E\gamma)$ with T_p for the $n(\gamma, \pi^-)p$ reaction at either a free neutron or a quasi-free surface neutron.

Meadows [A2] has determined experimentally the cross sections of several reactions produced by bombarding the stable separated

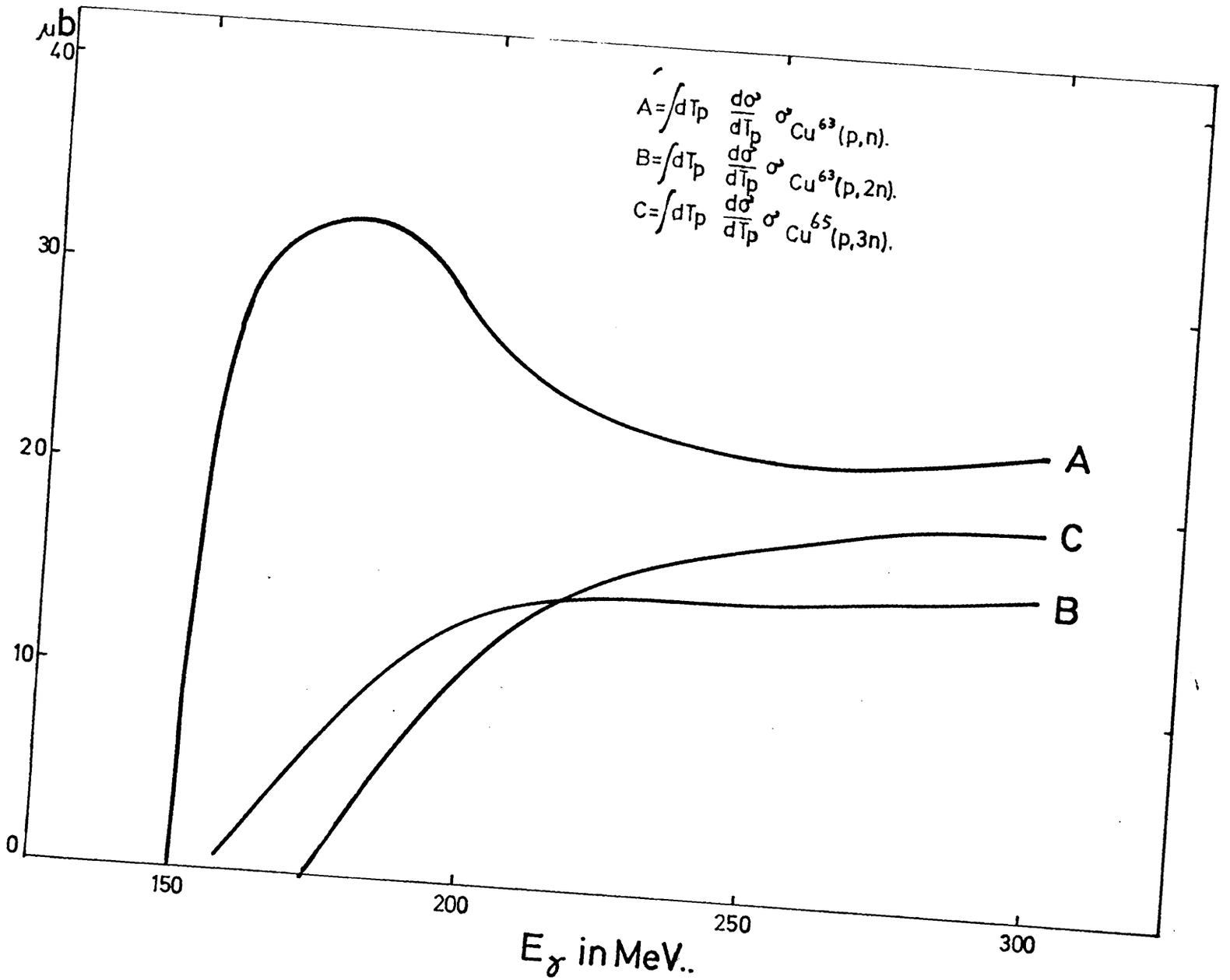
μb
40
30
20
10
0
150
200
250
300
E_γ in MeV..
$A=\int dT_p \frac{d\sigma}{dT_p} \sigma_{Cu^{63}(p,n).}$
$B=\int dT_p \frac{d\sigma}{dT_p} \sigma_{Cu^{63}(p,2n).}$
$C=\int dT_p \frac{d\sigma}{dT_p} \sigma_{Cu^{65}(p,3n).}$
A
C
B

Figure A 2.

isotopes of copper with high energy protons (to 100 MeV). These are shown in Fig. A1 along with "$\frac{d\sigma}{dT_p}$". They do not in fact refer to reactions involving exactly the same compound nucleus as the (γ, π^-) reactions but may well be typical in which case integrals of the type $\int dT_p \frac{d\sigma}{dT_p} \sigma_{Cu(p,xn)}$ should give the shapes and relative magnitudes of the cross sections for the $(\gamma, \pi^- xn)$ reactions of immediate interest.

Curves A, B, C of Fig. A2 show the result of performing the indicated integrals for proton induced reactions producing one, two and three neutrons respectively. The "σ" scale was added later as will appear below. The relative contributions of Cu^{63} $(\gamma, \pi^- n)Zn^{62}$ and $Cu^{65}(\gamma, \pi^- 3n)Zn^{62}$ to the total cross section for the photoproduction of 9 h Zn^{62} from natural copper may now be estimated by multiplying A and C by the isotopic abundance ratios of Cu^{63} and Cu^{65} respectively. The shape of the total cross section curve obtained by adding may be compared with the experimental result (Fig.A3). The scale of the "theoretical" cross section curve of Fig.A3 was adjusted to give the same area ($\int \sigma dE_\gamma$) as the experimental curve. A corresponding scale was attached to Fig.A2. Using this scale, the contribution of the $Cu^{65}(\gamma, \pi^- 2n)Zn^{63}$ reaction to the total cross section for the photoproduction of 38 m Zn^{63} from natural copper was deduced by multiplying curve B of Fig.A2 by the isotopic abundance ratio of Cu^{65}. This contribution is shown in Fig.A4 together with the experimentally obtained total cross section, the difference representing the contribution of the $Cu^{63}(\gamma, \pi^-)Zn^{63}$ reaction. The cross section for Cu^{63} $(\gamma, \pi^-)Zn^{63}$ may now be extracted by dividing the difference curve by

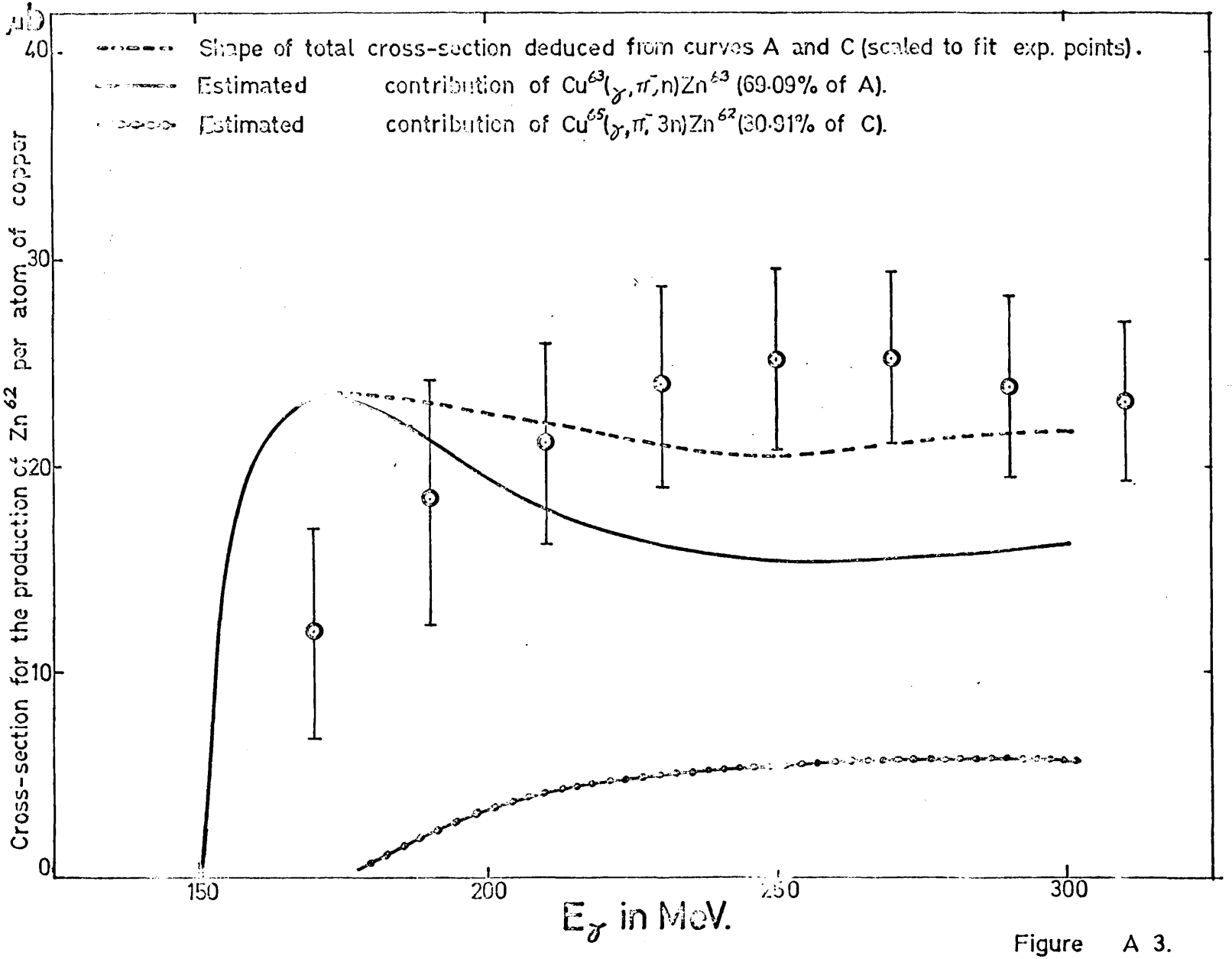
μb
Shape of total cross-section deduced from curves A and C (scaled to fit exp. points).
Estimated contribution of $Cu^{63}(\gamma,\pi^-,n)Zn^{63}$ (69·09% of A).
Estimated contribution of $Cu^{65}(\gamma,\pi^-,3n)Zn^{62}$ (30·91% of C).
Cross-section for the production of Zn^{62} per atom of copper
40
30
20
10
0
150
200
250
300
E_γ in MeV.

Figure A 3.

the isotopic abundance ratio of Cu^{63} (Fig.A5).

The above analysis suggests that for photon energies from threshold to about 200 MeV, Zn^{62} is produced almost entirely from Cu^{63} by the $(\gamma, \pi^- n)$ reaction. At higher photon energies the yield of this reaction decreases rather slowly and an increasing contribution is produced by $(\gamma, \pi^- 3n)$ on the less abundant Cu^{65}. The yield of this reaction rises to 25% of the total at 320 MeV. Zn^{63} is produced mainly from Cu^{63} for photon energies up to almost 300 MeV, the contribution of $(\gamma, \pi^- 2n)$ on Cu^{65} being less than 15%. At the extreme energy (320 MeV) where the measured total cross section has fallen to 18 μb, the contribution of the Cu^{65} reaction is 30%. (In the body of the Thesis it was stated that the <u>average</u> contributions of the Cu^{65} reactions over the whole energy range 140 MeV to 320 MeV were believed not to exceed 15%. This more detailed analysis suggests average contributions of 10% (Zn^{63}) and 20% (Zn^{62})).

It may be remarked that the Leiss and Penfold method of analysis underestimates a rapidly rising cross section. A better fit to the "theoretical" curve for Zn^{62} production would be obtained by assuming a cross section which increases linearly over the first energy bin. In fact, if the "theoretical" cross section (Fig. A3) is folded with the bremsstrahlung spectrum, the experimental yield curve may be fitted within experimental error. Clearly, a more detailed investigation of the cross section near threshold using smaller energy increments would be desirable.

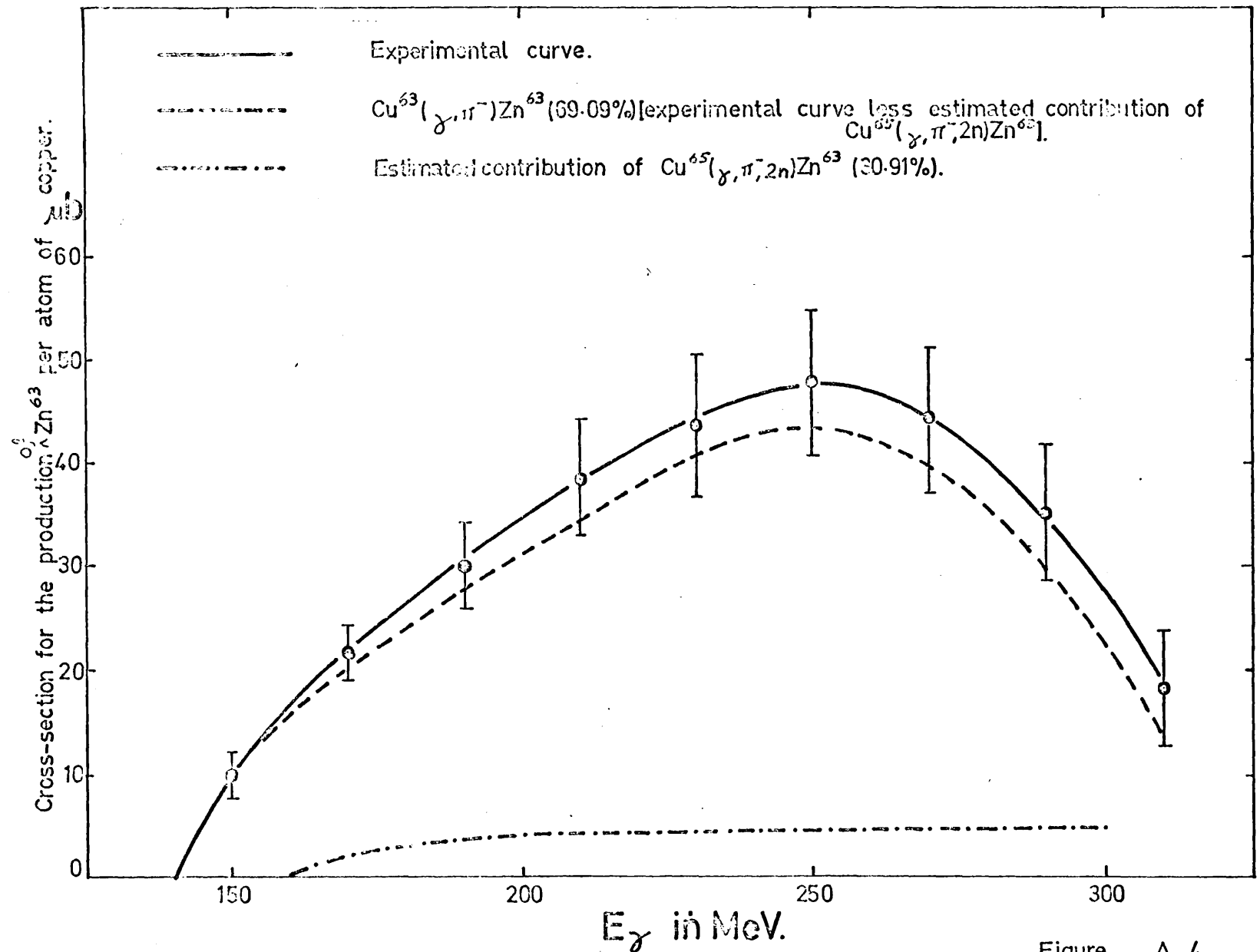
Experimental curve.
$Cu^{63}(\gamma,\pi^-)Zn^{63}$ (69·09%) [experimental curve less estimated contribution of $Cu^{65}(\gamma,\pi^-,2n)Zn^{63}$].
Estimated contribution of $Cu^{65}(\gamma,\pi^-,2n)Zn^{63}$ (30·91%).
Cross-section for the production of Zn^{63} per atom of copper.
μb
0
10
20
30
40
50
60
150
200
250
300
E_γ in MeV.

Figure A 4.

On the basis of the scale assigned to Fig.A2, an estimate was made of the sum of the cross sections for the reactions $Cu^{63}(\gamma,\pi^- xn)$ and $Cu^{63}(\gamma,\pi^- pxn)$ where x = 0,1,2,3,4,5,6 in each case, for E_γ = 255 MeV. This amounted to~500 μb. and may be compared with a total of ~1100 μb calculated according to Butler's [A3] theory using the systematics of Littauer and Walker[A4] (π^-/π^+ = 1.1) and the value for the total cross section of C^{12} measured by Steinberger & Bishop[A5]. In view of the fact that other processes such as $Cu^{63}(\gamma,\pi^- 2p)\ Ni^{61}$ and $Cu^{63}(\gamma,\pi^-\alpha)Ni^{59}$ are energetically possible and might have relatively large cross sections, it is considered that the present results are in good agreement with the Butler-Wilson[A6] surface production model. The cross section for the reaction $Cu^{63}(\gamma,\pi^-)Zn^{63}$ is in good agreement with the Laing and Moorhouse[A7] calculation for surface production.

Meyer and Hummel[A8] have measured the cross section for $V^{51}(\gamma,\pi^- 2n)\ Cr^{49}$ and obtained a peak value of 100 μb at ~ 200 MeV. The total cross section for (γ,π^-) reactions on V^{51} calculated on the same basis as above would be about ~ 500 μb. The branching ratio for two neutron emission appears very high for this nucleus but as Meyer & Hummel remark, branching ratios are very sensitive to the threshold energies and level densities involved. There are no experimental results for proton induced reactions on V which could be used to attempt an explanation on the lines of the above analysis of the copper reactions.

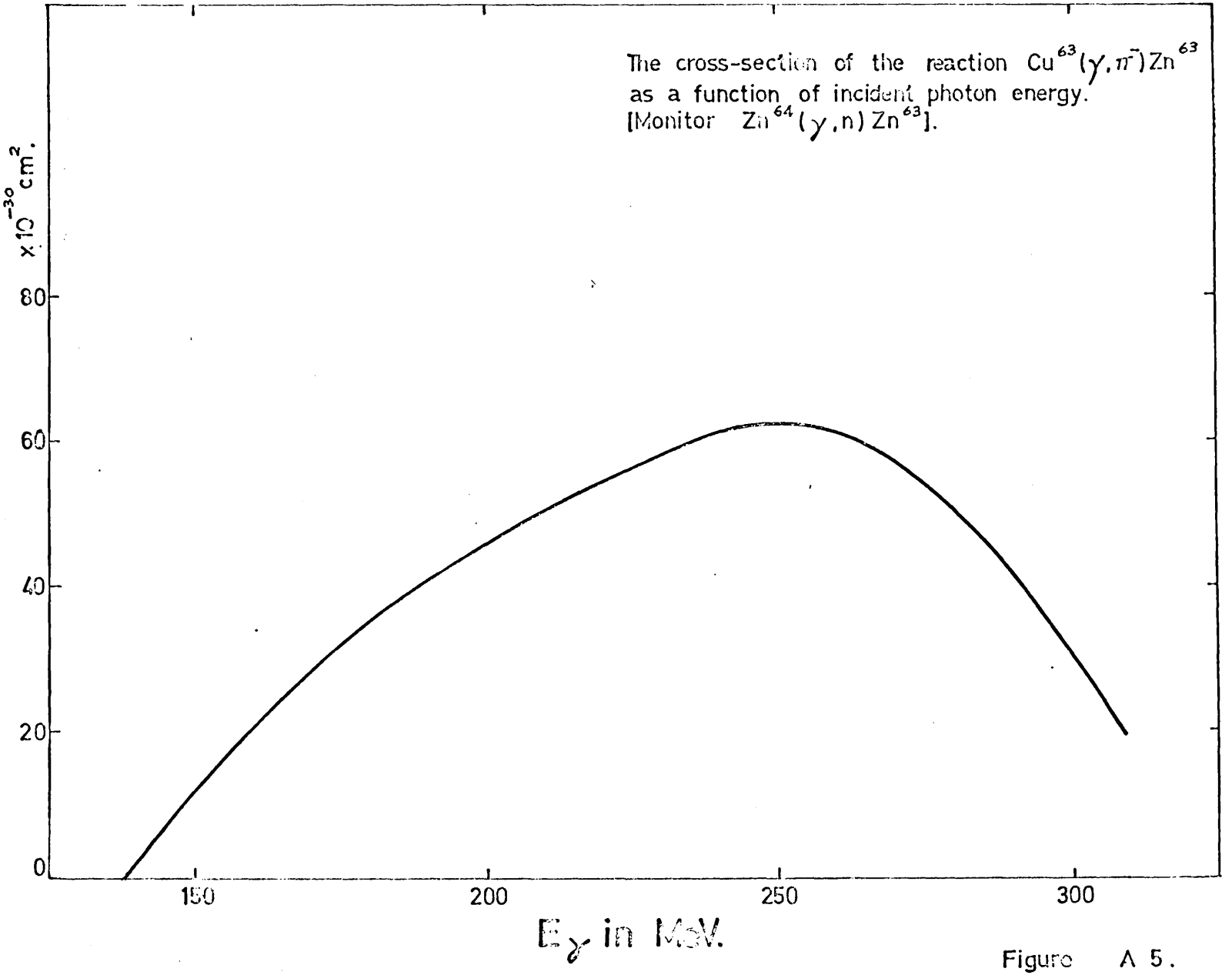
The cross-section of the reaction $Cu^{63}(\gamma, n^-)Zn^{63}$ as a function of incident photon energy.
[Monitor $Zn^{64}(\gamma, n)Zn^{63}$].
x 10^{-30} cm^2.
80
60
40
20
0
150
200
250
300
E_γ in MeV.

Figure A 5.

REFERENCES

A1. ROBINSON, C. S., PHYSICS RESEARCH LABORATORY REPORT, UNIVERSITY OF ILLINOIS, 1959.

A2. MEADOWS, J. W., PHYS. REV. 91, 885 (1953).

A3. BUTLER, S. T., PHYS. REV. 87, 1117 (1952).

A4. LITTAUER, R. M. and WALKER, D., PHYS. REV. 86, 838 (1952).

A5. STEINBERGER, J. and BISHOP, A. S., PHYS. REV. 86, 171 (1952).

A6. WILSON, R. R. PHYS. REV., 86, 125 (1952).

A7. LAING, E. W. and MOORHOUSE, R. G., PROC. PHYS. SOC., 70B, 629, (1957)

A8. MEYER, R. A. and HUMMEL, J. P., PHYS. REV. 140, B 48 (1965).

INTRODUCTION

The photoproduction of pions has been studied for the purpose of investigating mesons as well as to find out more about the nucleons themselves. Most experimental information about the basic photoproduction processes can be learned from the production of pions from simple nuclei like hydrogen and deuterium. Such information is useful in determining the properties of the pion field and the nature of the pion-nucleon interaction. The study of pion production in complex nuclei reveals, in general, information about the behaviour of pions and nucleons in nuclear matter and the "competing reactions" in the core of the nuclear volume.

The basic photoproduction reaction on a free nucleon is a two body problem which is quite amenable to calculation. It has been extensively studied both theoretically and experimentally. The photo-production processes from complex nuclei are more complicated. If, however, pion production is considered as the result of the interaction of a photon with a single nucleon in the nucleus, then comparisons of the reactions from bound and free nucleons will yield information on the effect of nuclear matter on the interacting system.

Photo production processes can be expressed by the following reactions:

(I) From free nucleons

$$\gamma + p \longrightarrow \pi^{+} + n \qquad (1a)$$

$$\longrightarrow \pi^{o} + p \qquad (1b)$$

$$\gamma + n \longrightarrow \pi^{-} + p \qquad (1c)$$

$$\longrightarrow \pi^{o} + n \qquad (1d)$$

(II) From complex nuclei - Bound Final state

$$\gamma + X_Z^A \rightarrow \pi^+ + Y_{Z-1}^A \qquad (2a)$$

$$\rightarrow \pi^o + X_Z^A \qquad (2b)$$

$$\rightarrow \pi^- + Y_{Z+1}^A \qquad (2c)$$

(III) Continuum final state with single nucleon emitted

$$\gamma + X_Z^A \rightarrow \pi^+ + n + Y_{Z-1}^{A-1} \qquad (3a)$$

$$\pi^o + n + Y_Z^{A-1} \qquad (3b)$$

$$\pi^- + n + Y_{Z+1}^{A-1} \qquad (3c)$$

There are similar reactions for pion production involving the emission of several nucleons.

The reactions investigated in this thesis are those of type (2c) and (3c).

Activity below meson threshold is investigated in this thesis. This activity was reported in previous photopion works but no definite explanation was offered.

Also investigated in this thesis are the relative yields of several photonucleon reactions at high photon energies.

CHAPTER I

REVIEW OF PUBLISHED WORK

INTRODUCTION

The production of charged π-meson by high energy x-ray bombardment of nuclei was first observed by McMILLAN, PETERSON and WHITE[1.1]. Since then a number of workers have studied photopion production phenomena. The earlier works of this type involving complex nuclei were performed by MOZLEY[1.2], STEINBERGER and BISHOP[1.3], and LITTAUER and WALKER[1.4]. MOZLEY determined the relative cross-sections per proton for the production of π^+ mesons from a few different elements. STEINBERGER and BISHOP studied the same from hydrogen and carbon. LITTAUER and WALKER studied the production of π^- and π^+ mesons from a wide range of nuclei. Two main features emerged from these experiments.

(1) The yields are considerably less than from appropriate equal numbers of free nucleons.

(2) The total yield of charged mesons is very closely represented by a law of the form $Y = KA^{\frac{2}{3}}$ where A is the mass number of the target nuclei.

Apart from these two general features LITTAUER and WALKER also observed wide variations of the π^-/π^+ ratios from element to element which tend to suggest that they are connected with some detailed feature of nuclear structure rather than with a variation of the elementary production process itself. In an effort to find some empirical correlation that would give a clue to the nature of this nuclear factor, they plotted the mass differences $M_{z-1} - M_{z+1}$ side by side with the π^-/π^+ ratios

(Fig. 1.1), M_{z-1} and M_{z+1} being the masses of the ground states of the final isobars z-1 and z+1 produced by (γ, π^+) and (γ, π^-) reaction on the initial target nucleus z. It becomes at once apparent from the resulting curves that a strong correlation exists between the mass differences and the π^-/π^+ ratios. In the following paragraphs various theoretical models, which were put forward in an effort to explain the main features of photopion production from complex nuclei, and their respective experimental support will be discussed.

(a) MOMENTUM DISTRIBUTION OF NUCLEONS

LAX and FESHBACH[1.5] argued that because of the momentum distribution of nucleons in a nucleus, it is not energetically possible for all the protons or all neutrons to participate in the production. They employed GOLDBERGER'S and CHEW'S[1.6] momentum distribution for the protons in carbon and obtained a value for π^+ meson production cross-section from carbon. Comparing with STEINBERGER and BISHOP'S experimental results they obtained excellent agreement for the meson energy spectrum at 90° and for the decrease in efficiency of meson production compared with free protons as targets. PALFREY et al[1.7] measured the π^- and π^+ yields from carbon as a function of peak bremsstrahlung energy (205-335 MeV) at three different angles. These authors found adequate agreement between the relative yields (π^-/π^+) and the predicted yields which consider the internal-momentum distribution of the target nucleons, but real disagreement was observed in the rate of decrease of the differential cross-section at high photon energies. The authors

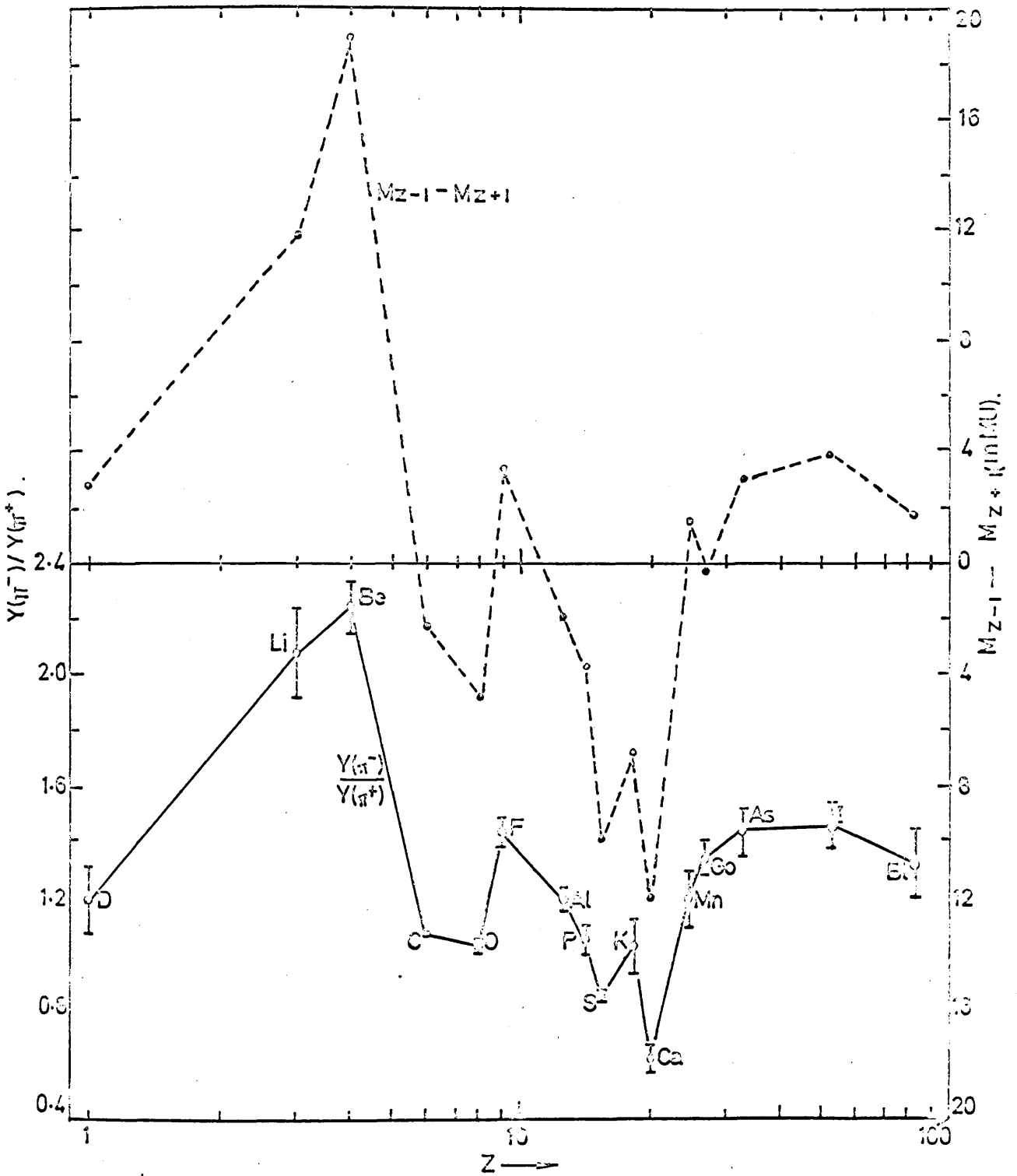

π^-/π^+ ratios & mass differences plotted aganst Z.

Figure 1·1

believe it to be due to a two-step process, not included in the model of LAX and FESHBACH, in which the high energy photon produces a high energy meson which scatters (internally in the parent nucleus) into the pion energy and angular bin in which the authors were counting. This scattering inherently prevents measurement of the internal momentum distribution of nucleons in a nucleus by photoproduction experiments of the type discussed by the authors.

(b) OPTICAL MODEL

BRUECKNER, SERBER and WATSON[1.8] tried to explain the results from a different angle. They assumed that some of the mesons which are produced will be absorbed before they escape from the nucleus. They tried to interpret photoproduction on complex nuclei on the basis of an optical model taking into account the finite mean free path for the absorption of pions in the nucleus before they could escape. According to this model they expressed the production cross section σ_a for π^+ mesons from a nucleus as

$$\sigma_{a/z} = \eta \sigma_a f_a$$

where z is the atomic number of the nucleus A, σ_a, fa and η represent the production cross section for a free proton, the fraction of mesons produced in A which are not reabsorbed before leaving A and the effects of nuclear binding on the cross-section respectively.

fa was expressed in terms of λ_a the mean free path for absorption of a pion on the assumption that the cross-section for absorption is much larger than that for scattering as

$$f_a = \frac{1}{v_a} \int_v e^{-D/\lambda_a} \, d\tau$$

$$= 3\left\{ \frac{1}{2}\frac{1}{x} - \left(\frac{1}{x^3}\right) + \left(\frac{1}{x^3}\right) \quad (1 + x)\, e^{-x} \right\}$$

where the integration is taken over the nuclear volume and D is the distance the meson travels from the point at which it is produced to that at which it leaves the nucleus, $x = 2R/\lambda_a$ where $R = a_o A^{\frac{1}{3}}$ is the nuclear radius.

When $x \gg 1$ i.e. the mean free path for absorption is small in comparison with the nuclear dimensions σ_a is written as

$$\sigma_a/z \simeq \eta \sigma_p \left[\tfrac{3}{4} \lambda a/a_o\right] A^{-\frac{1}{3}}$$

It could be seen that as long as the condition $x \gg 1$ is satisfied σ_a/z varies as $A^{\frac{1}{3}}$ which is equivalent to σa varying as $A^{\frac{2}{3}}$ (supposing $Z = \frac{A}{2}$), since η is not expected to show a uniform trend with A. This is what was observed by MOZLEY and LITTAUER and WALKER whose experiments indicate a general $A^{\frac{2}{3}}$ dependence for a series of elements.

The earlier experiments of LITTAUER and WALKER and CHEDESTER et al[1.9] on the interaction of pions and nuclei suggested a short mean free path for nuclear interaction of pions. This was in line with the optical model of BRUECKNER et al. However, BYFIELD et al[1.10] from a careful analysis of their own scattering experiments, indicated λ to be of the order of 8×10^{-13} cm. FRANCIS and WATSON[1.11] indicated that an even larger mean free path ($\lambda = 0.5 \times 10^{-12}$cm $\sim 10^{-12}$cm) could be shown to be in satisfactory agreement with experiment. IMHOF et al[1.12] measured the relative yields of positive pions (12 - 125 MeV) from H, C, Al, Cu, Ag and Pb at angles varying from 45° - 150°. The maximum bremsstrahlung energy used was 335 MeV. The experimental results showed a clear $A^{\frac{2}{3}}$ dependence. By considering the effects of the coulomb potential, the

potential arising from the pion-nucleon interaction, the internal momentum distribution of the nucleus and scattering of the pions inside the nucleus, the authors obtained fair agreement between the experimental results and the prediction of optical model. The same conclusion was drawn by WILLIAMS, CROWE and FRIEDMAN[1.13] who studied the Z-dependence of positive pion photoproduction from different nuclei. The maximum photon energy used was 550 MeV. Taking into account the variations in the production cross-section due to the real potential, including the coulomb potential and using the real and imaginary potentials given by FRANK et al[1.14], they obtained good agreement between the experimental results and the optical model for pion energies ranging from 33 to 152 MeV, for which the observed mean free path varied from 9×10^{-13}cm. to 1×10^{-13}cm. Their results were normalised to copper. WATERS[1.15] studied the photoproduction of 40 MeV and 80 MeV charged π-mesons from different nuclei at maximum photon energies of 800 MeV and 1000 MeV. The author normalised his results to Beryllium. The yields for 80 MeV and 40 MeV mesons were found to vary as $A^{2}/3$ and $\sim A$ respectively. Using the optical model and considering the effect of the Pauli Principle which reduces the number of states available, and the coulomb barrier effect causing reflection of some of the mesons at the nuclear surface, the author obtained reasonably good agreement between theoretical prediction and experimental yield of 80 MeV mesons, but the yield for 40 MeV mesons deviated sometimes by a factor of 2. The deviation between this experiment and that of WILLIAMS, CROWE and FRIEDMAN is surprising since the only difference is in photon energy. By using the optical model plus the

effect of inelastically scattered mesons the author found a better fit for 80 MeV mesons, but not for 40 MeV mesons, though the correction was in the right direction. The author made clear that due to the complex nature of the observed low-energy meson yield, other factors could also affect the yield. Thus the linear dependence of the meson yield on A, the atomic number, rather than on $A^{\frac{2}{3}}$ as observed in the part of this experiment, is to a great extent fortuitous. It is strongly dependent on the fact that the observed low-energy mesons were produced by high-energy bremsstrahlung giving plenty of scope for intermediate processes to affect the yield. McCLELLAND[1.16] also studied the photoproduction of charged π mesons in different nuclei produced by a 1000 MeV bremsstrahlung beam. The meson energies studied ranged from 100 - 400 MeV. By using the optical model the author predicted an upper and lower limit for the meson yield, the upper limit corresponded to the case where the mesons were lost due to absorption only and the lower limit corresponded to meson loss due to both absorption and scattering. The experimental yields were found to lie between these two limits and the measured cross-section showed an $A^{\frac{3}{4}}$ dependence. The result of the previous work (of WATERS) was shown by this author to be consistent with $A^{\frac{2}{4}}$ dependence. The optical model, however, could make no prediction for π^-/π^+ ratio. So far as the meson production cross-section is concerned, the result of McCLELLAND'S experiment seems to be consistent with an optical model treatment of an assumed initial production of mesons throughout the nuclear volume. No recourse to a surface production mechanism is necessary, and if such a process does occur, its effect is indistinguishable

from the uncertainties in the volume-production model which was employed. This initial production of pions throughout the nuclear volume rather than production only at the surface was also supported by SEIJI KABE[1.17] et al's experiment on Carbon.

(c) SURFACE-PRODUCTION MODEL

As discussed earlier, it was indicated by BYFIELD et al and others that the mean free path of pions in nuclear matter is of the order of 8×10^{-13} cm. This was not so short as suggested in the earlier experiments of, for example, LITTAUER and WALKER. It was found that on the basis of estimates of the absorption mean free path for mesons in nuclear matter, the very good experimental $A^{\frac{2}{3}}$ dependence is difficult to understand as due merely to absorption of mesons. It also appeared that the optical model is not by itself sufficient to explain the observed yield, in particular the characteristic features such as π^- to π^+ ratios. Consequently the question was raised whether the $A^{\frac{2}{3}}$ dependence of the photo cross-section can be correctly interpreted as due merely to the reabsorption of mesons. A completely different approach was made to the problem of photoproduction of pions by BUTLER[1.18].

BUTLER assumed that pion production is possible on surface nucleons and that production in the core is suppressed by some method. Accordingly he worked out the production cross-section by considering only the surface nucleons. The surface nucleons were defined as those nucleons which the photon catches beyond the boundary defined by the radius r_o of the nucleus. r_o was to be the radius of the central core of a nucleus, inside of which the density of nucleons is roughly constant, but outside

of which the density falls off rapidly. Any one nucleon outside this radius is subject to only weak interaction with other members of the nucleus. In fact in working out the cross-section this nucleon was considered to be free and to have an energy (in general negative) depending on the particular state of the nucleus it leaves behind. The production cross-section was worked out on this model by taking r_o to be equal to 1.2 fermis (1.2×10^{-13} cm). It was found that apart from having the correct $A^{\frac{2}{3}}$ dependence, the calculated cross-section actually accounted for a large fraction (60 - 70 per cent) of the observed cross-sections (LITTAUER and WALKER). By considering the differences in the average binding energies of neutrons as compared with protons in a nucleus and thus in the number of neutrons as compared with protons in the nuclear surface and the coulomb interaction between protons, the variations in the ratio of the individual π^- to π^+ surface yields were found to have the same trend as the experimental results. The success of BUTLER'S theory in explaining LITTAUER and WALKER'S experimental results suggest that the interior production of mesons must contribute to only a small extent and must therefore be quite heavily damped. In fact it was estimated that the production from the interior of a nucleus must be suppressed by a factor $\tilde{>}$ 3. This suppression cannot be explained as due to meson reabsorption, since the absorption mean free path was found to be large. This suppression can be understood by a mechanism proposed by WILSON[1.19].

WILSON argued that the suppression of meson production in the

interior of the nucleus can be explained as the result of a large competing photodisintegration process due to meson exchange effects between strongly interacting nucleons within the nucleus. When a free nucleon forms an excited state due to the absorption of a high energy photon, there are only two modes of decay - either the re-emission of the photon or the emission of a meson. Whereas, when a high energy photon interacts with a nucleon which is itself interacting with one or more neighbours in a nucleus and capable of exchanging energy with them, there exists the possibility that there will occur a direct photodisintegration of this interacting nucleon group via meson exchange, i.e. a meson in the excited state of the first nucleon transfers to the ground state of a second nucleon, the excess energy going into kinetic energy of separation of the nucleon group. This process would then compete with meson production, some of the mesons which would have escaped the influence of the parent nucleon had it been free being retained by one member of the interacting nucleon group, the excess energy producing disintegration of the group. The probability of such a competing process will depend, among other things, on the extent to which nucleons in a nucleus are coupled by their interaction. It was shown by WILSON that inside the core of the nucleus the probability of a given nucleon interacting with a neighbouring nucleon is almost unity. This, then, explains the way by which meson production inside the core of the nucleus can be suppressed. Of course, once a meson does escape from the influence of the parent nucleon and any strongly interacting neighbours, there is also the possibility of reabsorption in other parts of the nucleus

before it finally escapes altogether. This also produces photo-disintegration, but is just the absorption allowed for by use of the mean free path. Thus the absorption of photons in nuclei may lead via meson exchange between strongly interacting nucleons in the core, to photo-disintegration which has a greater probability than the formation of a real meson. This view was supported by the experimental results obtained by ROSENGREN and DUDLEY[1.20] who reported the existence of an isotropic component in the angular distribution of photoprotons with an energy close to 70 MeV, which appeared to be due to the absorption of pions by pairs of nucleons. GEORGE,[1.21] from a study of the photoproduction of stars and mesons in nuclear emulsions, also supported WILSON'S theory of the mechanism by which meson production in the core is suppressed.

COMPARISON BETWEEN THE TWO MODELS

We thus have two competing mechanisms for the suppression of meson production in the core of the nucleus namely reabsorption of meson (optical model) and photodisintegration in the core of the nucleus via meson exchange (surface-production model). In all previous works, discussed above, the meson had relatively high energy, 60 - 100 MeV. The mean free paths for absorption associated with mesons in this energy range were relatively short. However, it was shown by STORK[1.22] and FRANK et al that the mean free path of a meson in nuclear matter depends greatly on the meson energy. It increases as the energy decreases

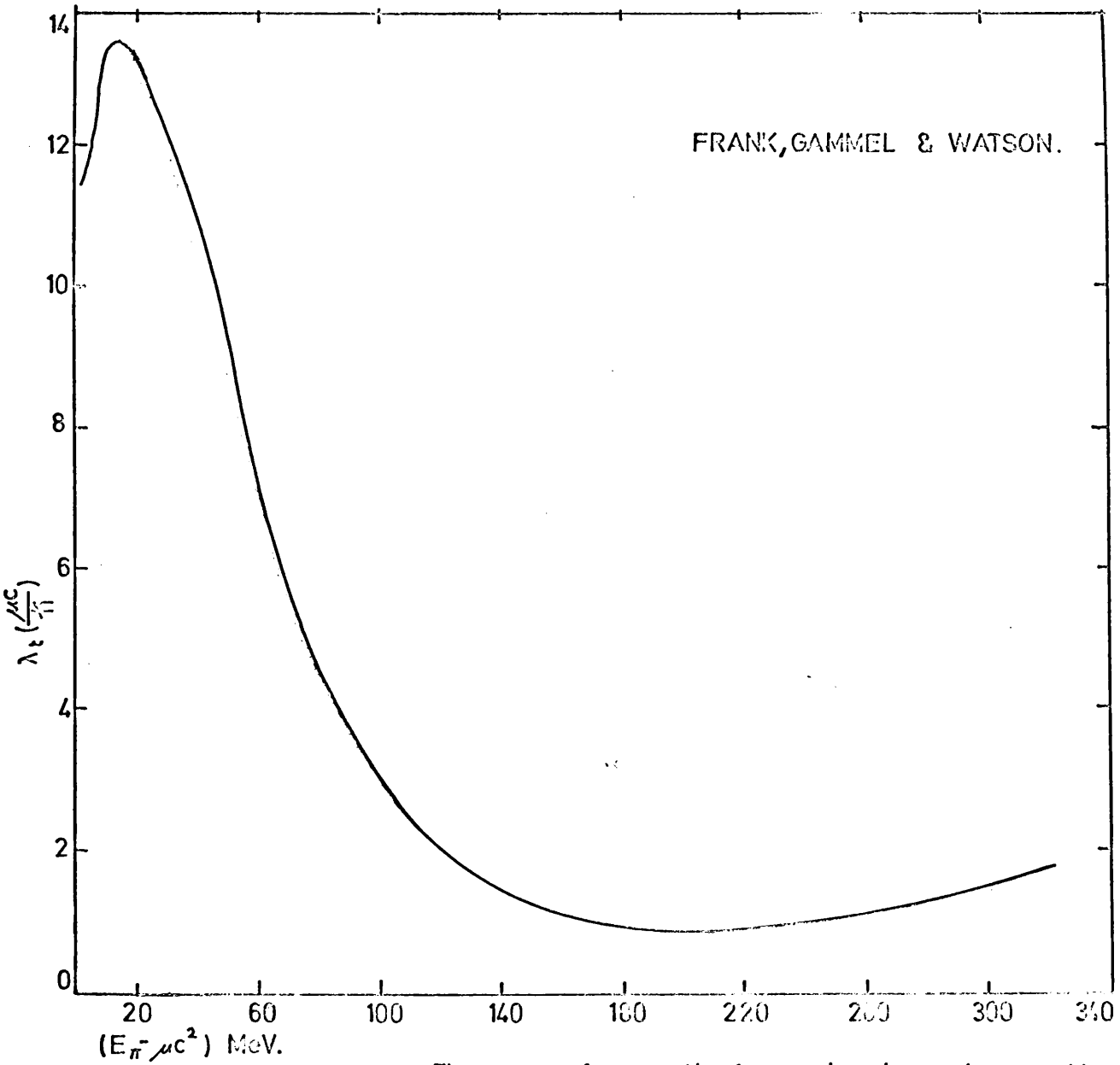

Figure 1·2. The mean free path for a pion in nuclear matter.

(Fig. 1.2). It therefore seemed possible by investigating the photoproduction of relatively low energy pions (~ 20 MeV) for which the nucleus must be to a considerable extent transparent, to obtain an unambiguous answer as to where the mesons are produced in the nucleus.

BELOUSOV et al[1.23] investigated the photoproduction of low energy π^0 mesons from different nuclei. The study of the photoproduction of π^0 mesons has the additional advantage that in this case there is no coulomb interaction to complicate the interpretation of experimental results. The measurements were made with 265 MeV and 200 MeV bremsstrahlung. By using two counter telescopes in coincidence, located 180^0 apart, π^0 mesons were recorded in an energy range of 1 - 15 MeV. An analysis of the absorption of slow π^0 mesons in nuclei leads to the conclusion that the average mean free path for the absorption of mesons in the nucleus in this particular energy range amounts to 20 r_0 ($20 \times 1.4 \times 10^{-13}$ cm). Therefore all nuclei right up to the heaviest must be transparent to such mesons. The results of BELOUSOV et al at both 265 MeV and 200 MeV show a clear $A^{\frac{2}{3}}$ dependence. This cannot be explained by the absorption of all mesons formed inside the nucleus, as is done in the description of the process of photoproduction of mesons from the point of view of the optical model, since that should have shown a clear A-dependence. These results, therefore, support the theory of surface production. POPOVA et al[1.24] observed the photoproduction of π^- mesons (0 - 3 MeV) for which the nucleus is practically transparent. The results, which agree with the theoretical predictions of BALDIN and LEBEDEV[1.25] for slow mesons produced from the

surface nucleons, also confirm the surface production model. POPOVA et al also pointed out the absence of any maxima for photoproduction from nuclei with excess neutrons in contrast to the work of LITTAUER and WALKER. BELOUSOV et al[1.26] in a later experiment, has observed the production of neutral π mesons from different nuclei. By considering two factors (1) the reabsorption of mesons at the instant of their creation inside the nucleus by a pair of strongly interacting nucleon (quasi-deutron process) and (2) the usual reabsorption inside the nucleus (single nucleon) predicted by the optical theory they were able to show fairly good agreement between the experimental results and theoretical conclusions. The calculations tend to suggest an A dependence intermediate between volume and surface production, though very close to surface production.

LAING AND MOORHOUSE CALCULATION

The only discrepancy between experimental results (LITTAUER and WALKER) and the calculated value based on the BUTLER-WILSON surface production model, is the 30 - 40% difference in the magnitude of the cross-sections. The calculated values tend to be on the lower side. The calculations of BALDIN and LEBEDEV and BELOUSOV et al, were normalised to carbon and produced no absolute cross-sections.

A more detailed calculation using the surface production model has been made by LAING and MOORHOUSE[1.27]. Their assumptions, based on a simple independent particle model, were (1) the primary photoproduction is essentially a single nucleon process (2) the nucleons in the struck

nucleus are taken to be bound in a potential well, which may be different for neutrons and protons. Inter-particle forces and spin orbit coupling are neglected. (3) In the primary process the struck nucleon goes into a discreet or continuum state and the nuclear potential is unchanged during this transition. (4) After production, the pions may be scattered or absorbed by other nucleons in the nucleus and this effect may be taken into account by an optical model. Their main difference from BUTLER'S treatment lies in assumption, (3). In BUTLER'S treatment the struck nucleon may go only to a continuum state. Although LAING and MOORHOUSE considered a simple independent particle model and assumed the primary photoproduction to be essentially a single nucleon process, they pointed out that pion production does not in fact take place as if no other nucleons were present. Their presence is felt through operation of the Pauli Principle and inter-particle forces, which will be most important in the nuclear core and may lead to competing photodisintegration processes (WILSON), which combined with pion scattering and absorption inside the nucleus, will cause a suppression of pion production from the core. For their calculations LAING and MOORHOUSE considered both surface and volume production assuming that on their model only the outer nucleon shells contribute. As an example of the case in which the struck nucleon is left in a discrete state they worked out the cross-section for the process "B (γ, π^-) "C. As an example of the case in which both discrete and continuum states are involved, differential cross-section and the π^-/π^+ ratio were calculated for the combined processes Ca^{40} (γ, π) X^{40}, Ca^{40} $(\gamma, \pi\, N)^{39}$ Y^{40} where π is the charged pion, N the ejected nucleon and X and Y the appropriate residual nuclei. Both

surface and volume production values were calculated.

The experimental determination of these processes affords a good test for the surface production model. HUGHES and MARCH[1.28] measured the cross-section of the reaction "B (γ, π^-) c" as a function of energy from 70 - 320 MeV. Their experimental values are in good agreement with the LAING and MOORHOUSE theoretical values for surface production. The experimental values of π^-/π^+ ratios for 80 - 100 MeV mesons from Ca were found to be in fairly good agreement with calculated surface production values (HOGG and SINCLAIR[1.29]). BELLAMY and HOGG[1.30] indicated that calculations both for surface and particularly for volume production based on the LAING and MOORHOUSE independent particle model would not be compatible with their experimental π^-/π^+ ratios for low energy mesons (15, 28, 48 MeV). MARCH and WALKER[1.31] measured the cross-section for the reaction Ni^{60} (γ, π^-) Cu^{60} as a function of energy. Their result was absolutely incompatible with the LAING and MOORHOUSE prediction (extrapolated from B") for volume production. On the other hand, their value for cross-section averaged over the photon energy range 140 - 320 MeV is 40 - 50% of that expected by an $A^{\frac{2}{3}}$ extrapolation from B". Their experiment strongly suggests that surface production rather than volume production is responsible for this type of reaction. DYAL and HUMMEL[1.32] measured the cross-section for the reactions B" (γ, π^-) C" and B" (γ, π^+) Be" as a function of energy. The resulting cross-sections for the production of B" (γ, π^-) C" reaction agree with those calculated by LAING and MOORHOUSE for surface production

of pions. Although detailed theoretical calculations of the cross-sections expected for the B" (γ, π^+) Be" reaction have not been made, they found the observed cross-sections to be in qualitative agreement, with those expected for surface production by making an estimate of the production of Be" on the basis of the number of states available. The results of LAING and MOORHOUSE depended more on the total number of states available than on the specific details of the states. Using this argument MEYER et al[1.33] successfully explained the cross-sections for the reaction $O^{16}(\gamma, \pi^+)$ N^{16} in terms of the surface production model. More recently DEVANATHAN and RAMCHANDRAN[1.34] have investigated theoretically the elastic photoproduction of charged pions from complex nuclei. They obtained an expression from which impulse approximation claculation could be made for any nucleus with n equivalent nucleons outside closed shells. This situation is of practical importance as it obtains in almost all cases of light and medium heavy nuclei. Considering all types of angular momentum coupling between the nucleons and using CHEW et al[1.35] amplitudes for the photoproduction from free nucleons (valid up to 500 MeV) they carried out numerical calculations to obtain cross-sections as a function of energy for the reaction $^{60}Ni_{28}$ $(\gamma, \pi^-)^{60}Cu_{29}$. They considered both the oscillator well (r_o = 1) function and the square well (r_o = 1.2, 1.4) function. However, when compared with available experimental data, very poor agreement, both in respect of shape and magnitude was obtained. The agreement was particularly poor for the assumption of an oscillator well function.

PION EMISSION ACCOMPANIED BY NEUTRON EMISSION

A reaction of the type (γ, π^- x n) where n = 1, 2, 3... is not one in which the recoiling nucleon leaves the nucleus. The recoiling nucleon in the basic π^- production is a proton which must stay in the nucleus if one is to study the reaction of this type. The neutron then must come from one of two processes. (1) For low proton energies (Ep ~ 30 MeV) the nucleus can be regarded as in an excited state. The neutrons can then be evaporated according to the statistical theory. (2) For high proton energies (Ep ~ 100 MeV) one or more neutrons may be emitted by direct interactions with the protons. Even after one or more neutrons have been emitted as a result of direct interactions with the recoiling proton, the nucleus can be left behind in a sufficiently excited state to allow further evaporation of neutrons.

So a (γ, π^- x n) type of reaction involves the following processes, (a) a photon interacts with the target nucleus causing a neutron to change into a π^- and a proton, (b) the π^- leaves the nucleus, (c) the recoil proton stays in the nucleus, (d) x neutrons are emitted. It can be further assumed that (1) the π^- is photoproduced from a free nucleon close to the surface (assuming that photoproduction in the core is somehow suppressed) (2) the π^- is emitted without undergoing any collision, (3) the neutron emission results from the interaction of the recoiling proton with the nucleus (4) this process can be treated as a (p, x n) reaction initiated by a free proton. This last assumption raises an interesting possibility. If true, the ratio of the relative yields of

$(\gamma, \pi^- n)$, $(\gamma, \pi^- 2n)$ ... etc. in a certain target nucleus should be the same as that of (p, n), (p, 2n) ... etc. in the same target nucleus.

At the present moment very little is known about this type of reaction. YAVIN and PASQUALI[1.36] measured the relative yields of (γ, π^-) and $(\gamma, \pi^- \times n)$ where $\times$ = 1, 2, 3, 4, 5 reaction from Bi^{209} at a maximum bremsstrahlung beam energy of 250 MeV. The authors found that within experimental error the relative yields of $(\gamma, \pi^- \times n)$ reactions agree very well with the relative yields of (p, x n) reactions on Bi^{209} as measured by JACKSON[1.37]. This tends to suggest strongly that $(\gamma, \pi^- x n)$ type of reaction can be treated as (p, x n) reaction after the π^- leaves the nucleus. The authors also found that the total cross-section is compatible with the surface production model. More recently MEYER and HUMMEL[1.38] measured the cross-section of V^{51} $(\gamma, \pi^- 2n)$ Cr^{49} reaction as a function of energy. By using (1) the cross-section for photoproduction of π^+ meson from hydrogen (2) $\frac{\pi^-}{\pi^+}$ ratio for V from LITTAUER and WALKER's curve (3) cross-section for (p, 2n) reaction on Cu^{63} the authors were able to calculate theoretically the cross-section for V^{51} $(\gamma, \pi^- 2n)$ Cr^{49} reaction as a function of energy. Very good agreement was obtained with experiment.

The present position appears to be as follows. Experimental work resulting in the production of high energy mesons can be interpreted in terms of the optical model. Mesons are supposed to be created at nucleons throughout the nuclear volume and the observed $A^{\frac{2}{3}}$ dependence results from reabsorption of mesons produced in the core. The observed $A^{\frac{2}{3}}$ dependence for the production of low energy mesons cannot be similarly

explained, since even heavy nuclei are relatively transparent to low energy mesons. The surface production model of BUTLER-WILSON proposes a mechanism by which meson production in the core of a nucleus is suppressed.

In order to test further the predictions of the optical and surface production models, it seems particularly useful to measure the total cross-section for photopion production especially for photon energies near threshold where the emission of low energy pions is expected. Counter experiments which select high energy pions can usually be interpreted successfully using either model.

The study of reactions of the type (γ, π^- x n) where x = 1, 2, 3 ... has other interesting possibilities. This type of reaction can be used for the investigation of problems in nuclear structure. It may also be possible to test the assumption that pion production in a complex nucleus is a single nucleon process.

It will also be interesting to know the relative cross-sections of (γ, π^-) and (γ, π^- x n) reactions as a function of energy in a particular target nucleus. It can be argued that provided the (γ, π^- x n) type of reaction can be taken as identical with (p, x n) type of reaction, the determination of the cross-section of any one of the (γ, π^- x n) reactions will enable one to predict others from known (p, x n) reactions.

In this thesis measurements are described for the determination of the cross-section of the reaction Cu^{63} (γ, π^-)Zn^{63} and Cu^{63}(γ, π^- n) Zn^{62} as a function of energy from 100 - 320 MeV. The cross-sections are then compared with the predictions of the surface production and optical models.

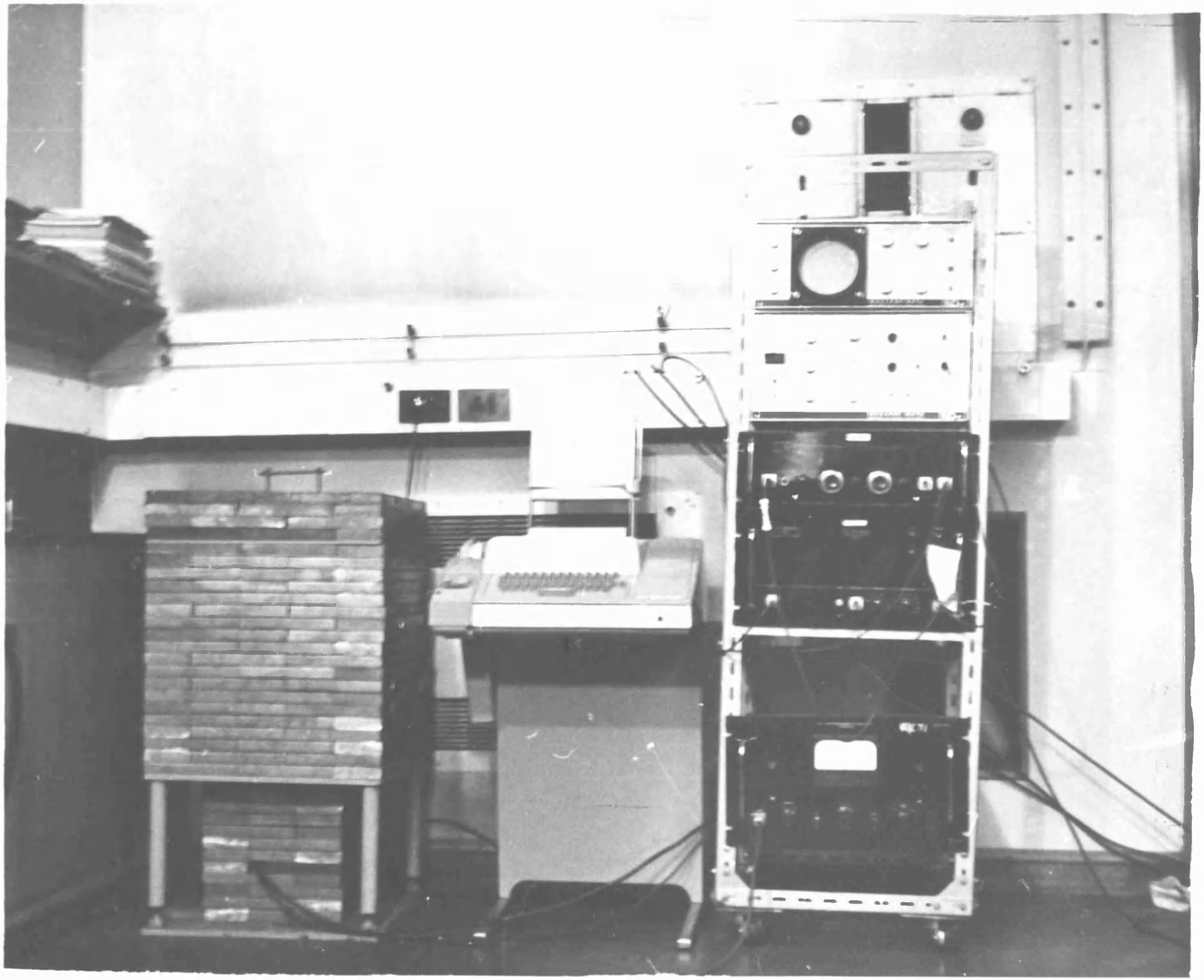

DETECTION SYSTEM

Figure 2

CHAPTER 2

DETECTION SYSTEM

INTRODUCTION:

In most of the previous experiments the measurement of total cross-section for the photoproduction of pions depended upon the detection of the pions in certain fixed energy ranges and angular intervals. The total cross-sections were then evaluated from differential measurements by extrapolating to angles at which no measurements were made and integrating over all angles. This method has the limitation that no distinction is made between reactions in which the meson is the only particle emitted and reactions in which the meson is accompanied by the simultaneous emission of other particles.

Photopion emission from a complex nucleus, unaccompanied by other nucleons results in the formation of a nucleus of the same mass as the target nucleus, but having either one charge less, the same charge or one charge more than the target nucleus according to whether the emitted pion is positively charged, neutral or negatively charged. When the emitted pion is charged, the final nucleus is radioactive. The production cross-sections can be found by measuring the different radioactivities - such as β-activity, α-activity. Also some of these radio-active nuclei have their own characteristic γ-rays, so that cross-sections can also be determined by measuring these γ-rays.

2.1

As pointed out by MARCH and WALKER, the $(\gamma, \bar{\pi})$ type of reaction can be studied more readily than the (γ, π^{+}) reaction because the former type of reaction normally results in a positron-emitting nucleus. The total cross-section can then be determined by counting the 0.511 MeV annihilation quanta. This method is preferable to a direct counting of positrons, since it permits of the use of thick samples.

When the pion is accompanied by simultaneous emission of nucleons, the mass of the final nuclei will be equal to the mass of the target nucleus minus the mass of the emitted particles. The charge of the final nucleus will, however, depend upon the charges of both the pions and emitted particles and the final nuclei may be stable or radioactive. The present work has been confined to the investigation of reactions ${}_{A}X^{Z}(\gamma, \bar{\pi})\ {}_{A}Y^{Z+1}$ and ${}_{A}X^{Z}(\gamma, \bar{\pi}n)\ {}_{A-1}Y^{Z+1}$. Both these reactions result in final nuclei with different mass numbers but with the same atomic number. They may therefore be separated simultaneously from the target nucleus by radio-chemical techniques. The two reactions can be identified by the half-lives of the final nuclei. The production cross-section can be measured by counting 0.511 Mev annihilation quanta or any characteristic γ-rays that may be present.

γ-RAY SPECTROMETER

It was shown in the preceding paragraph that the total cross-section can be measured by detecting the 0.511 Mev annihilation quanta and other characteristic γ-rays. It is therefore necessary

to set up an efficient γ-ray spectrometer. The first two considerations are the choice of a suitable "phosphor" and the size of the phosphor.

Since its introduction as a γ-ray detector by HOFSTADTER,[2.2] NaI(Tl) has remained the most important detector for γ-ray scintillation spectrometry. Its high density (3.67 gm/cc) makes it a suitable material for the efficient absorption of electro-magnetic radiation. Single crystals of large size can be grown and these have proved of great value in the spectrometry of both particle and electro-magnetic radiations. The presence of iodine gives a high cross-section for photo-electric and pair production interactions. The emission spectrum with a maximum of 4100 Å is suitable for good matching to many types of commercial photomultiplier. The speed of response makes it suitable for most applications, its decay time is 0.25 micro second. These properties combined with the high transparency of the crystal to its own fluorescence mean that there is inherently good resolution making a convenient detector for both counting and identifying, by virtue of the γ-ray energies, the activity of the source.

The choice of the size of the detector is based upon a consideration of several factors. The table below gives the interaction ratios and photofractions of γ-rays of different energies for crystals of different sizes. It becomes clear that the bigger the crystal size the higher is the interaction ratio and the photofractions. This is because as the detector size and hence the path

length traversed by a photon increases, the probability for the occurrence of multiple compton processes increases markedly. Since the resolution time of the phosphor is long compared with the time for many collisions, the events will add. This results in relatively more events which ultimately leave the total photon-energy in the detector. At 0.511 Mev approximately 76% of the events result in total energy loss in the 5" x 5" detector as opposed to 57% for the 2" x 2" detector. The bigger size of the crystal also allows one to measure with good "geometric" efficiency the activity from a larger source.

TABLE (2.3).

Point source on NaI-crystal face at axis

Crystal size dia. x ht. (in.)	Energy (Mev)							
	0.142	0.662	1.330	2.620	4.450	7.100	10.000	14.000
				INTERACTION RATIO				
8 x 8	1.000	0.966	0.897	0.810	0.802	0.809	0.820	0.842
6 x 6	1.000	0.930	0.828	0.750	0.714	0.717	0.727	0.748
4 x 4	1.000	0.833	0.705	0.597	0.572	0.567	0.586	0.606
2 x 2	0.999	0.598	0.456	0.379	0.345	0.348	0.361	0.386
½ x ½	0.865	0.210	0.145	0.112	0.102	0.102	0.105	0.115
				PHOTOFRACTIONS				
8 x 8	0.912	0.764	0.626	0.531	0.455	0.407	0.377	0.309
6 x 6	0.913	0.709	0.572	0.441	0.361	0.300	0.272	0.205
4 x 4	0.916	0.627	0.460	0.320	0.252	0.183	0.139	0.086
2 x 2	0.919	0.457	0.294	0.172	0.101	0.049	0.032	0.008
½ x ½	0.879	0.221	0.092	0.031	0.0049	0.0004	0.0001	0.0000

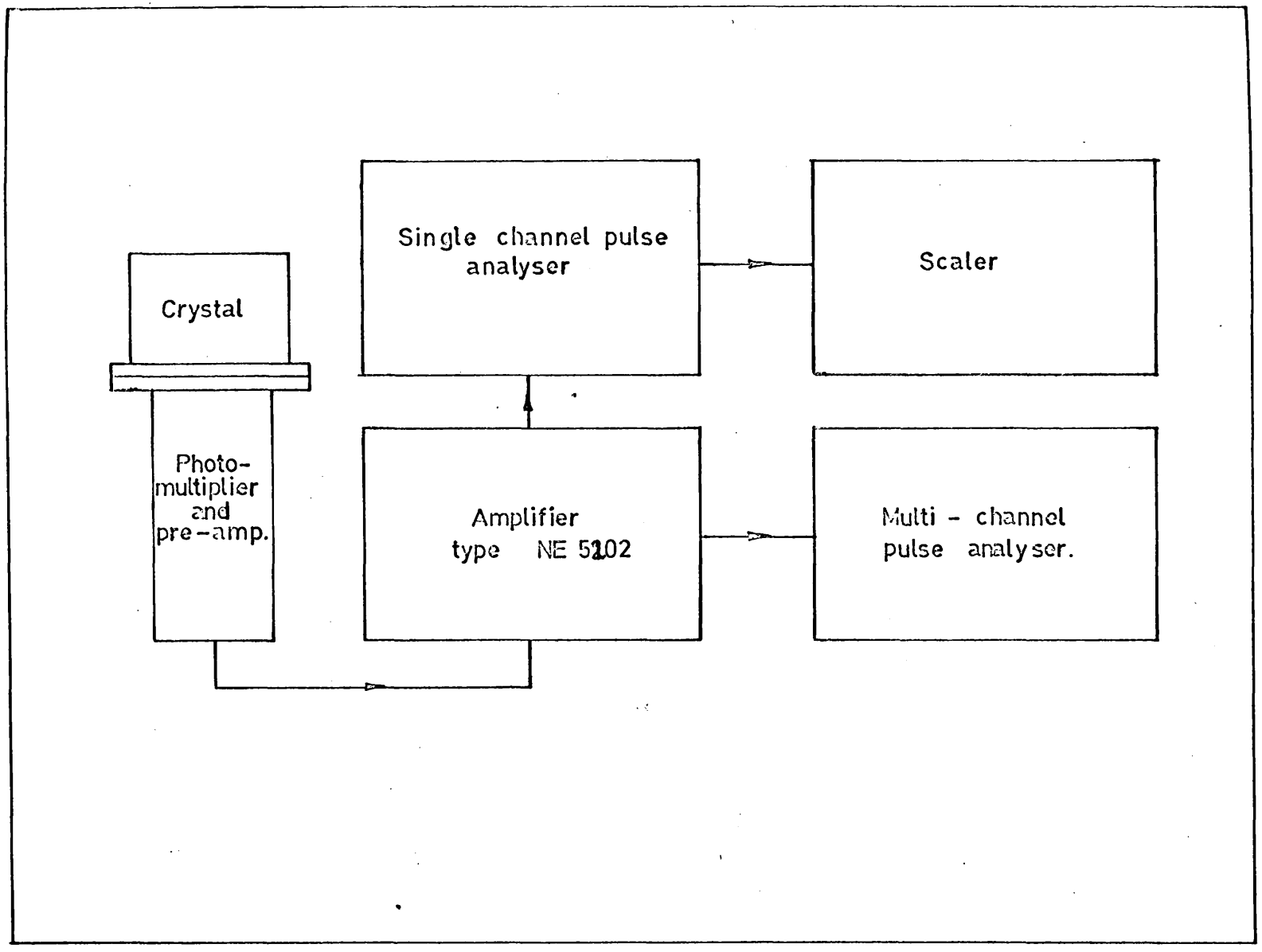

Block diagram of electronics.

Figure 2·1.

In the analysis of complex spectra it would be ideal completely to suppress the compton electron distribution. For a number of reasons, however, a compromise is necessary. To go to a large phosphor would require the use of a larger phototube with an appreciable increase in cost. This also results in some loss of resolution for low energy γ-rays. For this reason it was decided to set up the 5" x 5" NaI(Tl) crystal, which was already in the Department, as a γ-ray spectrometer.

ELECTRONICS CIRCUITRY

Fig. 2.1 is a block diagram of the electronics circuitry used. The output pulses from the photomultiplier, after being followed by a White Cathode Follower, were amplified by a non over-loading linear amplifier (N.E. 5202) which is a double delay-line amplifier based on the FAIRSTEIN[2.4] system. The amplifier is specifically designed for operation with a sodium iodide crystal. It has a gain of 50,000 with a recovery time of 5 microseconds for 100 times overload. The overload due to large cosmic ray pulses gives rise to a bump in the low energy region. This is due to the squiggles produced in the output pulse when a large overload pulse (cosmic-ray) is amplified by the double delay line amplifier. However, this is not important because the energy-region where it occurs is considerably below the energy region of interest. Apart from that the intensity is very much less than the intensity of the normal background. In the earlier stages of

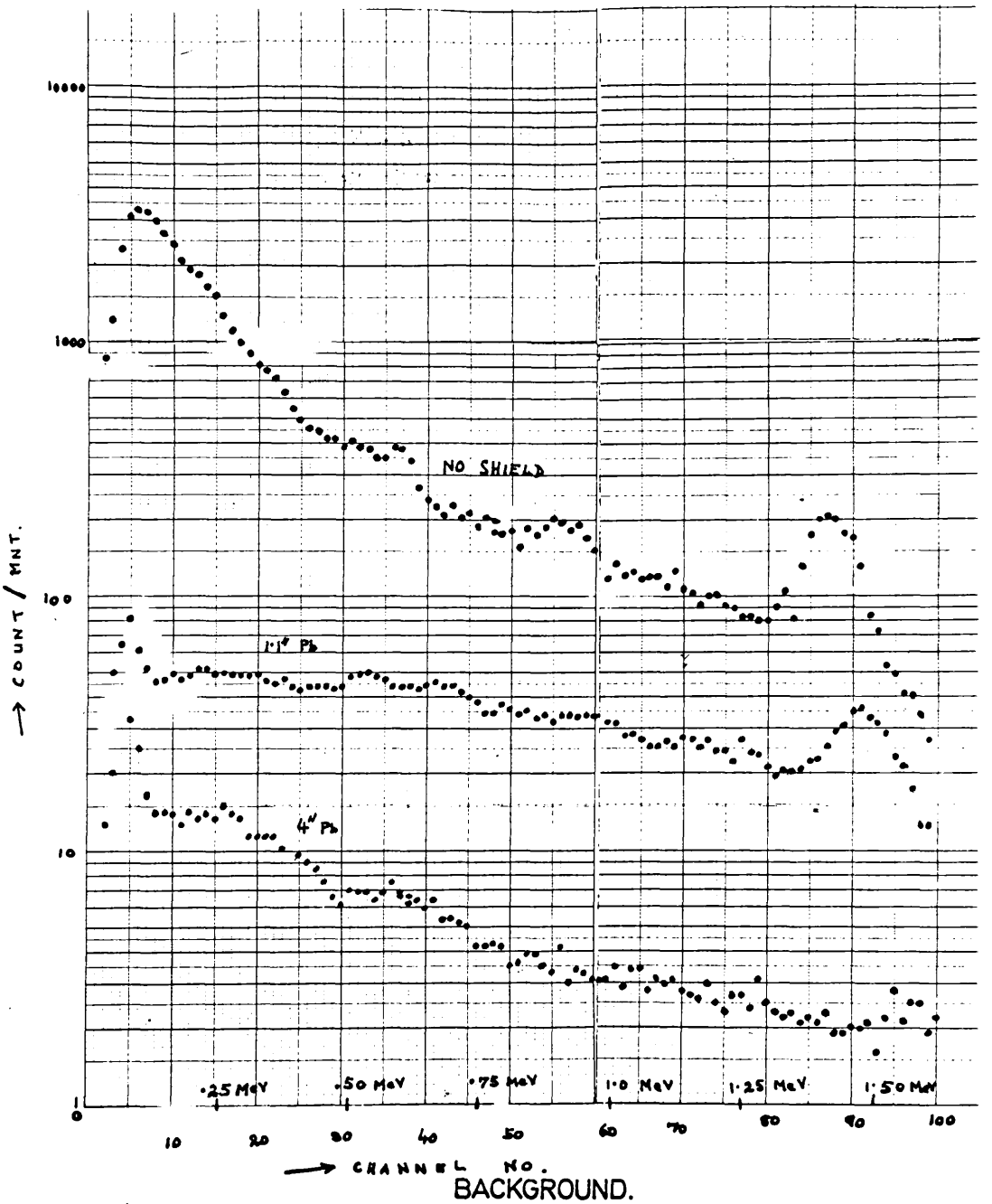
10000
1000
100
10
1
0
→ COUNT / MNT.
NO SHIELD
1·1" Pb
4" Pb
·25 MeV
·50 MeV
·75 MeV
1·0 MeV
1·25 MeV
1·50 MeV
10
20
30
40
50
60
70
80
90
100
→ CHANNEL NO.
BACKGROUND.

Figure 2·2.

this research the amplified pulses were analysed by a single channel pulse height analyser or a multi-channel instrument when available. A multichannel analyser is almost indispensable for this type of work and a suitable model was eventually acquired specifically for use with the large NaI crystal. A single channel pulse height analyser can also be used to set bias limits in order to measure the activity within a certain energy range.

DETECTOR SHIELD

One of the important considerations in obtaining good data in scintillation spectrometry is the design of the detector radiation shield. This is particularly important in the present case since the large crystal is more sensitive to background radiation and cosmic-rays. It is desirable to reduce the background radiation level to a point where corrections to the data will be small even for weak sources.

The common method of shielding a detector is to build a lead box and place the detector within it. Three spectra of the background radiation from 0 - 1.5 Mev energy range were drawn, first with no shield, then with 1.1" thick circular lead shield (this was immediately available) and finally with a 4" thick lead shield (8" x 8" x 15"). The spectra are shown in Fig. 2.2. It is obvious from the figure that the 1.46 Mev γ-ray from K^{40} is from surrounding materials. This was expected since the potassium content of the crystal as quoted by the manufacturer is too low (1 p p m) to give rise to such a peak

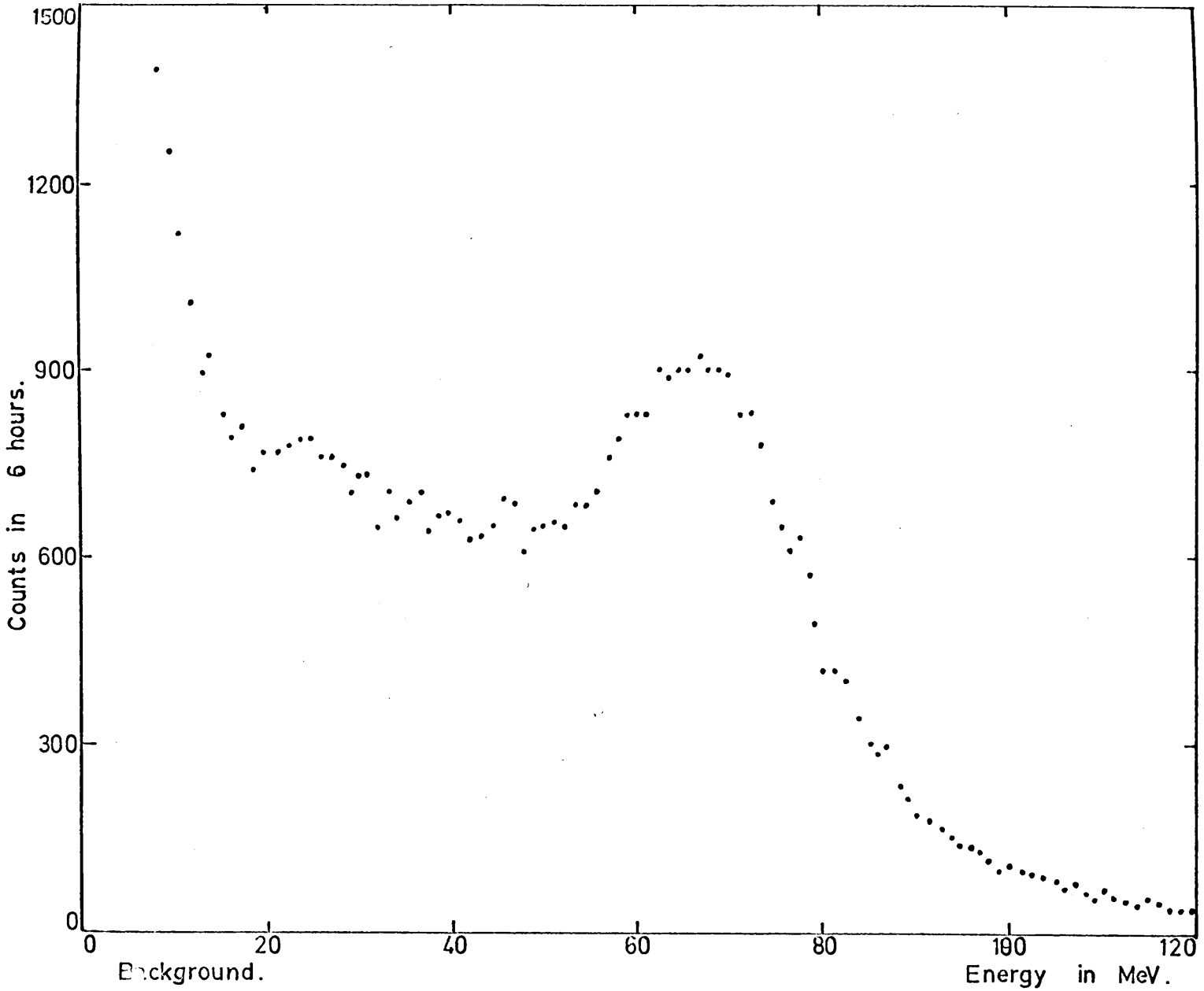
1500
1200
900
600
300
0
Counts in 6 hours.
0
20
40
60
80
100
120
Background.
Energy in MeV.

Figure 2·3.

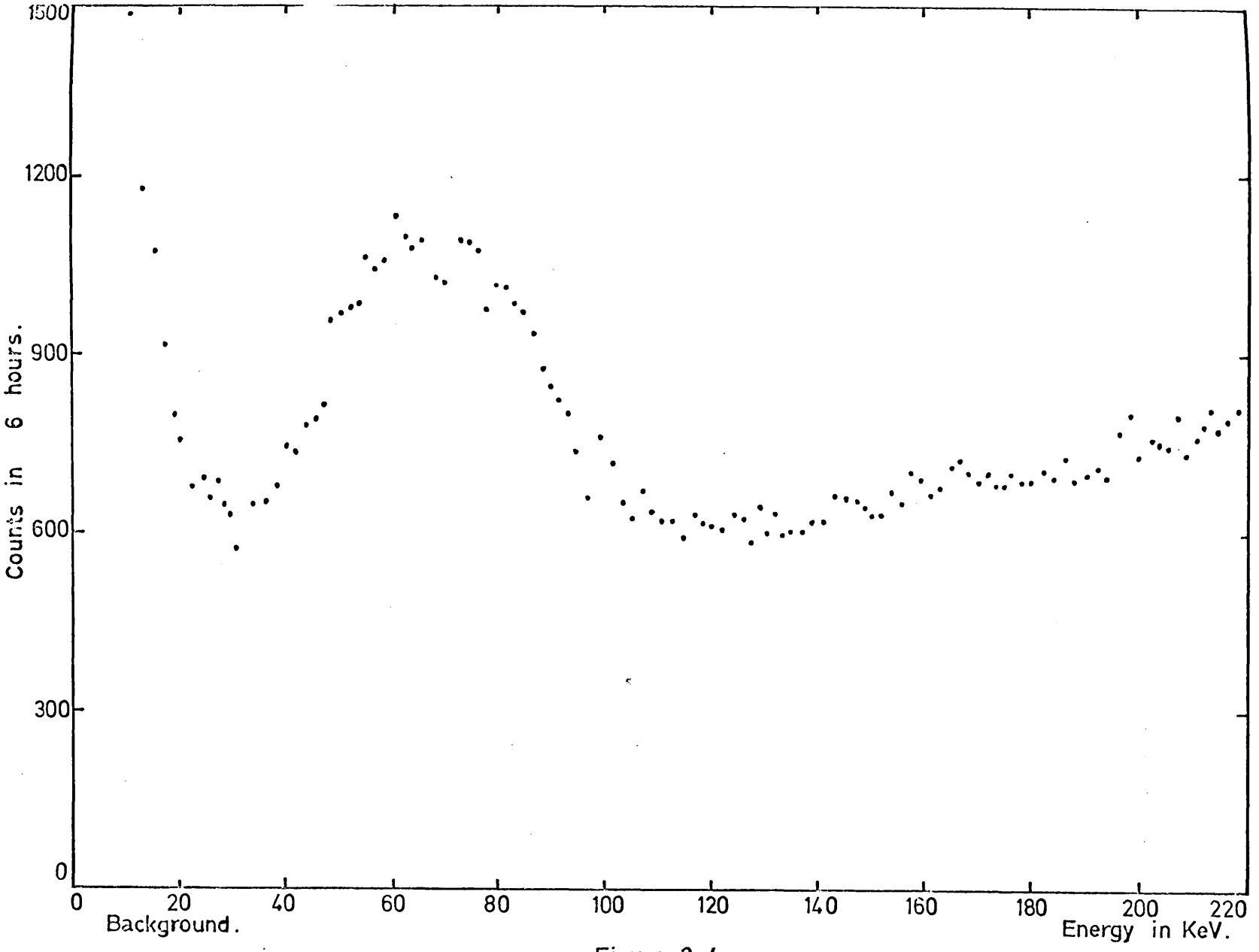
1500
1200
900
600
300
0
Counts in 6 hours.
0
20
40
60
80
100
120
140
160
180
200
220
Background.
Energy in KeV.

Figure 2·4.

of its own. The total count between an energy range 0.13 Mev - 1.5 Mev for 4" of lead is about 625 counts per minute. This compares well with the results of other workers including GUSTAFSON et al[2.5] who obtained about 700 counts per minute for a 5" x 4" crystal using the same thickness of lead shield.

Using the 4" lead shield a systematic investigation of the background radiation was carried out up to an energy of 120 Mev. Two broad bumps were apparent one at an energy from 55 - 90 Mev (Fig. 2.3) the other at about 70 Kev (Fig. 2.4). The energy loss of cosmic-ray mesons in 1.51 cm. of NaI was determined by BROWN[2.6] and STERNHEIMER[2.7], which ranges from 6.50 - 7.13 Mev. The first bump agrees well with energy loss of cosmic-ray mesons in a 5" thick crystal. The count per minute under this bump also agrees well with the vertical intensity of these mesons (ROSSI[2.8] and PUPPI and DALLAPORTA[2.9]). The low energy bump was found to be due to squiggles produced when a large overload cosmic-ray pulse is amplified by the double-delay line amplifier, as already mentioned earlier. As each overload pulse due to a cosmic-ray should give rise to a pulse in the low-energy region, the areas under the two bumps were compared. They agree well.

In any type of analysis of data obtained on the scintillation spectrometer, a differentiation must be made between the response of the detector to radiation from the source and spurious scattered radiation arising from interaction with the surrounding material,

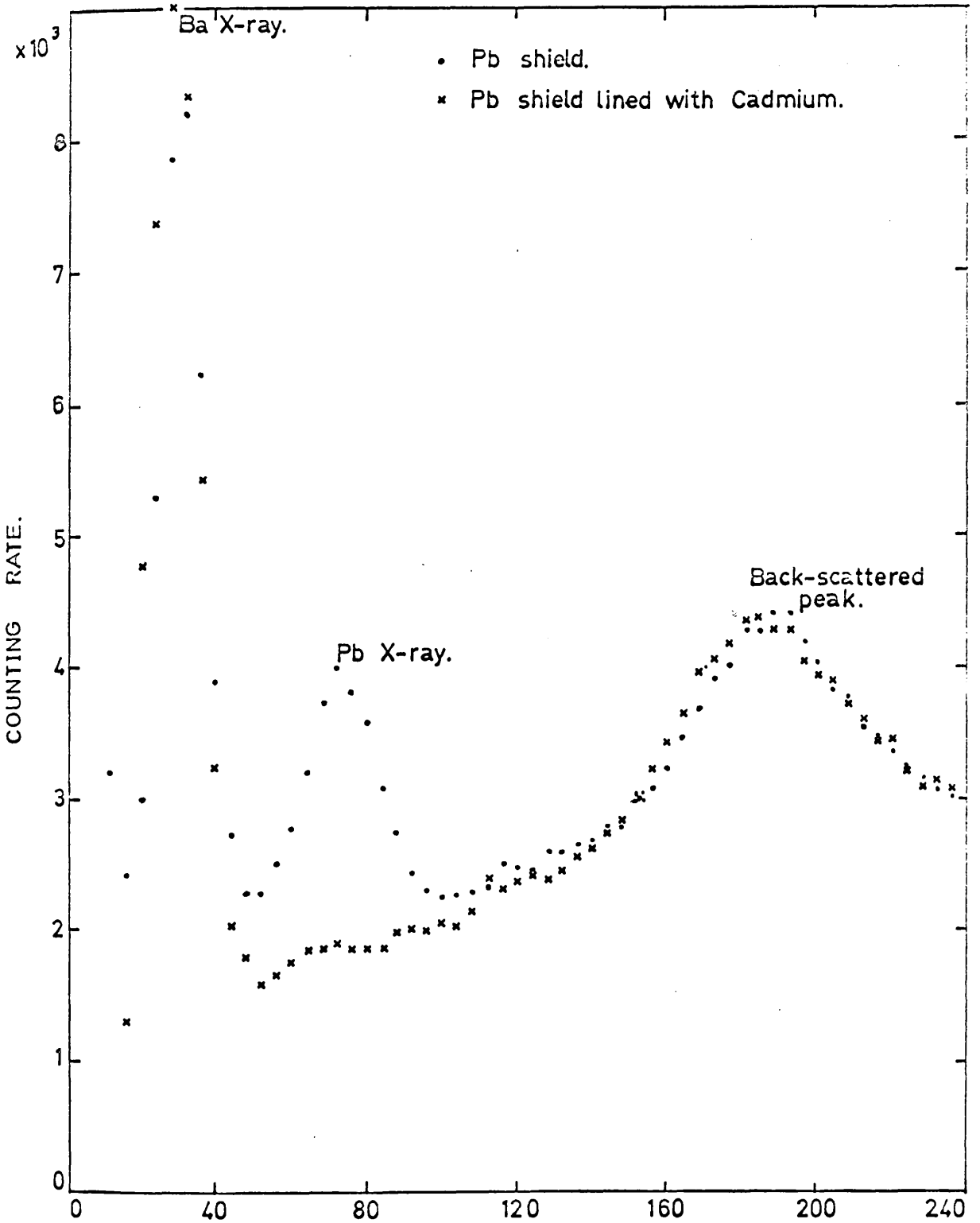

Figure 2·5.

Part of Spectrum of Cs^{137}.

source holder, beta absorber and radiation shield.

This scattered radiation results from two types of interaction (1) the photo-electric process, and (2) compton-scattering.

1. PHOTO-ELECTRIC PROCESS

The photo-electric effect is of particular importance in shield design since the cross-section for this process is high for low-energy photons, particularly in materials such as lead. This process results in the production of x-rays characteristic of the absorbing material. Spurious radiation from this source is generally reduced by the use of "graded" shield. In an arrangement of this type, the Pb radiation shield is lined with one or more materials in descending order of "Z". These materials are chosen to have a high cross-section for the absorption of fluorescent radiation from the preceding one. In the present case the lead shield was lined with 0.040" Cd. This thickness of Cd was found to be sufficient to absorb the Pb x-rays. Fig. 2.5 shows the effect of lining Pb with cadmium. Cadmium in turn gives rise to Cd x-rays. However, since the Cd x-rays (17.4 Kev) appear at the extreme lower end of the spectrum where amplifier noise is in any case a problem, no attempt was made to get rid of these x-rays.

2. COMPTON-SCATTERING

It is necessary to select a particular geometrical arrangement of source, shield and detector, since the response of the detector is intimately related to the position of the source. For a weak source,

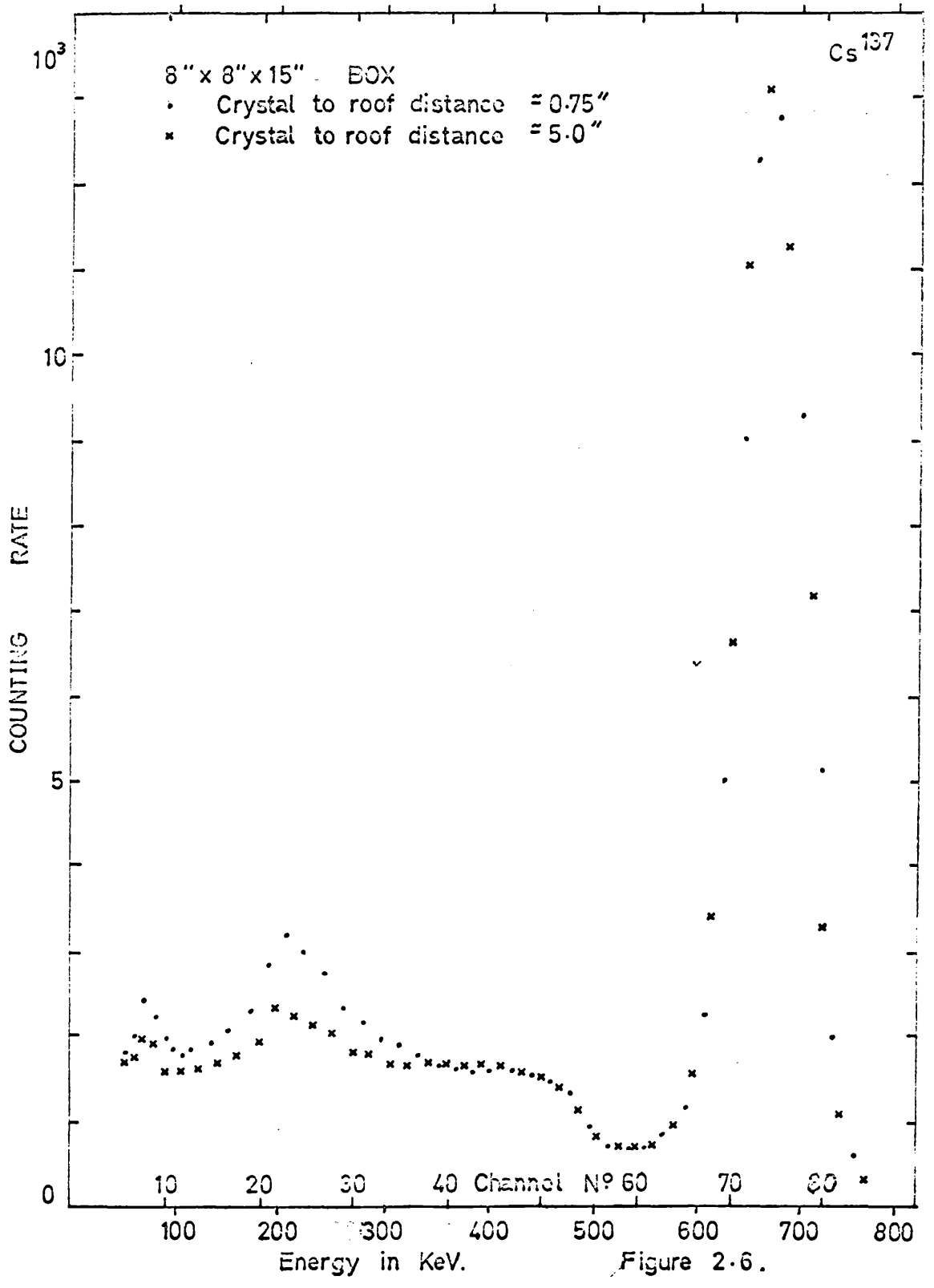
Cs 137
8" x 8" x 15" BOX
• Crystal to roof distance = 0·75"
× Crystal to roof distance = 5·0"
COUNTING RATE
10³
10
5
0
10
20
30
40
Channel Nº 60
70
80
100
200
300
400
500
600
700
800
Energy in KeV.

Figure 2·6.

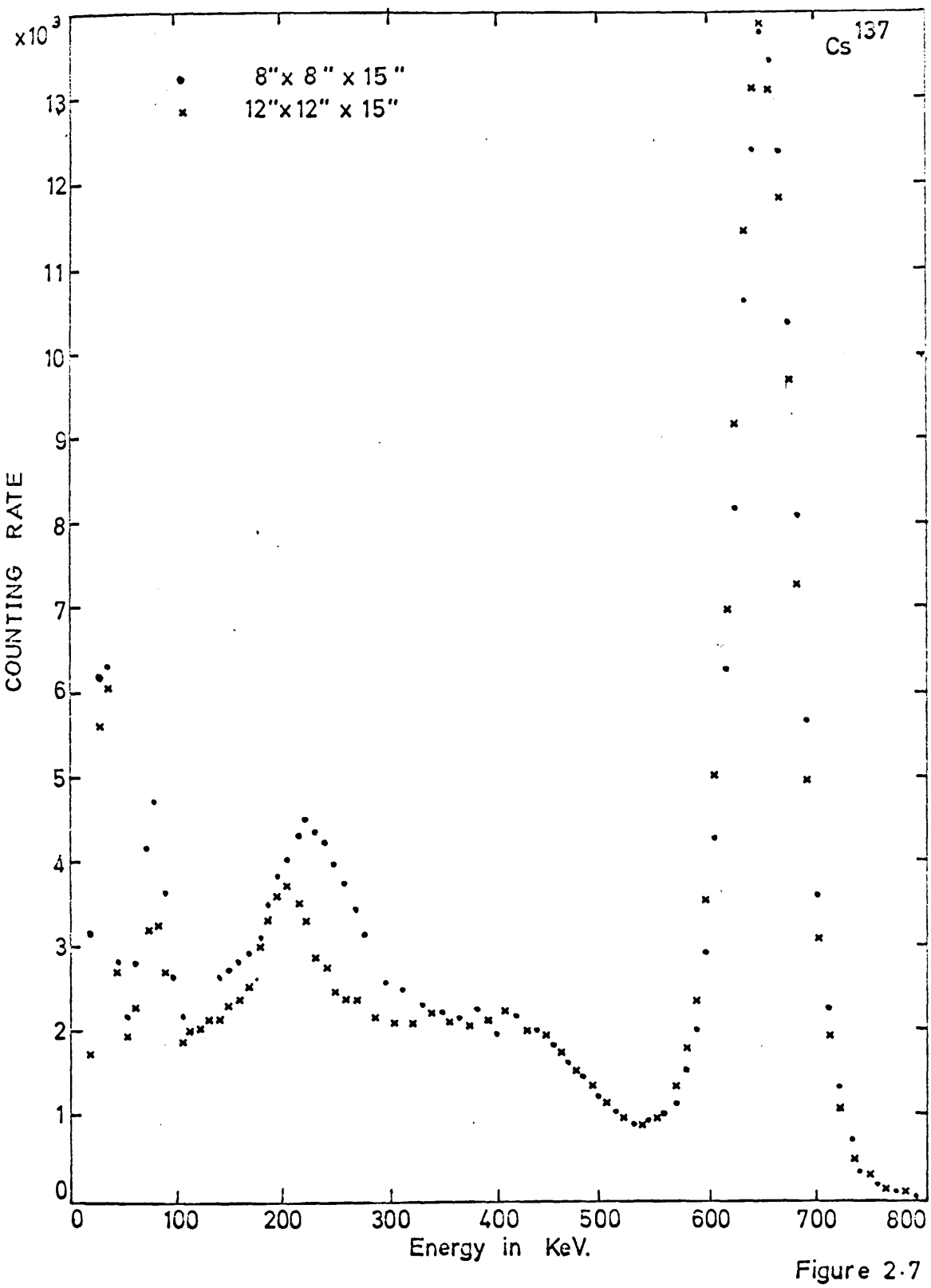
x10³
Cs 137
8"x 8" x 15"
12"x12" x 15"
COUNTING RATE
0
1
2
3
4
5
6
7
8
9
10
11
12
13
0
100
200
300
400
500
600
700
800
Energy in KeV.

Figure 2·7

when the overriding consideration is to obtain the highest counting rate, the best position is directly on the crystal which gives rise to a problem. As the source and the detector are both within the same lead shield, the radiations scattered back from the surrounding materials as a result of the compton process gives rise to a back-scattered peak in the resulting spectrum. One way to reduce this effect is to make the dimensions of the detector shield as large as cost and space will permit (R. L. HEATH[2.10]). This is due to a decrease in solid angle subtended by the detector for scattering from an elementary area on the surface of the shield wall. For most shield arrangements the magnitude of the scattered component will be relatively independent of source distance "h" while the efficiency for the detection of radiation will be proportional to $1/h^2$. It was found that by simply raising the roof of the shield by few inches, a considerable improvement in the spectrum could be obtained as seen in Fig. 2.6. Fig. 2.7 compares the spectrum of Cs^{137} obtained in two shields, one 8" x 8" x 15" and the other 12" x 12" x 15". The lower part of the crystal photomultiplier assembly (photo-multiplier and white Cathode-follower) was placed inside 4" x 4" x 12" lead wall while the upper portion (crystal) was placed inside the 12" x 12" x 15" lead wall. This was done in order to minimise the amount of lead required. Fig. 2.8 gives a diagram of the general arrangement. The use of the iron structure at the bottom reduced the amount of lead required while retaining effectively the desired dimension of the

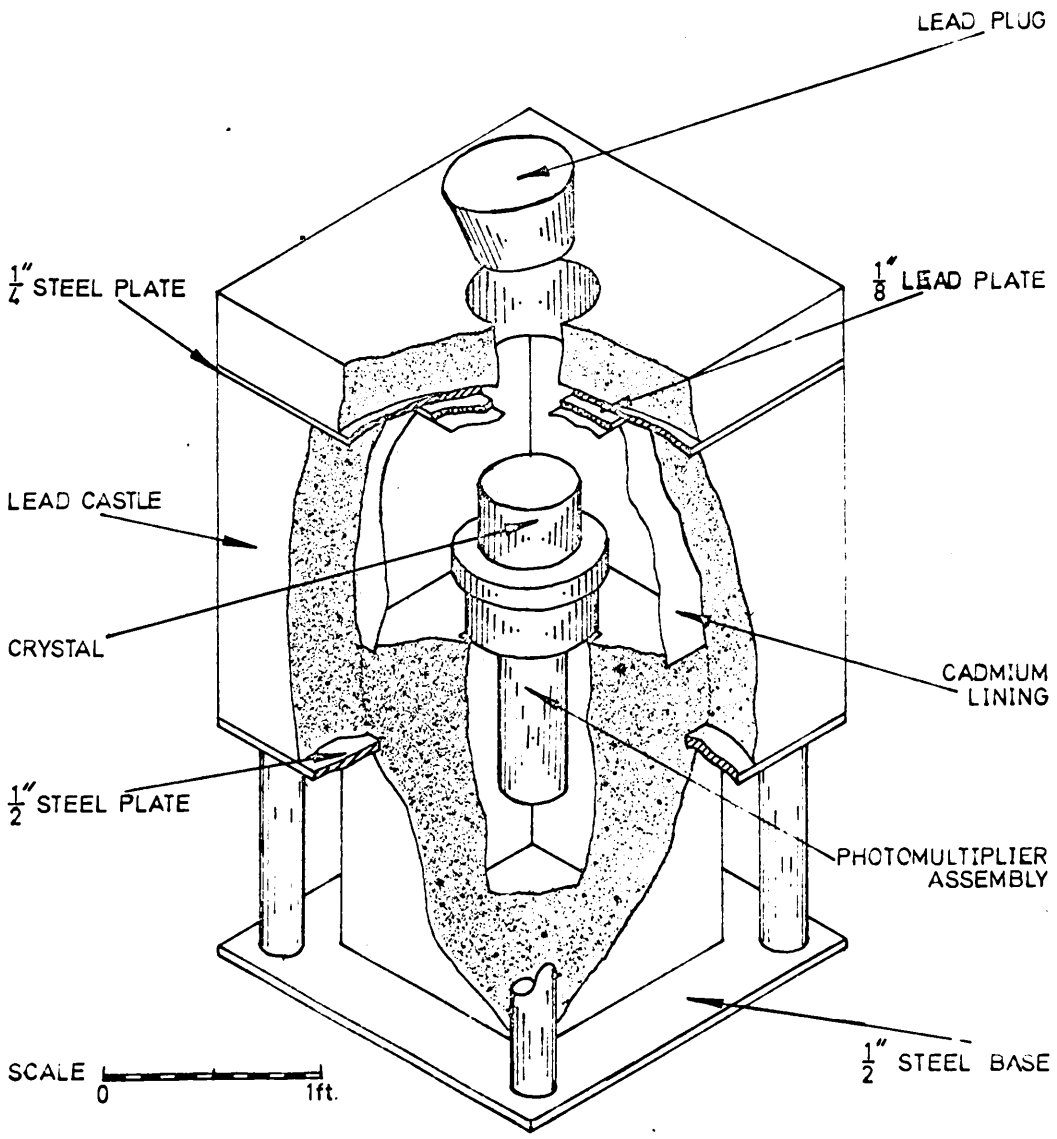
LEAD PLUG
1/4" STEEL PLATE
1/8" LEAD PLATE
LEAD CASTLE
CRYSTAL
CADMIUM LINING
1/2" STEEL PLATE
PHOTOMULTIPLIER ASSEMBLY
1/2" STEEL BASE
SCALE
0
1ft.

Figure 2·8

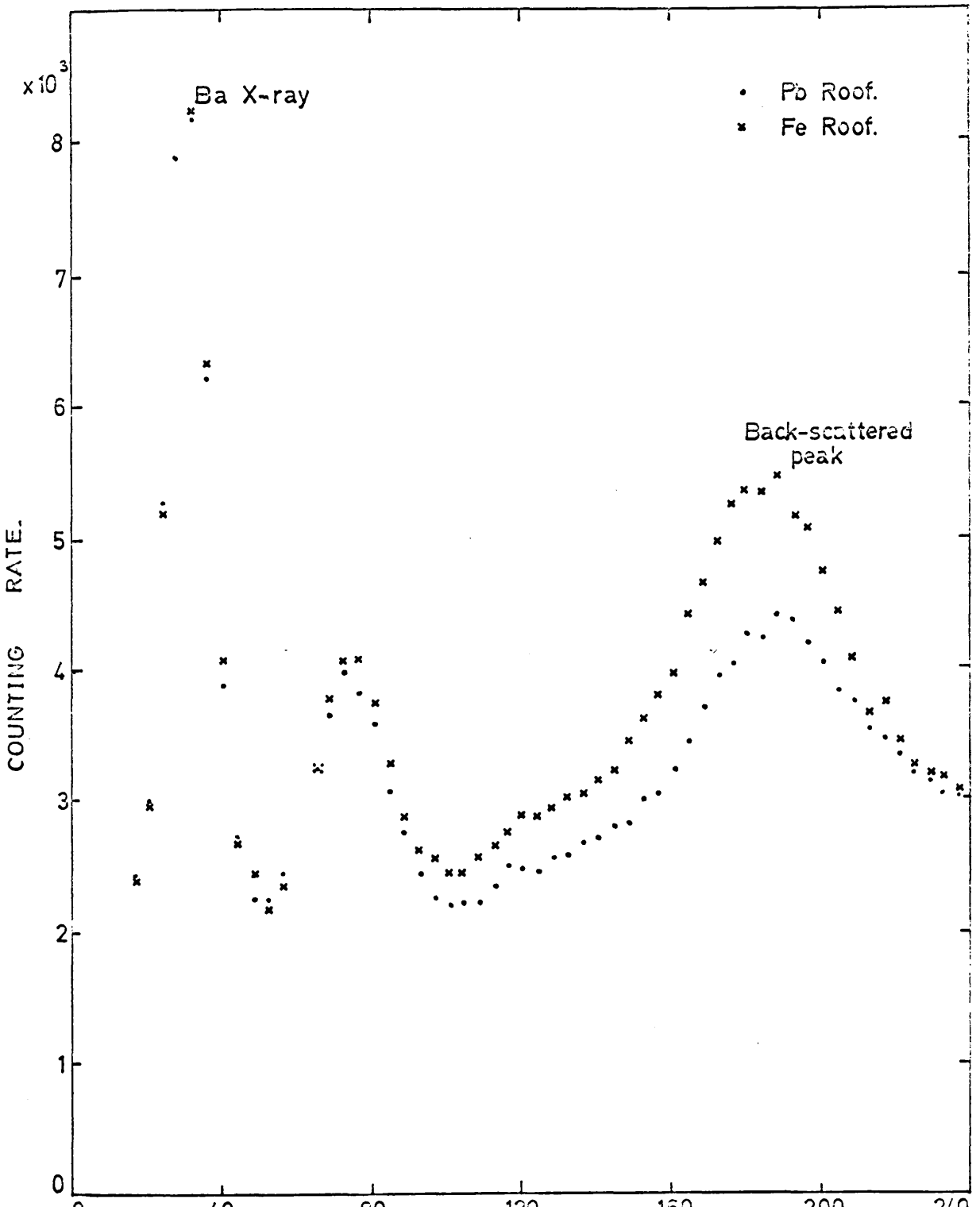

Figure 2·9.

Part of Spectrum of Cs^{137}.

box. The iron plate at the top was used to support the top portion of the lead shield. This was lined with lead and cadmium in order to minimise the effect of back-scattering, because the back-scattering effect is worst in case of iron, as can be seen from Fig. 2.9.

Another method of reducing back-scattered radiation is to use a collimator (BOSCH and CARACOCHE[2.11]). Accordingly a collimator with a narrow cone was designed. The back-scattered peak was almost completely removed. The compton distribution was also suppressed considerably due to the fact that now the photons were foreced to travel the whole length of the crystal as a result of which most of the scattered radiation due to the compton process inside the crystal was absorbed before it could leave. However, only a small fraction of the total radiation could now reach the crystal. For a weak source this is rather a high price for eliminating back-scattered radiation. For this reason another collimator was designed so that the face of the cone looking at the crystal completely covers the crystal face. For a source at a certain distance this represents the ultimate number of photons that would reach the crystal, even if no collimator were used. Fig. 2.10 gives the geometrical arrangement for the two collimators. Fig. 2.11 gives the spectron of Cs^{137} under two different conditions - source on crystal and source on collimator with the narrow cone.

During the actual experiment the source in the form of a solution contained in a conical flask was placed on the crystal. This was

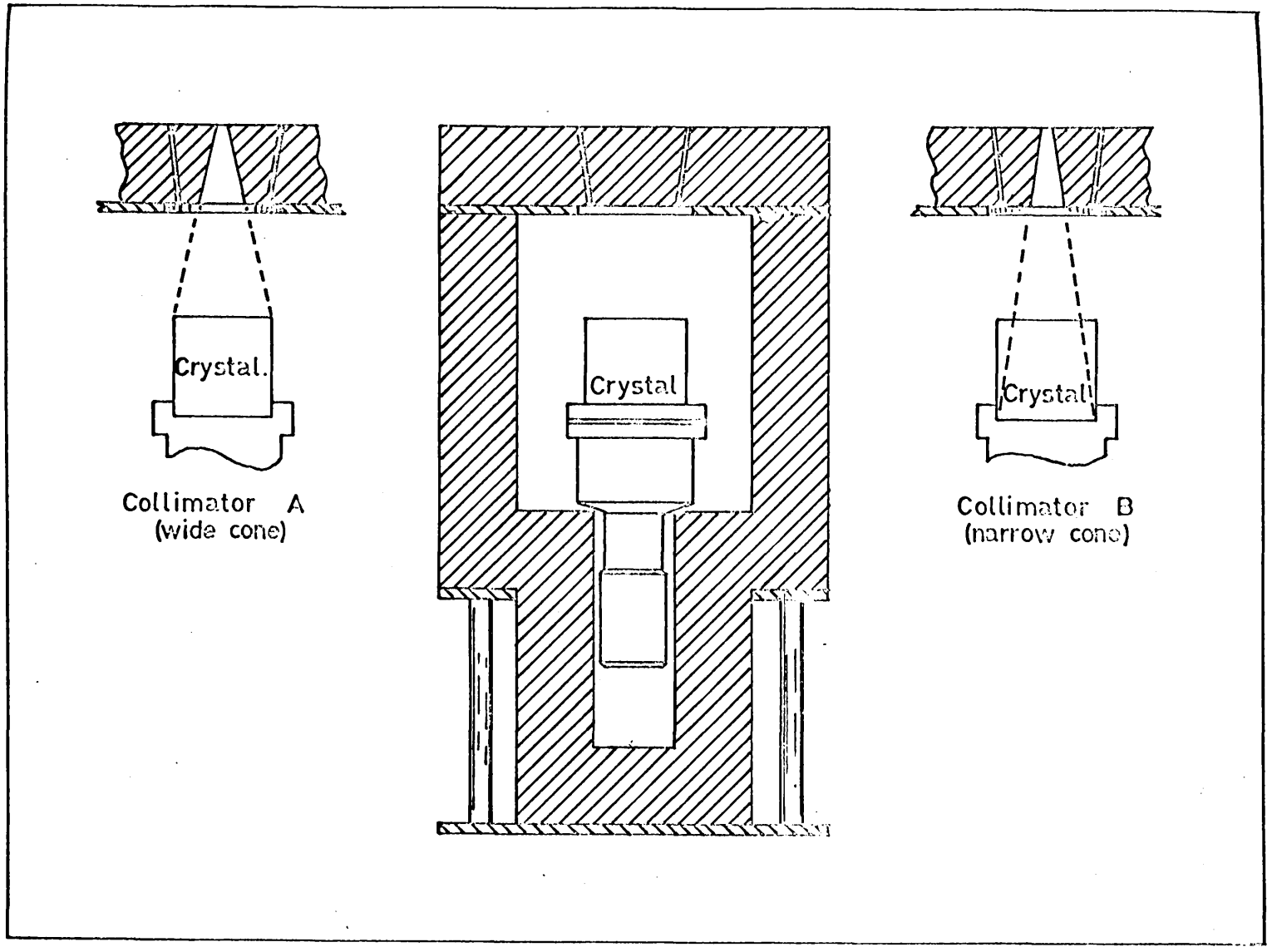

Geometric arrangement for collimators.

Figure 2·10.

because the source was so weak that the overriding consideration in this case was to obtain the best possible counting rate. A single-channel pulse height analyser was used to select only the 0.511 Mev annihilation quanta. These quanta were recorded continuously by means of a scaler. The stability of the whole system was watched by counting from time to time the 0.511 Mev annihilation quanta from a standard Na^{22} source. The equipment after an initial warming up period, remained quite stable throughout the entire period of counting.

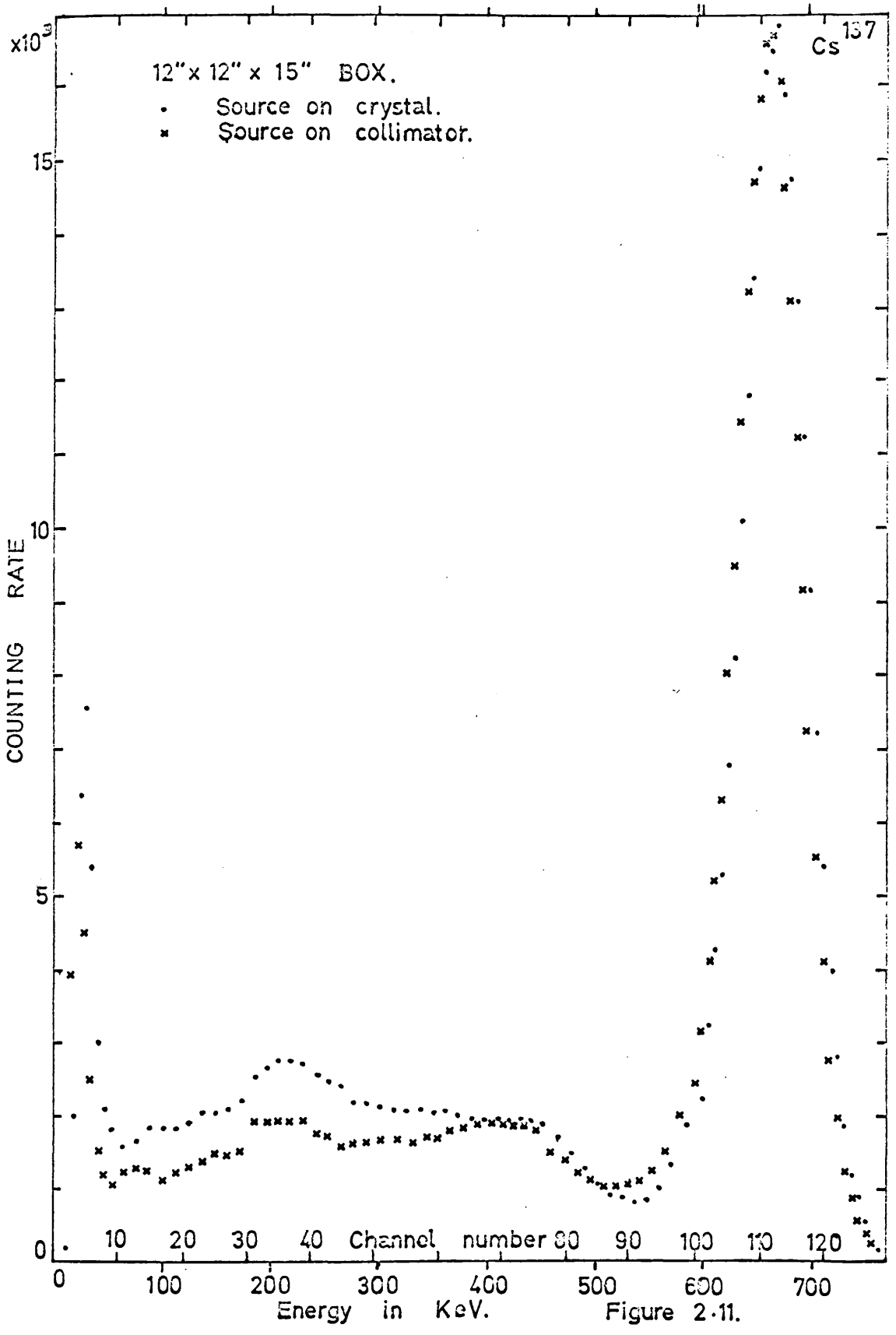
x10³
Cs 137
12"x 12" x 15" BOX.
• Source on crystal.
× Source on collimator.
15
10
5
0
COUNTING RATE
10 20 30 40 Channel number 80 90 100 110 120
0 100 200 300 400 500 600 700
Energy in KeV.

Figure 2·11.

CHAPTER 3

CHEMICAL SEPARATION

From an inspection of the chart of the nuclides in the region around copper (Fig. 3.1) it becomes clear that the success of studying (γ, π^-) and $(\gamma, \pi^- n)$ reactions on copper by the detection of annihilation γ-rays requires an efficient radio-chemical separation. This is necessary because by exposing a certain amount of target material to a high energy photon beam, one produces a large number of radio-active isotopes. Photo-nucleon reactions such as (γ, n), $(\gamma, 2n)$, (γ, p), (γ, pn) have much larger cross-sections than the photo-pion reactions of immediate interest. The products of these reactions are frequently positron emitters as are the Zn^{63} and Zn^{62} respectively. Moreover, they have half-lives of the same order so that it would be difficult if not impossible to effect a separation on the basis of half-life only (i.e. by analysis of the decay curve of the induced activity). That this was so was confirmed by exposing a copper target to the synchrotron beam. The resulting activity was found to be dominated by $Cu^{63}(\gamma, n)\ Cu^{62}$ (9.9 min), $Cu^{63}\ (\gamma, 2n)\ Cu^{61}$ (3.3 hr) and $Cu^{65}(\gamma, n)\ Cu^{64}$ (12.8 hr). It was impossible to assign any activity to Zn^{63}. The problem is then to separate both qualitatively and quantitatively a small amount of zinc from a large amount of copper and other interfering elements that may be produced by various photonucleon reactions. The amount of zinc produced by the reaction of interest may be as little as 10^{-12} gm. in one gm. of target material. The time of separation should be reasonably short, so that the zinc activity would be measurable.

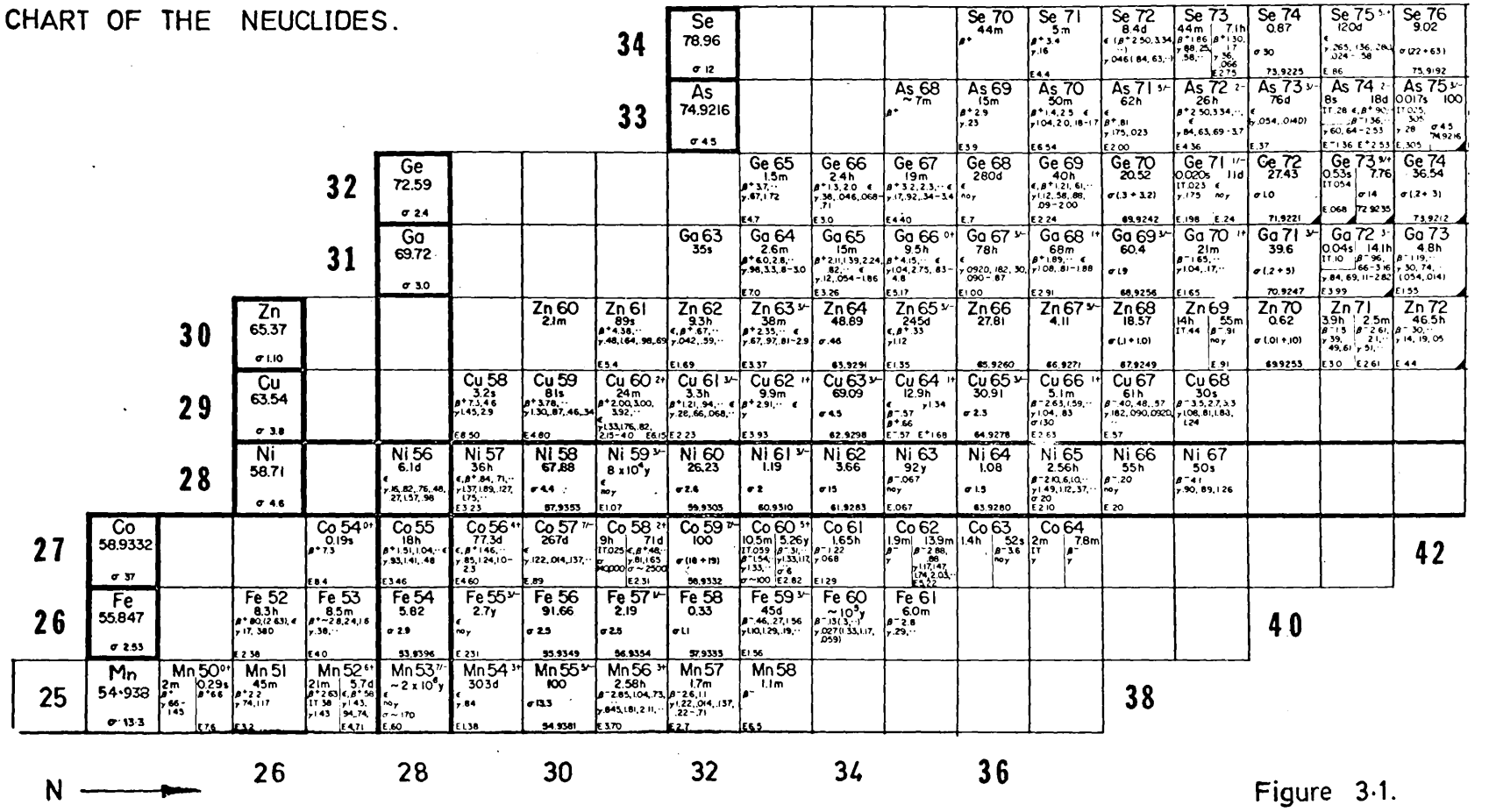
CHART OF THE NEUCLIDES.
Z
N
25
26
27
28
29
30
31
32
33
34
38
40
42
26
28
30
32
34
36

Figure 3·1.

It is important that the separation technique be easily reproducible with a high degree of accuracy. Such a separation is rather different from standard chemical procedures. The separation technique described in this chapter was determined by trial and based on the standard radiochemical separation and macro quantitative analysis. A great deal of time was spent in finding an efficient and easily reproducible method of separation.

Ideally one would like a chemical separation in which it is possible to extract zinc completely, leaving all the copper and other interfering metals in solution. However, such a separation could not be realised in practice. One was forced to look for the best possible alternative method of separation. It should be mentioned at this point that any method considered must start from a solution in nitric acid, since only this reagent will quickly dissolve metallic copper.

Standard methods of chemical separation are

(a) Precipitation

(b) Ion-Exchange Method

(c) Electrolytic Deposition

(d) Solvent Extraction.

The methods are discussed separately below. It may be noted at this point that the method of separation finally adopted consisted of a combination of electrolytic deposition to remove the bulk of the copper followed by solvent extraction to isolate zinc. Other approaches are described in so far as they illustrate some of the problems which

arise in the activation method.

Precipitation

No method was discovered of precipitating an insoluble salt of zinc leaving copper in solution. In orthodox qualitative analysis, copper is separated from zinc by passing hydrogen sulphide through an acid solution of (preferably) the chlorides, which precipitates copper sulphide. Nitric acid oxidises hydrogen sulphide to elementary sulphur and must be removed. In the present application this could be done by boiling with hydrochloric acid which, however, was time consuming. Since the amount of zinc produced by irradiating a target is so small it was necessary to add a weighed amount (500 mg.) of "carrier" zinc to the original solution in order to reduce the proportion of zinc adsorbed on the copper sulphide precipitate. "Hold-back" carriers of metals with insoluble sulphides were also added. The bulky precipitate of copper sulphide required thorough washing and the volume of filtrate, containing (hopefully) the zinc and invariably some residual copper, was almost unmanageable. Subsequent isolation of zinc was difficult and this approach was finally abandoned.

Copper can be precipitated from solution by the addition of sodium hydroxide. Sodium hydroxide solution was added to the boiling solution of copper nitrate containing suitable additions of carrier elements. Copper hydroxide was precipitated which was converted to insoluble cupric oxide by boiling. The precipitate was filtered

and washed. The filtrate was cooled and treated with additional sodium hydroxide to precipitate zinc as the hydroxide. The efficiency of this procedure was measured by oxidising the precipitate in a bunsen flame and weighing the zinc oxide produced to determine the proportion of zinc carrier recovered. The efficiency was not very good (50% - 70%) and could not be held constant in successive trials. It would therefore have been necessary to measure the efficiency separately for each run. Radioactive tracer experiments and a trial run with a sample irradiated in the synchrotron showed that the zinc hydroxide precipitate was always contaminated by copper although apparently free from other elements. The measurement of efficiency was confirmed. Since it was desired to study the production of 9h Zn^{62}, the search for a separation technique which would remove 12.8 h Cu^{64} was continued.

Ion Exchange

The ion exchange technique has obvious attractions but could only be considered as a refining process after the bulk of the copper had been removed by other methods. Otherwise the ion exchange resin would become saturated with copper. Moreover, the standard procedures are too slow for the present application and would require considerable development.

Electrolytic Deposition

It is possible by careful control of the pH of the electrolytic

solution and of the electrode potential to deposit metals electrolytically in the order of their reduction potentials. In acid solution advantage may be taken of the fact that the spontaneous evolution of hydrogen stabilises the electrode potential at the hydrogen evolution potential. Copper has a smaller reduction potential than that of the hydrogen ion while zinc (and nickel) have greater reduction potentials. It is therefore possible to deposit copper from acid solution and to inhibit the deposition of zinc. One would, of course, have preferred the reverse situation. However, it was found possible to employ high current densities without requiring external control of the electrode potential. Most of the copper would be deposited in a relatively short time, the whole of the zinc remaining in solution. Since this method formed part of the separation technique finally adopted, the experimental details are given below:

Copper was dissolved in a slight excess of Nitric acid. The electrolysis was carried out in a copper vessel which also served as the cathode. The anode was a platinum foil (4" x 4") which was wrapped round a perspex cylinder and was placed at the centre of the copper vessel. The vessel itself was placed in a water jacket containing cold water which served to keep the temperature of the electrolytic solution down during electrolysis. Since the time for deposition depends on the strength of the current, a very high current of 28 amps was used. This corresponded to a current density of 1.75 amp. per sq. inch. This was obtained from the three-phase mains by means

of a three phase variac and D.C. rectifier. During the electrolysis the current was kept constant by adjusting the variac. Fig. 3.2 shows the experimental arrangement for electrolysis.

The electrolytic solution consisted of a mixture of copper nitrate solution and a solution of hydrazine di-hydrochloride. In order to use maximum cathode area for the deposition of copper, the total volume of the electrolytic solution was made up to 360 cc. by the addition of deionized water. Hydrazine di-hydrochloride which is a reducing agent, served two purposes.

(1) It acted as an anodic depolarizer. A depolarizer is a substance which prevents interfering or undesirable reactions by being itself preferentially reduced at a cathode or oxidized at an anode. The depolarizer maintains the cathode potential less negative (less reducing) or the anode potential less positive (less oxidizing) than the potential at which interfering reactions occur. Hydrazine-di-hydrochloride prevents the formation of a layer of oxygen (evolved at the anode) which otherwise reduces the current efficiency. Nitric acid, already added in slight excess, is an oxidizing agent and acted as a cathodic depolarizer by preventing to some extent rapid evolution of hydrogen at the cathode. This improved somewhat the quality and uniformity of the deposit.

(2) In addition to functioning as an anodic depolarizer, hydrazine dihydrochloride played another important role. It enhanced the current efficiency for the deposition of copper. This was because the cupric

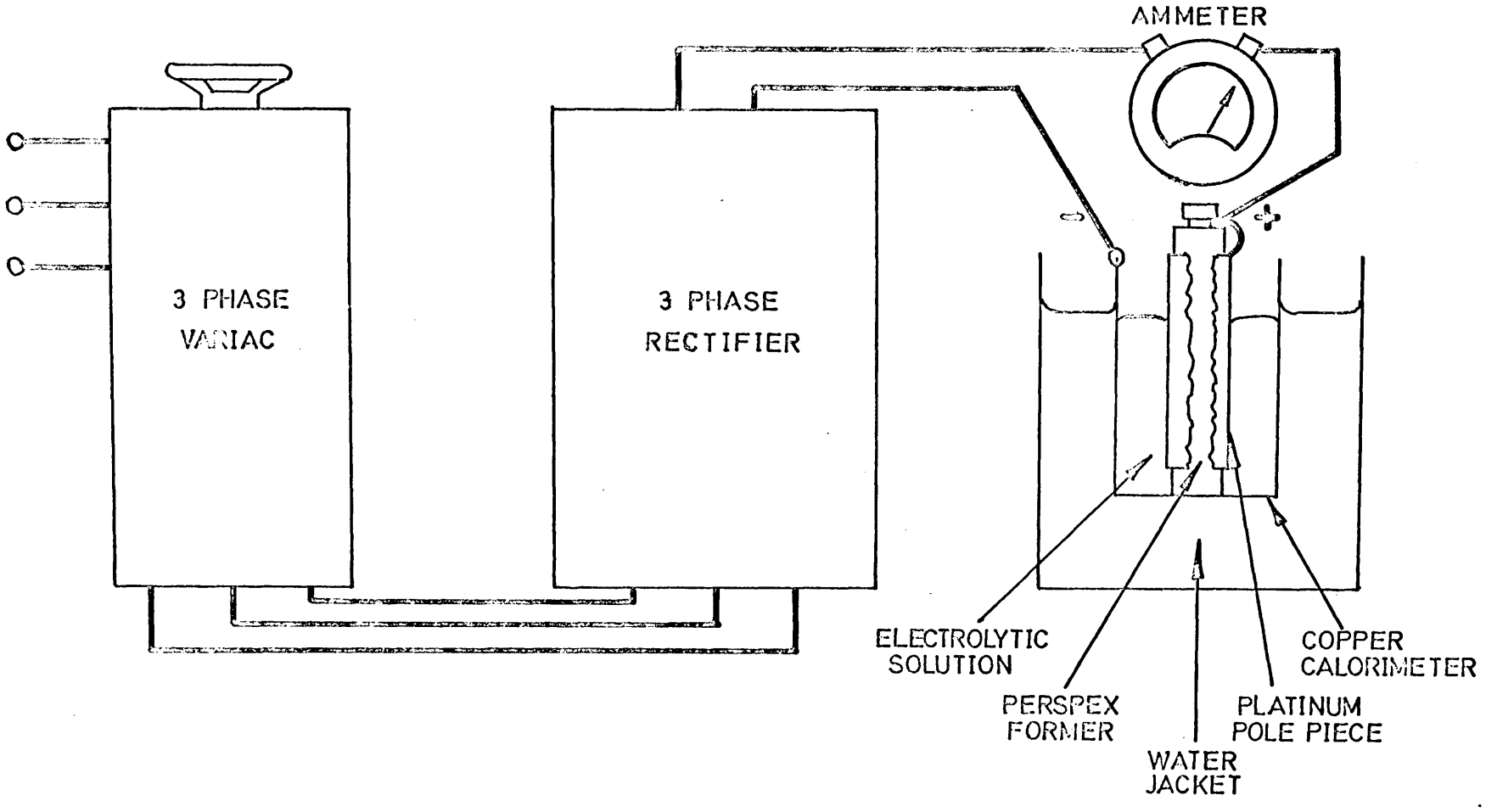
AMMETER
3 PHASE
VARIAC
3 PHASE
RECTIFIER
ELECTROLYTIC
SOLUTION
PERSPEX
FORMER
WATER
JACKET
PLATINUM
POLE PIECE
COPPER
CALORIMETER

Figure 3·2

complex was reduced to a considerable extent by hydrazine to a chloro complex of cuprous copper, which has a much larger diffusion co-efficient. Consequently the proportion of current carrying copper was larger and the electrolysis time correspondingly shorter.

The optimum amount of hydrazine dihydrochloride used was determined by a series of experiments and was found to be roughly 3.5 gm. for each gm. of copper. The electrolysis was carried out for about half an hour. The amount of copper left in the solution after this time was of the order of only a few milligrams, whereas the initial amount of copper was a little more than six gms. The rate of deposition becomes very slow at this point so that it is not profitable to continue electrolysis since the solvent extraction process described below can cope with this residual amount of copper. Solvent extraction works well with microgram quantities of zinc and effects a complete quantitative separation from copper and other interfering elements. Solvent extraction also helps to reduce the volume of the final solution, which is an important consideration from the counting point of view. For these reasons electrolysis was stopped after about half-an-hour and a solvent extraction was carried out with the remaining solution.

Solvent Extraction

The two solvents which are widely used for the extraction of zinc are dithizone (Diphenylthiocarbazone) and di-β-naphthylthio-carbazone, which is an analog of dithizone. It was demonstrated by

CHOLAK et al[3.1] that of the two, di-β-naphthylthiocarbazone is the better reagent since the conditions required for 100 per cent separation of zinc are less stringent. Fig. 3.3 shows the effect of pH of the solution on zinc partitions.

Elimination of Interferences

The reagent used in this experiment was a solution of di-β-naphthylthiocarbazone in chloroform which has a bluish green colour. When this solution is shaken with an aqueous solution containing different metal ions, it forms a coloured complex with some or all of the metals in the solution. These coloured complexes are the carbazonates of the metals concerned. At the pH range for quantitative extraction of zinc, shown in Fig. 3.3, di-β-naphthylthiocarbazone extracts not only zinc but also other metals including Cu, Ni, Fe, Co. All these metals must be prevented from forming carbazonates. Sodium diethyldithiocarbamate when added to the aqueous phase has been shown to be effective in preventing the formation of carbazonates of all metals except zinc. Other metals form carbamates. When di-β-naphthylthiocarbazone is used, zinc can be extracted quantitatively even in the presence of as much as 50 mg. of carbamates of all other metals.

Of the metals which react with carbamate, copper, nickel, cobalt and bismuth (when present in large quantity) have chloroform-soluble coloured complexes which, unless removed, affect the final separation

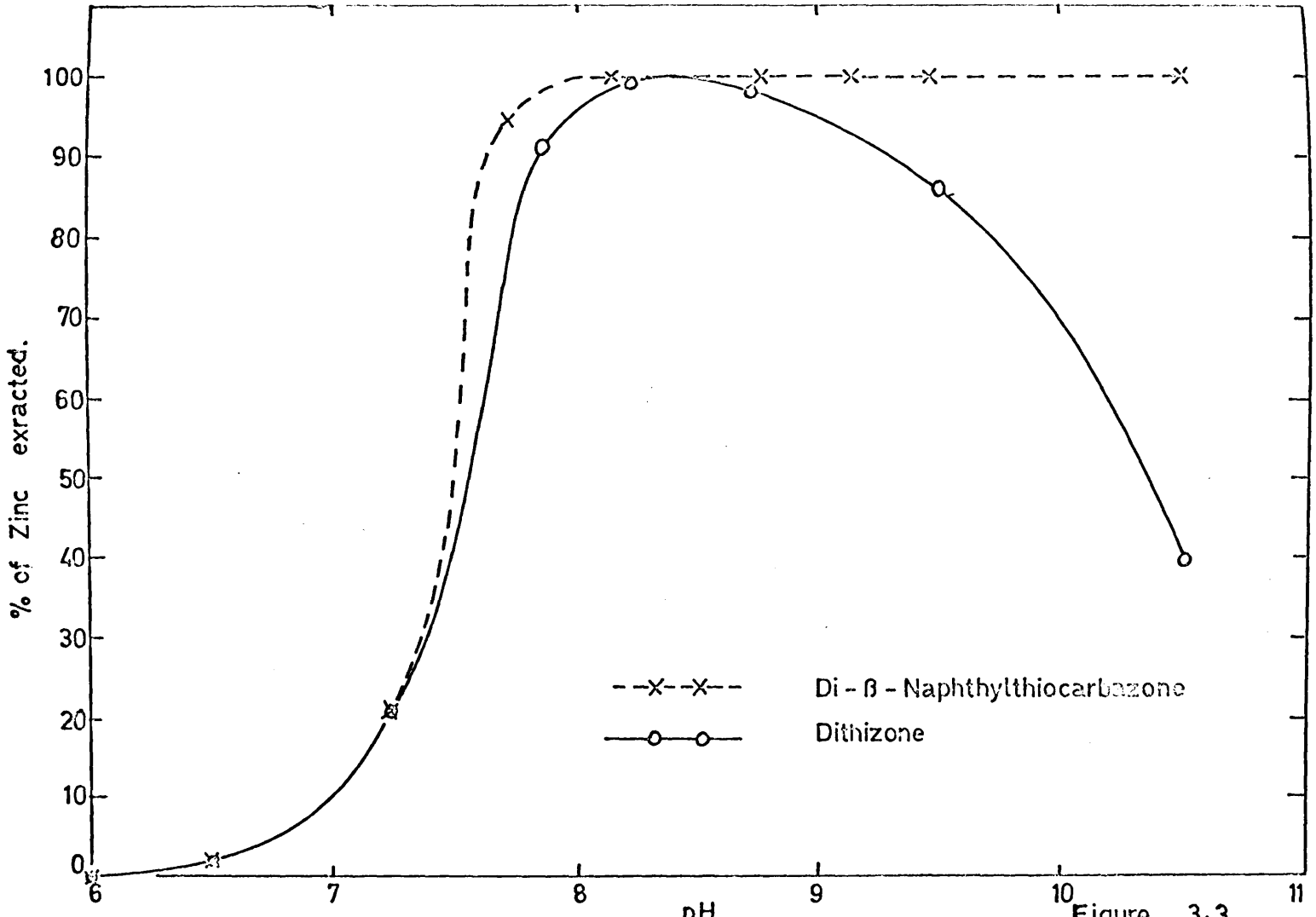

Figure 3·3.

Effect of pH on zinc partitions when Dithizone & Di-ß-Naphthylthiocarbazone extractions are made.

of zinc. This is very important in the present case, since even after the initial separation quite a large amount of copper (considering the amount of metals involved in solvent extraction) remains. So even after the addition of carbamate, some copper will probably accompany zinc into this penultimate stage. Fortunately the carbamate complexes of copper, nickel and cobalt which may enter the chloroform phase are insoluble in 0.2N Hcl acid, and therefore remain in the chloroform phase when the latter is treated with weak acid. In this way zinc can be finally separated from copper and other interfering metals produced by various photo-nucleon reactions.

The procedure for carrying out solvent extraction of zinc is breifly described below. This is essentially the same as that of CHOLAK et al.

The volume of the solution left after electrolysis was noted and placed in a 1000 ml. separatory funnel. To this were added 30 ml. of 20 per cent ammonium citrate solution, which acted as a buffer solution, and a few drops of aqueous thymol blue solution, which acted as pH indicator. Ammonium hydroxide solution was then added until the pH of the whole solution reached a value of 9 - 9.5. As could be seen from Fig. 3.3 this pH was not critical as long as it was from 8.3 to 10.5. A solution containing 50 mg. of sodium diethyldithiocarbamate was then added to this solution.

About 25 ml. of a strong solution of di-β-naphthylthiocarbazone in chloroform was then added to this solution and shaken vigorously

for a minute. This was then allowed to separate into the chloroform and aqueous layers. The colour obtained was faint violet which was indicative of the presence of metallic complexes. The chloroform layer was drained into a second separatory funnel. The aqueous layer was again shaken with another portion of di-β-naphthylthiocarbazone solution, the colour was noted, and the solution allowed to separate into two layers as before. The chloroform layer was again drained into the second separatory funnel. This was repeated until the di-β-naphthylthiocarbazone solution retained its original bluish green colour. This meant that zinc was extracted completely into the chloroform layer in the second separatory funnel. The colour was judged while shaking the solution, since the differences in colour were more readily discernible in the shaken mixture than in the small volume of the chloroform phase.

Di-β-naphthylthiocarbazone entrained in the aqueous phase was removed by shaking the latter with one or two 25 ml. portions of absolute chloroform, which were then added to the previously extracted chloroform phases in the second separatory funnel. In order to eliminate extraneous salts in the di-β-naphthylthiocarbazone extract, the collected chloroform extract was washed with about 100 ml. of deionized water. The chloroform layer was then drained into a third separatory funnel.

This washed chloroform solution was then shaken vigorously with 50 ml. of 0.2N Hcl acid and the phases were allowed to separate. After the two phases had completely separated, the chloroform phase

was discarded. Entrained di-β-naphthylthiocarbazone in the acid phase was removed by two successive washings with 25 ml. portions of absolute chloroform. The 0.2N Hcl. acid extract now contained all of the zinc free of copper, nickel, cobalt, iron, mercury, silver, aluminium, phosphates and sulphates.

The solutions mentioned in the procedure were prepared in the following manner:

(i) Di-β-naphthylthiocarbazone solution: About 600 - 700 mg. of di-β-naphthylthiocarbazone was dissolved in 1000 ml. of absolute chloroform containing 10 ml. of absolute ethyl alcohol. The solution was stored in brown bottles and was kept in the refrigerator when not in use.

(ii) Ammonium Citrate Solution: Four hundred gms. of citric acid was dissolved in water and sufficient ammonium hydroxide was added to make the solution just alkaline to thymol blue. The solution was made up to 1 litre (40 per cent) with de-ionized water. Before use the quantity required was measured out and equal volume of deionized water was added to make it 20 per cent.

Pyrex ware was used throughout.

Confirmation and Efficiency

A series of experiments was carried out to prove that after the entire chemical separation procedure (electrolysis + solvent extraction), the final extract was completely free of copper and that it also con-

tained the whole of zinc. In the first instance a known amount of radio-active Cu^{64} was added to the copper nitrate solution. The amount of Cu^{64} isotope chosen was such that the activity was a few times more than that of Cu^{64} produced in a copper target by exposure to a beam for about three hours. This figure was obtained from preliminary exposures. After the chemical separation no activity above background could be detected. This proved that the chemical separation technique described above got rid of all the copper. In the second case, a known amount of radio-active Zn^{65} was added to non-radioactive copper nitrate solution and the entire chemical separation procedure was carried out. By comparing the Zn^{65} activity before and after chemical separation it was found that 90 per cent of the zinc survived the chemical separation. The remaining 10 per cent was accounted for by the loss of electrolytic solution during electrolysis. The copper deposit was slightly porous in character and as a result a portion of the solution was trapped inside it. Although a part of this solution could be recovered by draining, it was decided unprofitable from a consideration of the time required. The solution lost in this way was found to be 10 per cent. From subsequent experiments it was established that for the same initial amount of electrolytic solution (360 cc) the loss was always close to 10 per cent. So the overall efficiency of the actual extraction of zinc was obtained by simply noting the volume of the electrolytic solution before and after electrolysis.

At this stage it was decided to put a copper target in the synchrotron beam. After an exposure lasting about 3 hours, the target was dissolved in HNO_3 acid and a chemical separation was carried out. The final 0.2 N HCl acid extract (50 cc. in volume) was placed in a 250 ml. conical flask and the activity was followed by means of the NaI(Tl) crystal. The activity clearly resolved itself into two components, one with a half life of 38 minutes and the other with 9 hours. These two activities could be at once attributed to Zn^{63} and Zn^{62} respectively. That the longer lived activity was entirely due to Zn^{62} and free from any Cu^{64} contamination was confirmed by means of successive electrolyses. In a single electrolysis the amount of copper left behind after the electrolysis was about 0.1% of the original amount. If now a solution of non-radioactive copper (of the same weight as that of the initial target) is added, and a second electrolysis is carried out, then the amount of radioactive copper left behind should be 0.0001% of the original amount. However, it was observed that the carrying out of one, two, or even three successive electrolyses made no difference to the ratio of short lived to long lived activities for the same exposure time. These experiments proved beyond doubt that the long-lived activity was indeed due to Zn^{62} (9.0 hr.) and was absolutely free from copper contamination.

During the initial period of development of the method of chemical separation, Cu^{64} and Zn^{65} isotopes produced in the East Kilbride reactor were used. The final separation technique was perfected by using samples activated in the synchrotron beam.

CHAPTER 4

EXPERIMENTAL PROCEDURE

GENERAL

Copper has two stable isotopes Cu^{63} and Cu^{65} of which Cu^{63} is more abundant (69.09%) than Cu^{65}(30.91%). A $(\gamma, \bar{\pi})$ type of reaction on these two isotopes results in Zn^{63} and Zn^{65} respectively. Zn^{65} has a very long half life (245 days) so that for a 2 - 3 hours exposure of natural copper the activity produced will not be detectable. A $(\gamma, \pi^- n)$ type of reaction on copper leads to Zn^{62} and Zn^{64}. Zn^{64} is stable. It then becomes clear that for a 2 - 3 hours exposure, reactions of the type $\gamma, \bar{\pi}$ and $\gamma, \pi^- n$ could be detected only on Cu^{63}.

PURITY OF THE TARGET

Throughout the whole experiment Analar grade natural copper was used. The copper was in the form of metallic sheets. Two different makes were used. The runs for the energy range 200 - 320 MeV were carried out with B.D.H. copper foil with a thickness of about 0.005". All low energy runs were carried out with H. and W. copper foil about 0.004" thick. In both cases the minimum purity quoted by the respective manufacturers was 99.9%. Detailed lists of maximum detectable impurities in these copper sheets were also supplied by the manufacturers which are tabulated in Appendix "A".

NEED FOR CHEMICAL SEPARATION

During the preliminary runs, a few foils of copper were

activated. The positron activity from these foils was followed for a couple of days. It was found impossible to assign any activity with half-lives of 38 minutes (Zn^{63}) and 9.0 hr. (Zn^{62}). The resulting decay curve was dominated by activities with half-lives of 9.9 minutes, 3.3 hr. and 12.8 hr. which were assigned to Cu^{62}, Cu^{61} and Cu^{64} respectively. This demonstrates the need for a highly effective chemical separation. The chemical separation technique has been discussed in detail in Chapter 3.

EXPERIMENTAL ARRANGEMENT

The actual target consisted of 30 or 38 circular copper discs (depending on whether they were 0.005" or 0.004" thick) +1 extra copper disc + 1 Zinc disc (0.004" thick) + 2 polythene discs ($\frac{1}{16}$" thick). All these discs were about 1.6 cm. in diameter and they were clamped together in a perspex box. There was a circular hole in the middle of the box so that the beam did not hit any other material before it passed through the target. The target was placed in the uncollimated beam in order to utilise maximum possible beam intensity. The position of the target is shown in Fig. 4.1. It was estimated from a separate "mozaic" experiment that the target in the position shown in Fig. 4.1 intercepted about 50% of the whole photon beam. In this experiment small pieces of zinc foil were formed into a "mozaic" and placed in the position of the target. The arrangement is shown in Fig. 4.2, where each foil is represented by a circle. The foils within the "dashed" circle occupied the same area as the target. After

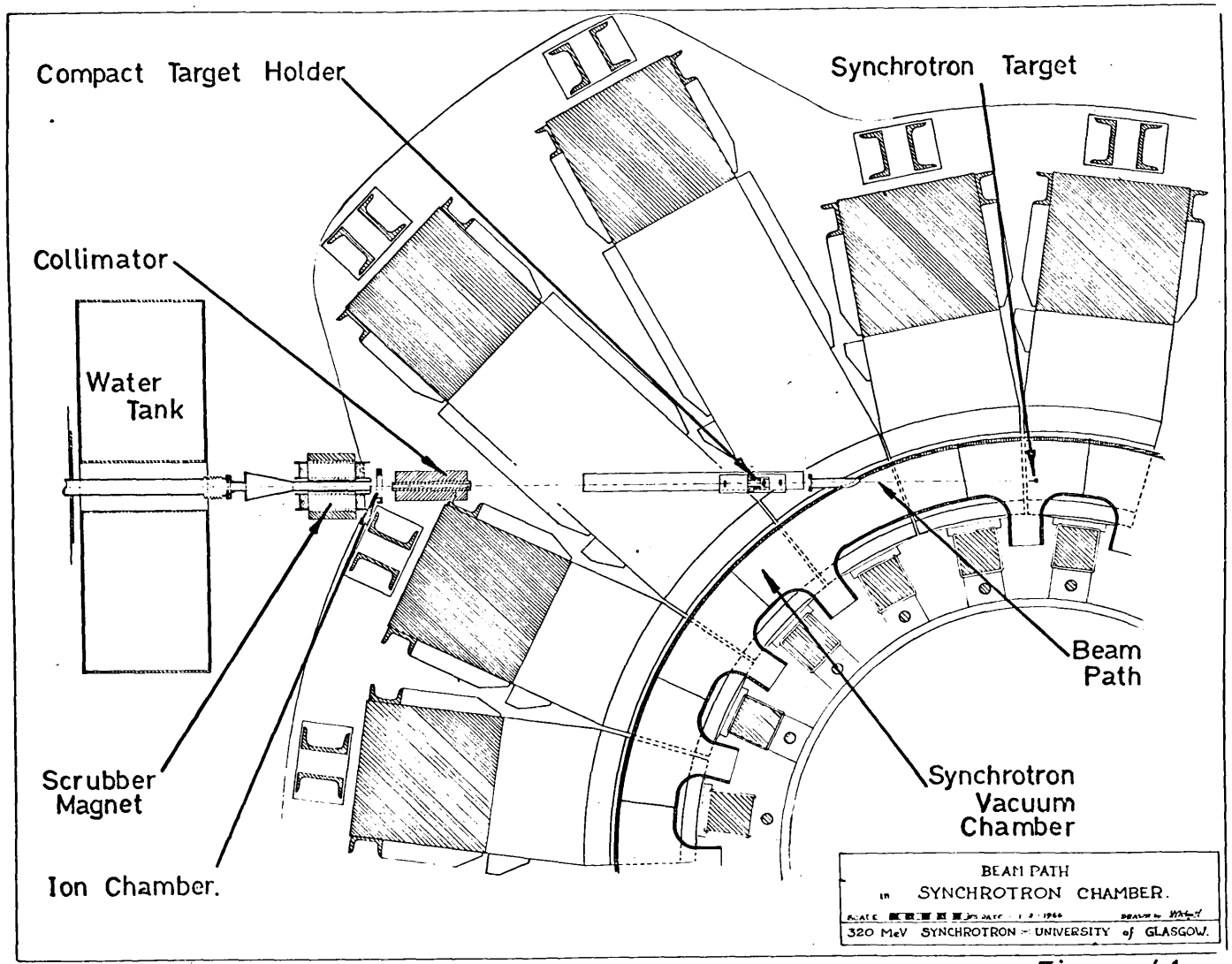
Compact Target Holder
Synchrotron Target
Collimator
Water Tank
Beam Path
Scrubber Magnet
Synchrotron Vacuum Chamber
Ion Chamber.
BEAM PATH
in
SYNCHROTRON CHAMBER.
320 MeV SYNCHROTRON - UNIVERSITY of GLASGOW.

Figure 4.1.

irradiation the activity produced in each foil was measured. Numbers on each component of the mozaic (Fig. 4.2) indicate relative activities corrected for decay. It was found that the total activity of the foils within the "dashed" circle was about 50% of the activity produced in all the foils. The "mozaic" also served to locate the centre of the beam. The number of copper discs was restricted to 30 or 38 because of chemical separation considerations. This number of discs usually amounted to 6.3 gms. of copper. From preliminary runs it was found difficult to electrolyze more than this amount of copper in a reasonably short time under optimum conditions.

The copper and zinc discs were sandwiched between the two polythene discs. These two polythene discs were used to find out if there was any significant loss in the beam intensity during its passage through the target and also as a beam monitor. It was found that within experimental error there was no loss in beam intensity. The zinc foil was specially used as a monitor for the reaction (γ, π^-) on Cu^{63}. The metallic zinc used was very pure (Appendix "A") and the reaction Zn^{64} (γ,n) Zn^{63} results in the same residual nucleus as Cu^{63} (γ, π^-) Zn^{63}. Since they are the same nuclei any variation in the beam intensity during the exposure will have no effect on the ratio of the production rates of source activity to that of the monitor activity. This explains why the choice of a reaction which results in the same nuclei as that from the reaction of interest as a monitor is so important. Moreover, since both the source and monitor products have the same

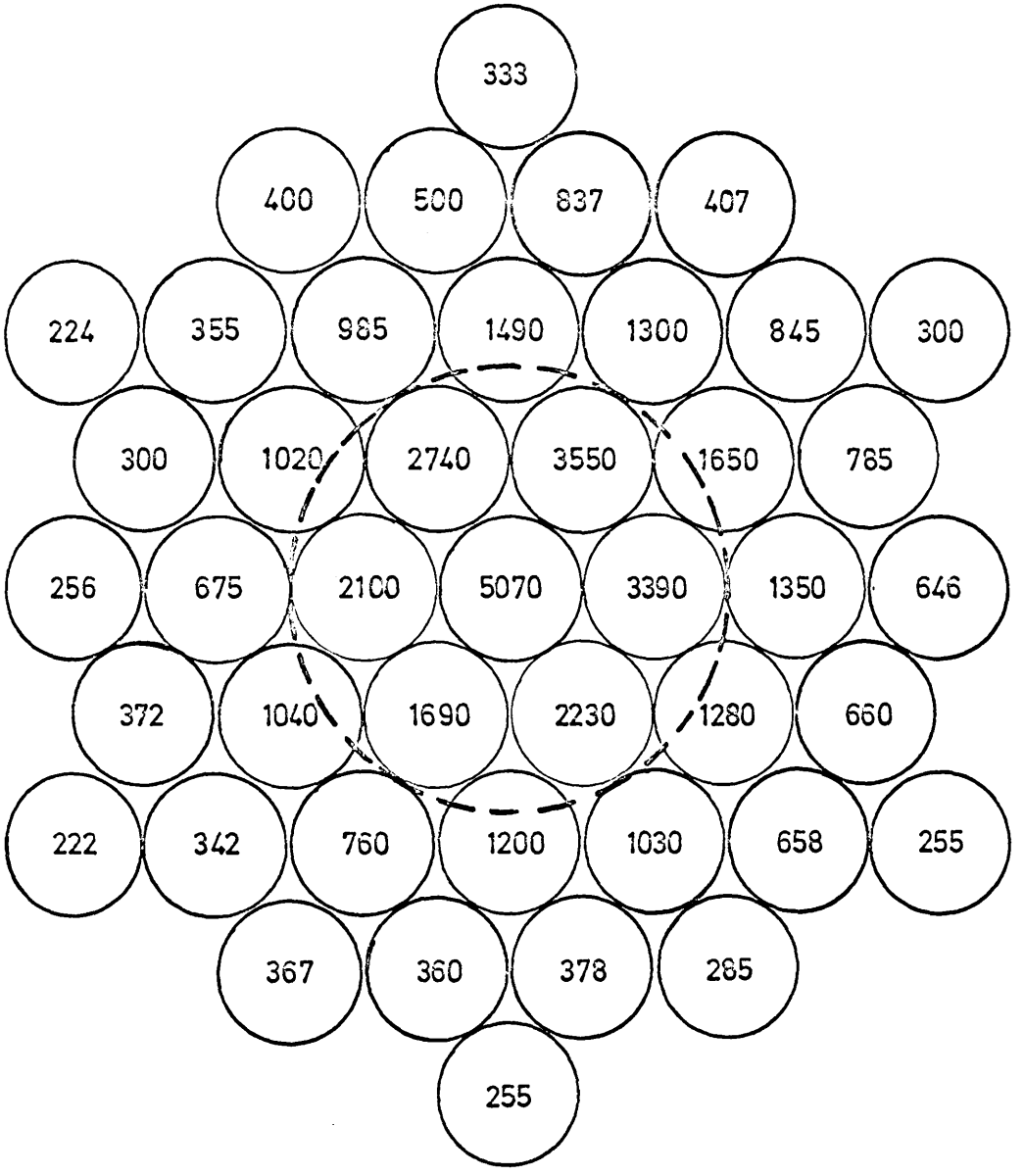

"MOZAIC" OF ZINC FOILS.

Figure 4.2

decay scheme, the determination of the efficiency of the counter for relative counting rates becomes very simple indeed. The one extra copper disc not subjected to subsequent chemical separation was activated to measure the activity resulting from (γ,n) and $(\gamma,2n)$ reactions on copper. A comparison can then be made of the magnitude of (γ,n) and (γ,π^-) reaction in the same target. $Cu^{65}(\gamma,n)\ Cu^{64}$ (12.8 hr. half-life) can also be used to monitor $Cu^{63}(\gamma,\pi^-n)\ Cu^{64}$ reaction. It has been pointed out earlier that the most suitable choice of monitor is a reaction which results in the same residual nuclei as that of the reaction of interest. However, if such a reaction is not available, the most obvious choice is a reaction of known cross-section which results in a residual nucleus with the same or similar half life. In that case the fluctuations in the beam intensity during the exposure will have no or very little effect on the relative production rates. During the exposure a continuous record was made of the beam intensity. The samples were activated for about 2 - 3 hours in a flux of approximately 10^{10} equivalent quanta per minute.

After exposure the copper discs were dissolved in a minimum amount of conc. HNO_3 acid. A complete chemical separation which results in the separation of zinc isotopes, was then carried out. After the chemical separation the 0.2N Hcl acid extract (50 cc.) was placed in a 250 cc. conical flask (pyrex), which was then placed on the NaI(Tl) crystal. The 0.511 Mev quanta resulting from positron annihilation was counted almost continuously for the first few hours and then intermittently over a period of two days. Zn^{63} decays by

90.4% positron emission straight to stable Cu^{63}. Zn^{62} decays by 18% positron emission and 82% electron capture to Cu^{62}. Cu^{62} in turn decays by 97.6% positron emission to stable Ni^{62} with a half life of 9.9 minutes. The observed activity of Zn^{62} will therefore consist primarily of the positrons from its daughter Cu^{62}. The resulting activity, surviving chemical separation, should therefore resolve itself into two activities with half-lives of 38 minutes and 9.0 hours. This is what was observed. Fig. 4.3 gives this decay curve for the activity resulting from a run at 320 Mev. That the activity is due to Zn isotopes only has already been demonstrated as described in Chapter 3, and no further confirmatory experiment was necessary. All the factors affecting the efficiency of chemical separation were noted. The time between the end of irradiation and start of counting was usually about one hour.

While the chemical separation was in progress the 0.511 Mev annihilation quanta from the polythene, copper and zinc discs were counted almost continuously one after another. The discs were placed between two copper plates of sufficient thickness to stop all positrons. After the initial period of almost continuous counting the discs were counted once an hour for the next few hours. Decays of copper and zinc activity were followed over a period of two days. The activities corresponding to different reactions were obtained by analyzing decay curves plotted from these observations.

Before these preliminary runs, a set of decay curves was con-

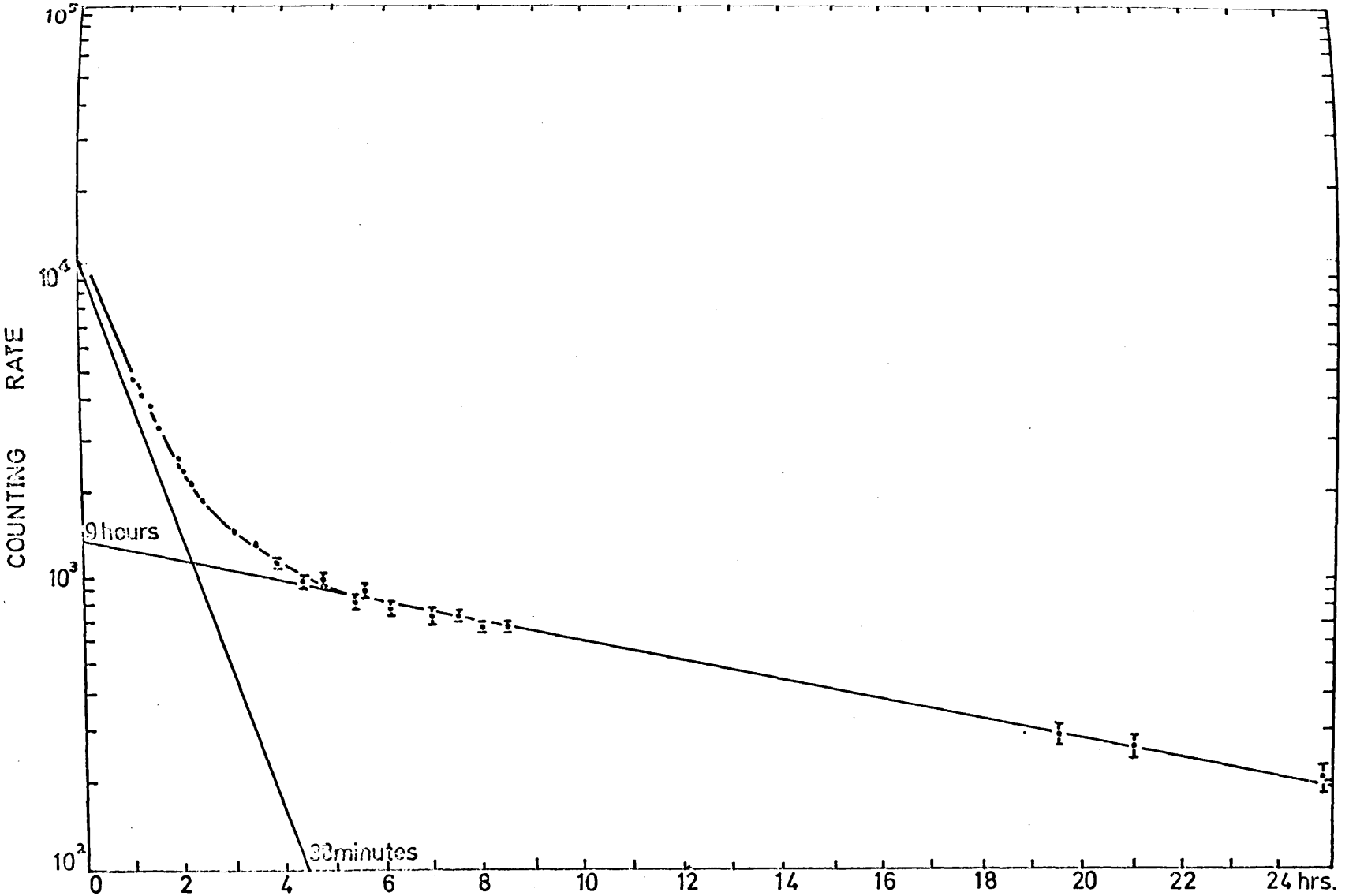

Figure 4·3.

320 MeV.

structed using appropriate half-lives. These proved to be very useful since the experimental decay curves could be plotted while the counting was still in progress and compared with the "constructed" curves from time to time to see if everything is moving in the right direction. This procedure also enables one to decide the best time for a count and when to stop counting.

After counting was over the activity present immediately after the end of irradiation was obtained from the decay curve by extrapolation of the resolved components. This was done both for the monitor and source activities. The relative efficiency of the different geometrical arrangements used when counting "source" and "monitor" activities was determined in an auxiliary experiment. Two weighed zinc foils were irradiated simultaneously. One of these was counted between copper discs under exactly the same conditions as the "monitor" foil. The other was dissolved in nitric acid in a conical flask. The volume was made up to the standard 50 cc. and counting was carried out under the same conditions as for the "source" activity. A factor for the relative efficiency of the two geometries was obtained by comparing the activities (referred to the same time). The ratio of production rates for the source reaction to the monitor reaction per atom was determined (method discussed in detail in Chapter 6). This ratio is referred to as the yield point at one particular energy of the bremsstrahlung beam.

The whole experiment was repeated for different end point

energies of the bremsstrahlung beam. In this way a set of yield points was obtained for different end point energies starting from 100 MeV to 320 MeV at intervals of 20 MeV. The resulting curve will be referred to as the "yield curve".

The ordinate of the "yield curve" exhibited in Fig. 4.4 is a measure of the rate of production of 38m. Zn^{63} in a copper target relative to that of the same isotope produced by the Zn^{64} (γ, n) Zn^{63} reaction in a Zn target when both are exposed to the same bremsstrahlung beam. It is proposed to calculate from this yield curve the cross-section for the reaction Cu^{63} (γ, π^-) Zn^{63} as a function of photon energy.

The threshold energy for pion production from a heavy nucleus is about 140 MeV and the sharply increasing relative yield from the copper target which commences at about this maximum photon energy may be assumed to be partly due to that reaction.

The yield of Zn^{63} from the copper target for photon energies below 140 MeV must be due to some other process taking place either in copper or an impurity. This same process is presumably responsible for part of the yield of Zn^{63} observed above the "meson threshold". It is clearly desirable that the nature of this interfering reaction be established and an assessment made of its contribution to the total yield of Zn^{63} at all energies. The "true yield" of the Cu^{63} (γ, π^-) Zn^{63} reaction of immediate interest may then be determined by subtraction, and calculation of the relevant

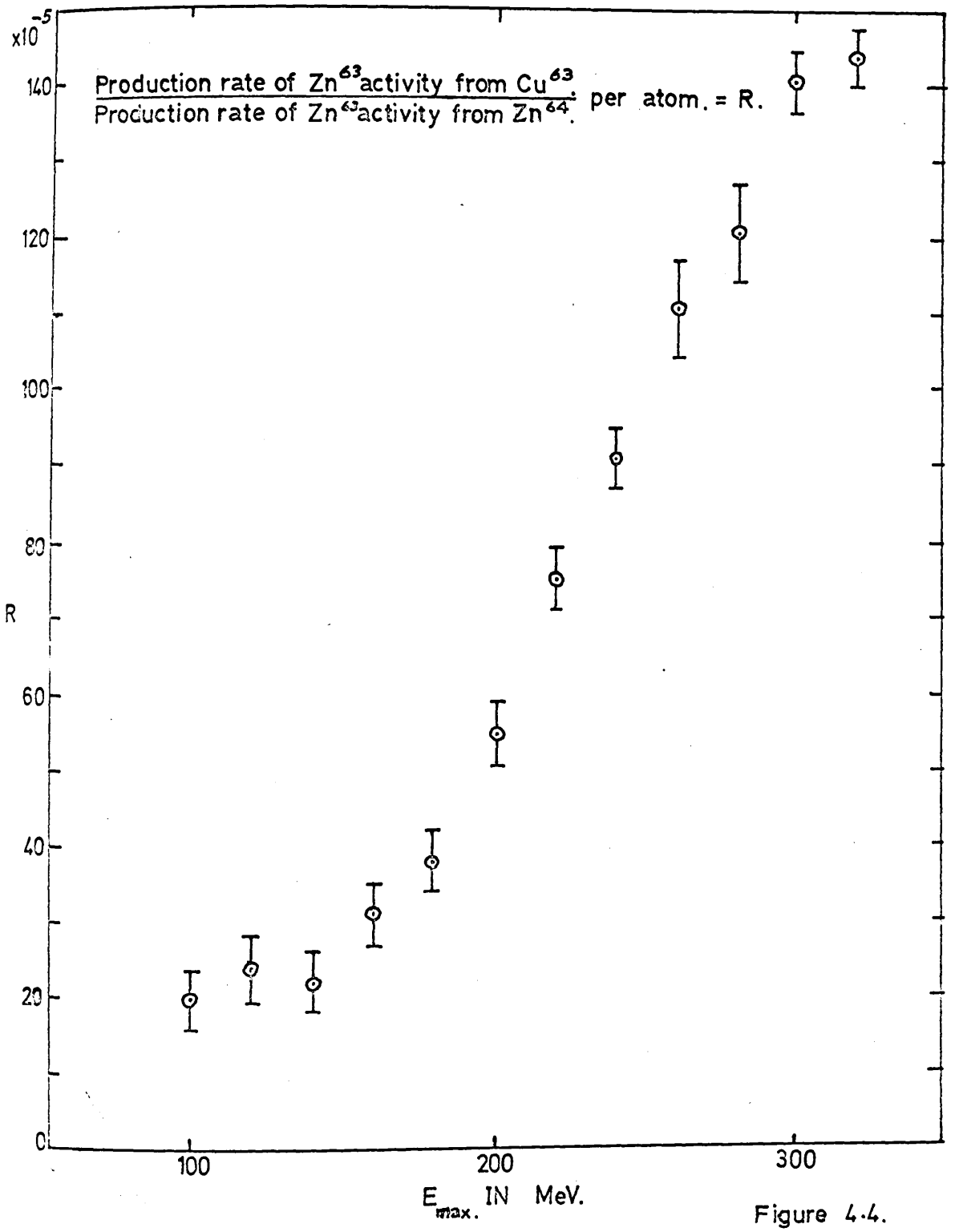
x10^-5
Production rate of Zn^63 activity from Cu^63 / Production rate of Zn^63 activity from Zn^64 per atom. = R.
140
120
100
80
R
60
40
20
0
100
200
300
E max. IN MeV.

Figure 4.4.

cross-section may proceed.

It will be noted that the required correction to the observed yield curve is quite large. If the contribution to the relative yield remained constant (an assumption which cannot be made if the nature of the interfering reaction is in doubt) it would amount to about 15% of the total yield of Zn^{63} even at the higher bremsstrahlung energies where it is probably least.

Similar considerations to those discussed above apply equally to the relative yield curve of Fig. 4.5 from which it is intended to calculate the cross-section for Cu^{63} $(\gamma, \pi^- n)$ Zn^{62}. There is evidently a competing process which produces Zn^{62} to an extent which varies from 100% to perhaps 10% at higher energies. Other workers who studied the γ, π^- reaction in different targets have also reported an "unexplained activity" below the photon threshold energy for meson production.

One of the reasons for undertaking the present research was the hope that a useful contribution might be made in this field by establishing the nature of the competing process. It was to this end that considerable effort was expended in devising an efficient chemical separation process and a sensitive detection system. Success in these directions has made it possible to state with confidence that the "extra" activities observed below the "meson threshold" in the present experiment were due to the same 38 m Zn^{63} and 9 h Zn^{62} as are produced by the photopion reactions under

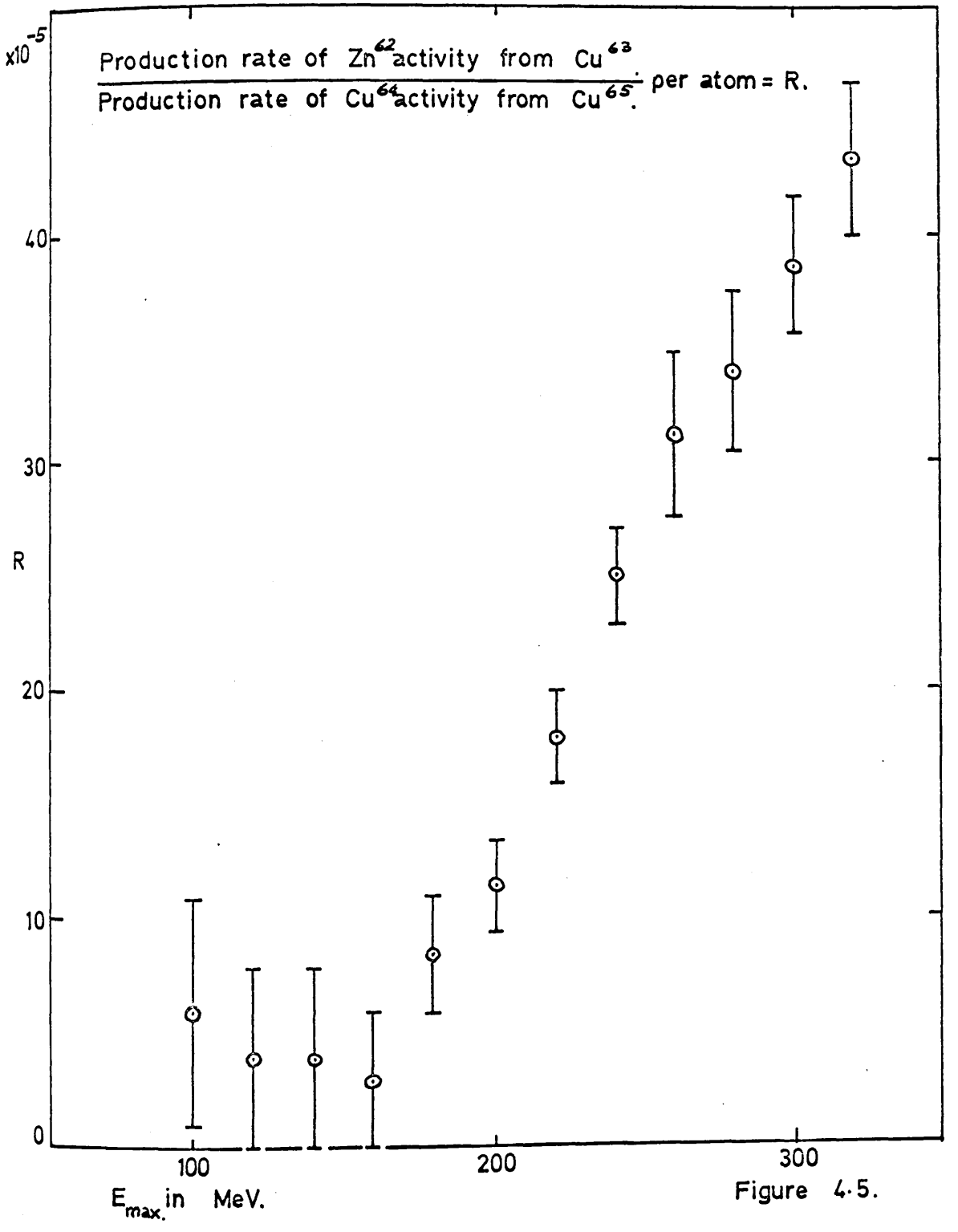
x10^-5
Production rate of Zn^62 activity from Cu^63 / Production rate of Cu^64 activity from Cu^65. per atom = R.
40
30
R
20
10
0
100
200
300
E_max. in MeV.

Figure 4·5.

investigation.

The results of earlier work are described in the following Chapter as an introduction to an account of further experiments designed to establish the source of the activity below threshold.

CHAPTER 5

ACTIVITY DUE TO REACTIONS OTHER THAN PHOTOPION REACTIONS

("THE ACTIVITY BELOW THRESHOLD")

INTRODUCTION

1.28

HUGHES and MARCH were the first to report an "activity below threshold" in their experiment on $B^{11}(\gamma,\pi^-)C^{11}$. The authors found this activity to be 75% of that at 320 Mev. This activity had the same half-life as that of C^{11}. They first considered the (γ,n) reaction on carbon impurity in the target. However, the percentage of carbon impurity in the boron sample would have to be at least 1.5% and the maximum percentage of this impurity was found by chemical analysis to be less than 0.3%. Nor could other impurities in the boron sample such as magnesium, aluminium, manganese, iron and oxygen be held responsible. Another possibility was the $B^{11}(p,n)C^{11}$ reaction. By using various thicknesses of Pb and copper shields, the authors were able to show that protons originating outside the sample were not responsible. Another possibility was the effect of protons produced inside the sample as a result of $B^{11}(\gamma,p)Be^{10}$ reaction. If the protons have a range greater than the thickness of the sample then the yield from the two stage process should vary approximately as the square of the sample thickness. The authors tried various thicknesses from 0.1 cm. to 1.0 cm. and found a linear variation of yield with thickness. This tends to suggest that the energy of the protons if responsible must be less than 6 Mev. For protons of this energy

according to the authors, the cross-sections for the (γ,p) and (p,n) reaction in the boron sample would be much too small to produce the observed activity. The only other possible source was a reaction of the type "$B(\gamma,e^-)C$", but such a reaction is not reported and is not expected to have a large cross-section. In order to explain the activity, the cross-section required should be of the order of 10^{-28} cm^2. So the activity remained unexplained.

MARCH and WALKER[1.31] reported a similar activity in their experiments on $Ni^{60}(\gamma,\pi^-)$ Cu^{60} which was about 25% of the activity at 320 MeV. They could not obtain an accurate determination of the half life of this activity as the counting rates at 140 MeV and 120 MeV were too low but it was comparable with that of Cu^{60}. Various explanations were offered including the presence of carbon impurity in the nickel sample, which chemical processing failed to remove and the two stage reaction mentioned earlier, but no definite conclusion was reached.

More recently, DYAL and HUMMEL[1.32] repeated the experiment of HUGHES and MARCH on boron with the intention of identifying the activity produced below the meson threshold. By using elemental boron, decaborane and repurified decaborane samples and noting the variation in the magnitude of this activity from sample to sample, they indicated carbon impurity as a major source of this activity in boron. Their estimates for the amount of carbon impurity that must be present to account for such activity were compatible with that

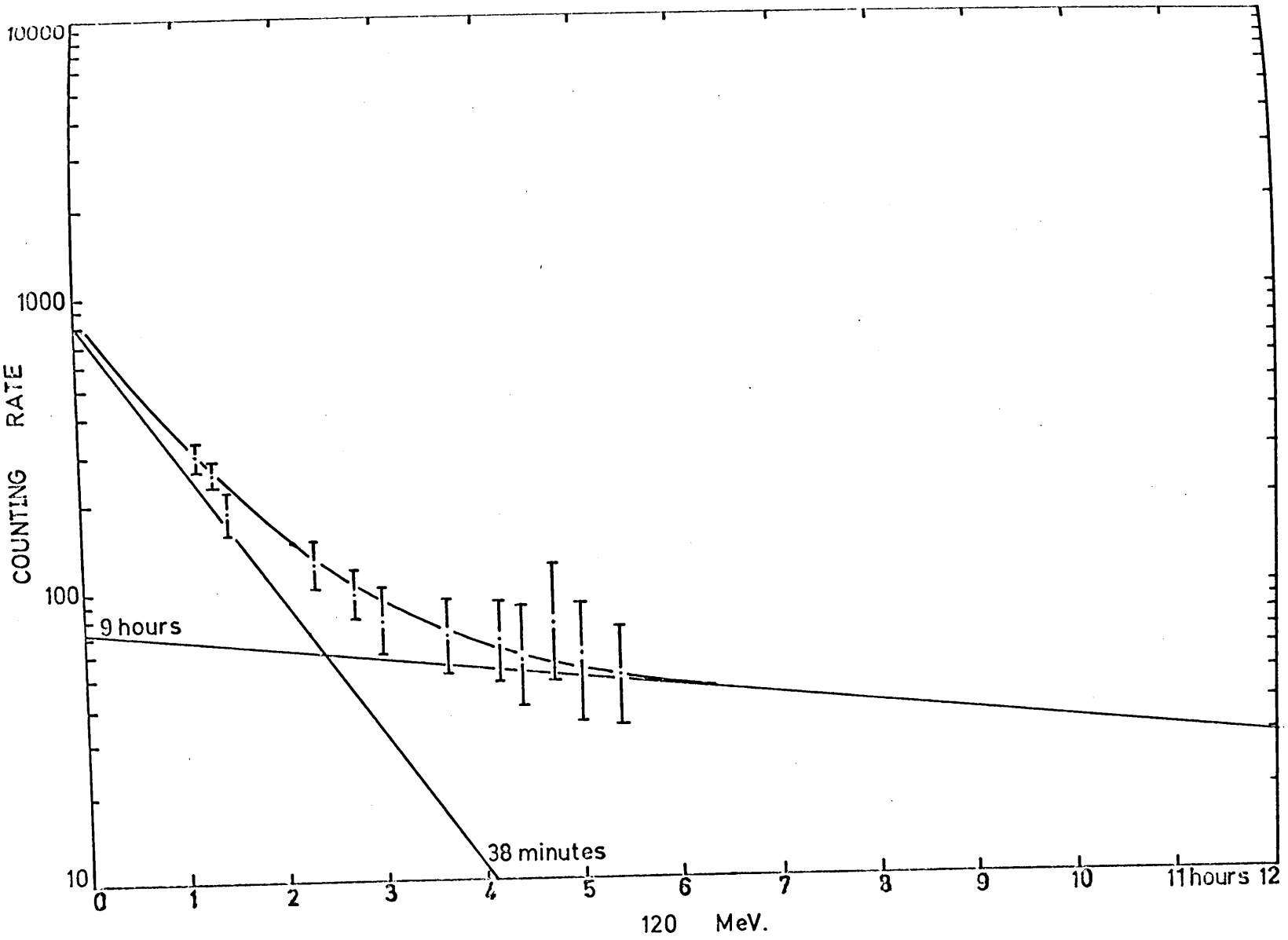
10000
1000
100
10
COUNTING RATE
9 hours
38 minutes
0
1
2
3
4
5
6
7
8
9
10
11 hours 12
120 MeV.

Figure 5·1.

possible in the decaborane samples, but the impurity required in the elemental boron sample was found to be much higher than indicated by chemical analysis. The authors did not rule out a possible contribution from two stage reactions. Their estimation for the possible contribution from this source ranged from 5- 50% for the repurified decaborane sample. Due to practical difficulties no further experiment was carried out from which a definite conclusion could be reached.

Present Experiment

As remarked above, it was considered virtually certain that the activities observed in the zinc separated from a copper target were in fact due to 38 m Zn^{63} and 9 h Zn^{62} both above and below the meson threshold. Fig. 5.1 shows the decay curve for the zinc extracted from a target exposed to a 120 MeV bremsstrahlung beam. Although weak, the activity was sufficient to allow a resonably accurate determination of the half-lives of the two components. These corresponded well with the known half lives of Zn^{63} and Zn^{62}. Fig. 5.1 may be compared with Fig. 4.3 of Chapter 4, the decay curve for a 320 MeV exposure. It seems clear that the same isotopes are responsible for the activity in each case.

The next step is to consider the reactions on a copper target that will result in these two isotopes. They are:

(1) (γ,π^-) and (γ,π^-n) reaction on Cu^{63},

(1a) (γ,π^-2n) and (γ,π^-3n) reactions on Cu^{65}.

(2) (γ,n) and $(\gamma,2n)$ reactions on zinc impurity in the copper sample,

(3) (p,n) and $(p,2n)$ reactions on Cu^{63} due to protons originating outside the sample,

(4) (γ,e^-) and (γ,e^-n) reactions on Cu^{63},

(5) (p,n) and $(p,2n)$ reactions on Cu^{63} due to protons originating in the sample.

Of these possibilities, no. (1) is not energetically possible. A detailed investigation has been made by HUGHES and MARCH of the possibility of no. (3) as the source of this activity. This was rejected. The possibility of no. (4) was also discarded. So the only two likely possibilities are no. (2) and no. (3).

It was mentioned in Chapter 4 that metallic zinc was used to monitor the beam. This served another useful purpose, since it enabled a direct estimate to be made of the amount of zinc impurity that must be present in the copper sample to account for the observed activity below threshold. Since the zinc monitor, the copper sample and the zinc impurity in the sample, if any, were irradiated simultaneously, the necessity for strict beam control was avoided. From the three runs at 100, 120 and 140 MeV it could be estimated that there must be a 0.03% zinc impurity in the copper sample if the activity below threshold were to be ascribed to this cause. However, the runs at this energy were carried out using copper foils with the analysis of Table II. The table does not mention

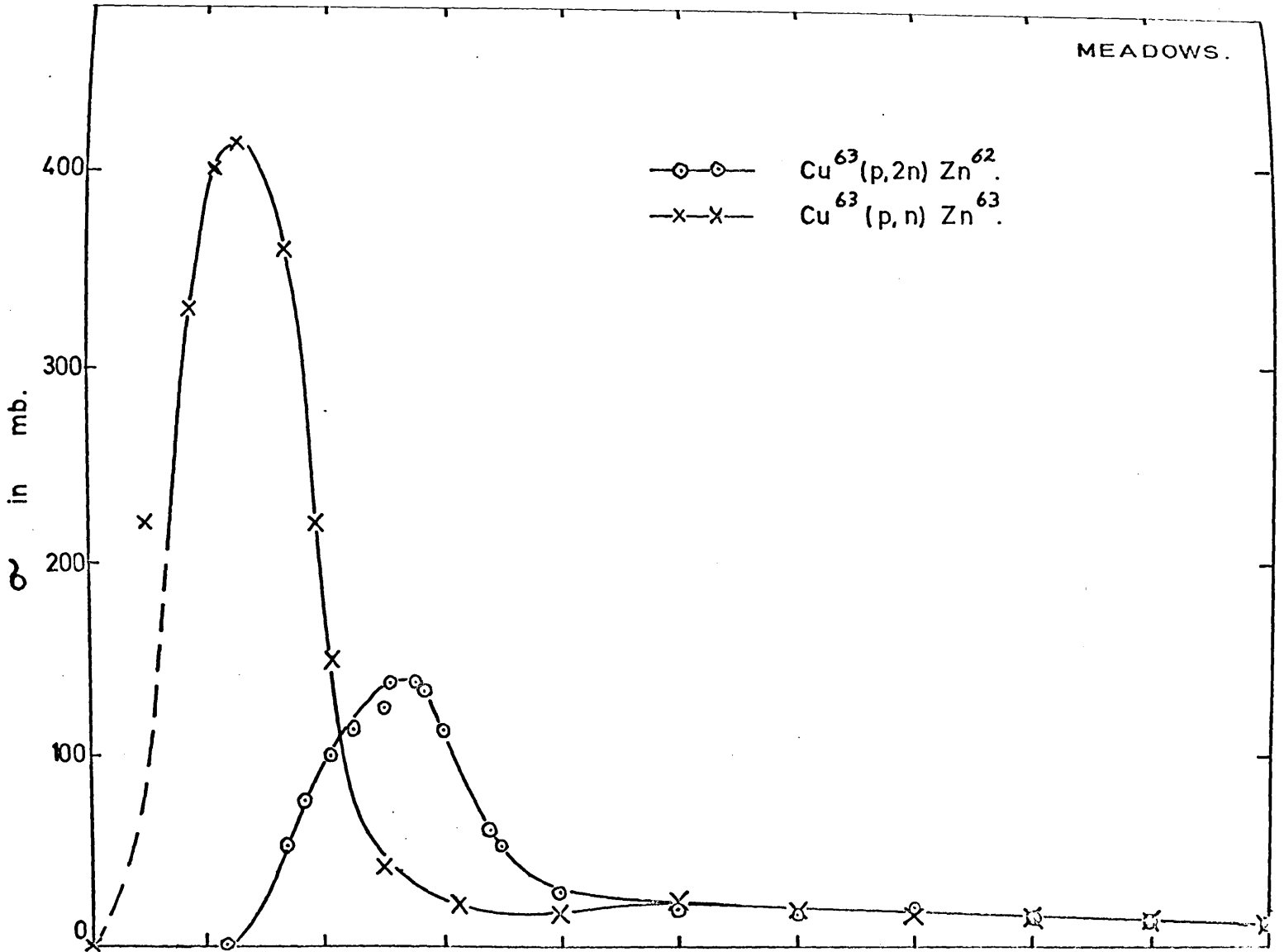

Zn^{62} and Zn^{63} from Cu^{63}.

Figure 5·2.

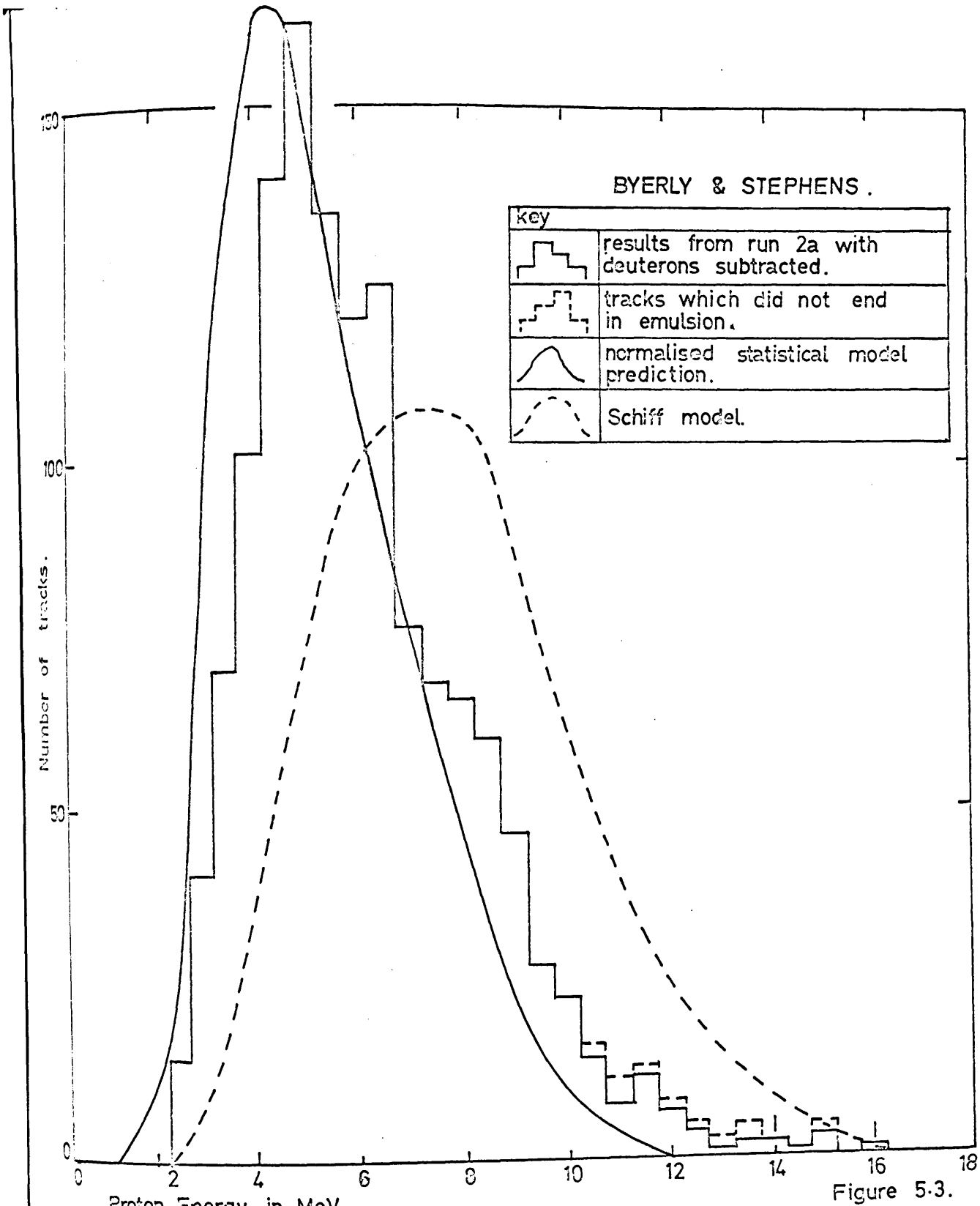

Figure 5.3.
Energy distribution of the Photoprotons.

zinc impurity at all from which it can be assumed that the zinc impurity in this sample is less than the minimum detectable 0.00001%. The possibility that the activity is produced in zinc impurity in the copper sample may therefore be discarded.

The only remaining possibilities are (p,n) and (p,2n) reactions due to protons produced inside the copper sample as a result of photo-disintegration. The protons responsible for these reactions, especially for the (p,n) reaction are probably low energy protons. Fig. 5.2 shows the cross-section for (p,n) and (p,2n) reactions on Cu^{63} (MEADOWS[5.1]) as a function of proton energy. In order to determine whether these (p,n) and (p,2n) reactions are responsible for the interfering activity, it is necessary to decide whether sufficient protons with appropriate energies might be produced in the target by (γ,p) processes. Unfortunately the distribution of proton energies from copper produced by high energy bremsstrahlung is not known. BYERLY and STEPHENS[5.2] have given the distribution of proton energies from a copper target exposed to 24 Mev bremsstrahlung (Fig. 5.3). It must be remembered at this point that the bremsstrahlung spectrum contains a continuous distribution of photon energies from zero to a maximum energy determined by the maximum energy of the electrons hitting the target. The shape of the spectrum for a given electron energy varies roughly as E_γ^{-1}, thus, there is a much larger number of low energy photons in the beam than of high energy photons. It seems possible therefore that (p,n) and (p,2n)

reactions are produced in a copper target mainly by low energy protons (10 Mev) produced by the low energy photons predominant in a bremsstrahlung beam. Such photoprotons would have a short range in copper (200 mg/cm^2) and would not escape except from a very thin target. The yield of the secondary (p,n) reaction would therefore be expected to vary linearly with the target thicknesses commonly used.

BONNER et al[5.3] faced problems similar to those encountered during the present work while investigating whether the photoproduction of mesons (μ) by x-rays was energetically possible at 100 Mev. At that time the mass of the meson was not accurately known. They found an activity at 100 Mev which could be interpreted either as due to meson production or a two stage process similar to that discussed above. By careful and detailed investigation, they concluded that the activity was in fact due to the two stage process. The authors carried out their investigation on two target samples, namely copper and aluminium. The target used in the present experiment was also copper, so that much of the author's argument is applicable. The actual experimental arrangement described in this Chapter is similar in principle to that of BONNER at al.

It can be shown from a consideration of cross-sections for (γ,p) and (p,n) reactions in copper-63 and the range of protons with the energy of interest that the ratio of the yield of this two stage reaction to that of the (γ,n) reaction on Cu^{63} should be of the order

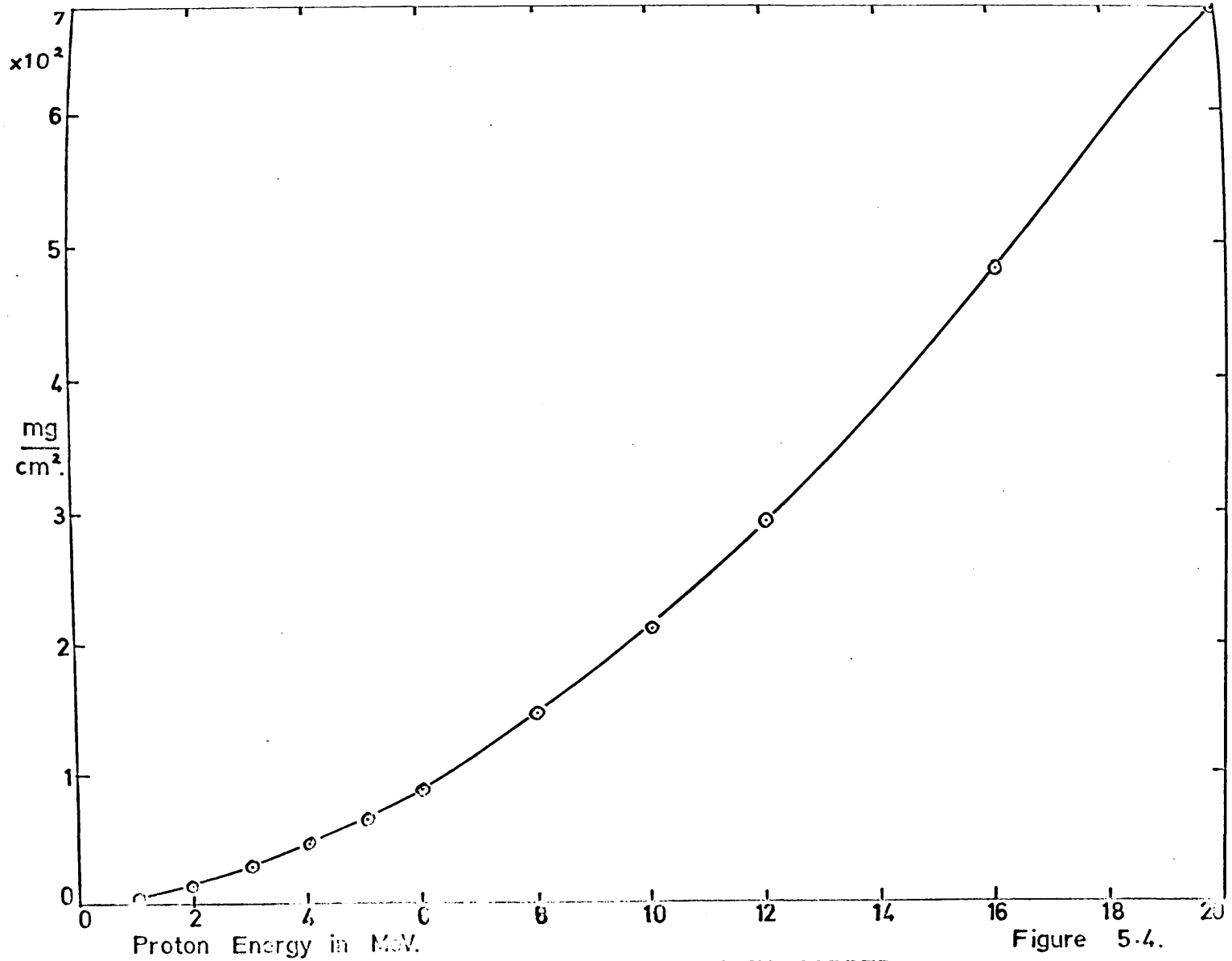

Figure 5.4.

RANGE OF PROTONS IN COPPER.

of 10^{-3} to 10^{-4}. Accordingly the production rate of Zn^{63} from the copper target was compared with that of Cu^{62} (obtained from one extra copper disc) for each of the three energies - 100, 120 and 140 MeV. They varied from 1.5 - 2 x 10^{-4}. This lends additional support to the hypothesis that the activity below threshold is due to the two stage process. However, until this can be confirmed experimentally, the doubt as to other possibilities will remain. The experiment described below is designed to prove the existence of the two stage reaction.

The targets at low energy usually consisted of about 38, 0.004" thick copper discs squashed together. The total thickness of the target was about 3.5 gm/cm^2. Even a single disc has a thickness of 90 mg/cm^2. From Fig. 5.4 it becomes clear that the proportion of protons of 6-7 Mev energy (typical of the energy of a proton resulting from the (γ,p) reaction and perhaps responsible for a subsequent (p,n) reaction) escaping from this disc and hitting the next or previous one is very small indeed. Hence if one carries out an experiment using different thickness of target constructed from .004" foil, the variation of induced activity would be expected to vary linearly with target thickness rather than quadratically. This point was checked by using a target containing 60 discs squashed together. Chemical separations were carried out separately on the two halves (30 discs) of the target. The activities were found to be same within experimental error.

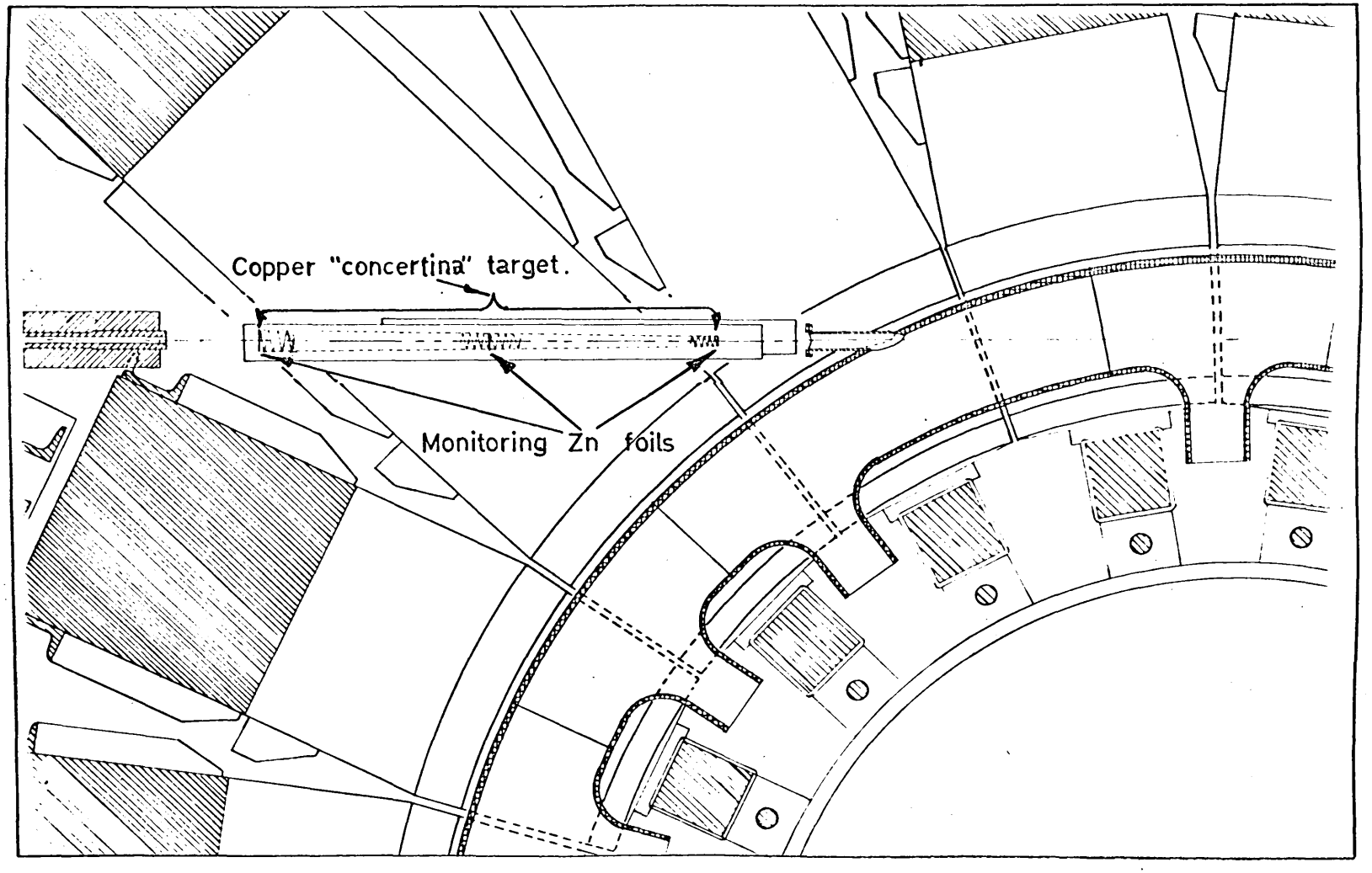

Figure 5·5.

The contribution of the two stage process could be reduced by using copper foil sufficiently thin to allow the escape of low energy protons produced within it. However, the activity produced in a single foil would not be detectable and it was therefore decided to use a large number of thin foils amounting to the same total thickness as the previous thick target. These were distributed in such a way that a large proportion of the protons produced in any one foil would miss the next or previous foil. A few runs were carried out with these thin foils, squashed together to form a thick target to make sure that theyproduced the same results as the previous targets when used under the same conditions. This was found to be true.

The thin foils mentioned above were 0.0005" thick. One of the problems faced was the design of a system by which they could be distributed along the beam while introducing as little other material as possible in the path of the beam. It is also necessary that all the copper foils should subtend the same angle at the synchrotron target so that each foil is traversed by the same beam. This angle was arranged to be the same as was previously used with the thick target. The foils must therefore be arranged along the beam with successively increasing diameters. After some preliminary experiments on this problem it was decided to arrange the foils "concertina" fashion, threaded on a thin central copper wire. The copper wire was adjusted along the axis of the beam. The "concertina" of 100

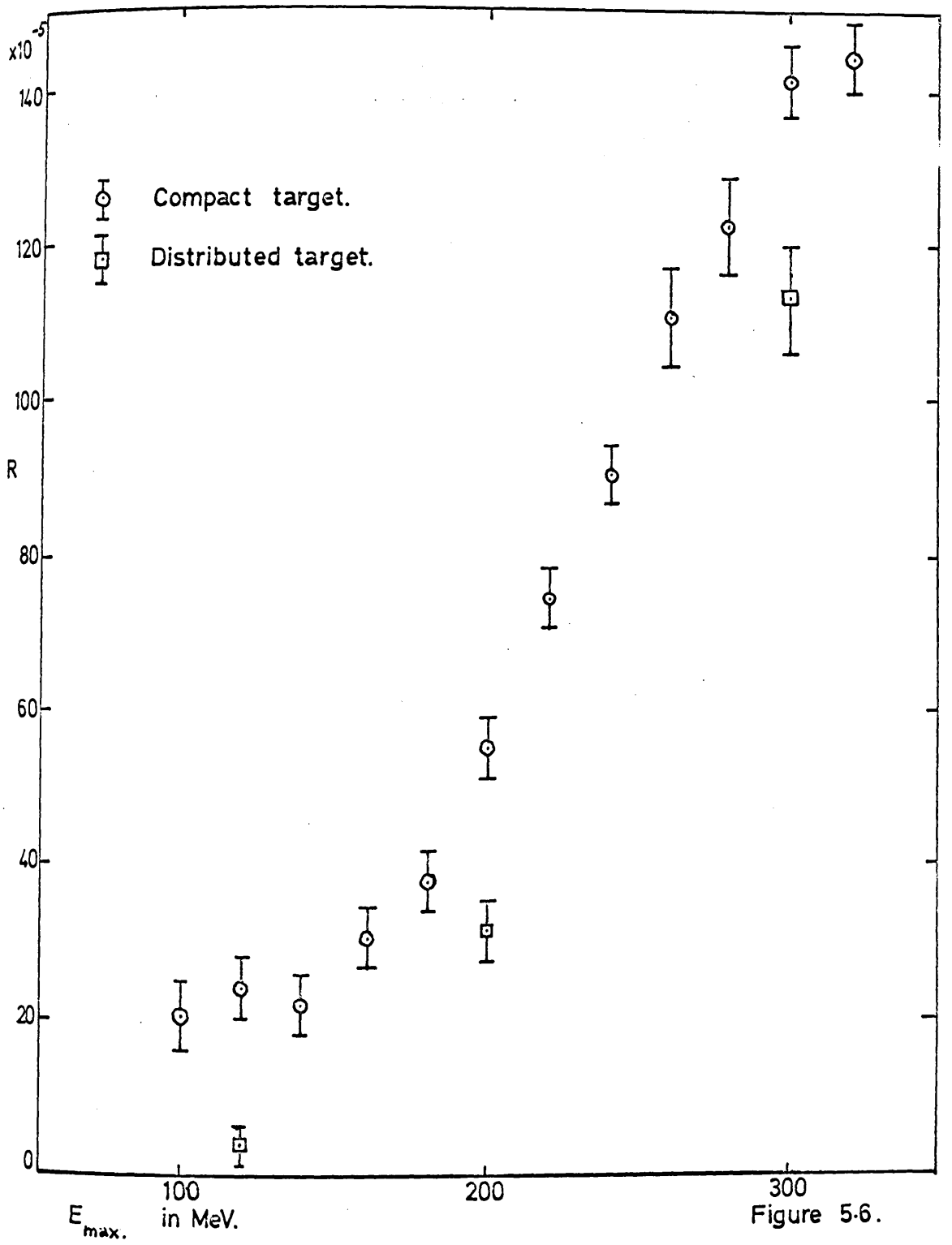
x10^-5
140
120
100
80
60
40
20
0
R
Compact target.
Distributed target.
100
200
300
E max.
in MeV.

Figure 5·6.

foils was spread uniformly over a distance of 70 cms so that the effective separation between two foils was about 0.7 cm. Three separate zinc foils, with appropriately increasing diameters, were placed in the beam along with the copper foils. One was placed in the front, one in the middle and the other at the rear of the copper foils. These served to check the alignment of the copper foils and to monitor the beam. Fig. 5.5 gives a schematic diagram of the foil arrangement. A rough calculation shows that if the activity produced below threshold is due to a two stage reaction, then the activity produced in the copper foils arranged as described above should be down by a factor of five or six as compared with the activity produced in a single target of the same thickness.

The experiment was performed at three different energies - 120, 200 and 300 MeV and the results are shown in Figs. 5.6 and 5.7. In the case of the 38 m Zn the "relative yield" at 120 MeV is down by a factor of six. This proves beyond doubt that the activity is indeed due to the two stage process mentioned above. The results at 120, 200 and 300 MeV show that the contribution of the two stage process is approximately constant throughout the energy range of the experiment. This would be expected since both the (γ,n) reaction in the monitor and the (γ,p) reaction which initiates the two stage process, are produced by the low energy component of the bremsstrahlung beam. One may therefore confidently subtract a constant activity from the yield curves of Fig. 4.4 and 4.5 to obtain corrected yield curves from which the cross-sections for $\gamma,\bar{\pi}$ and $\gamma,\bar{\pi}n$ may be calculated.

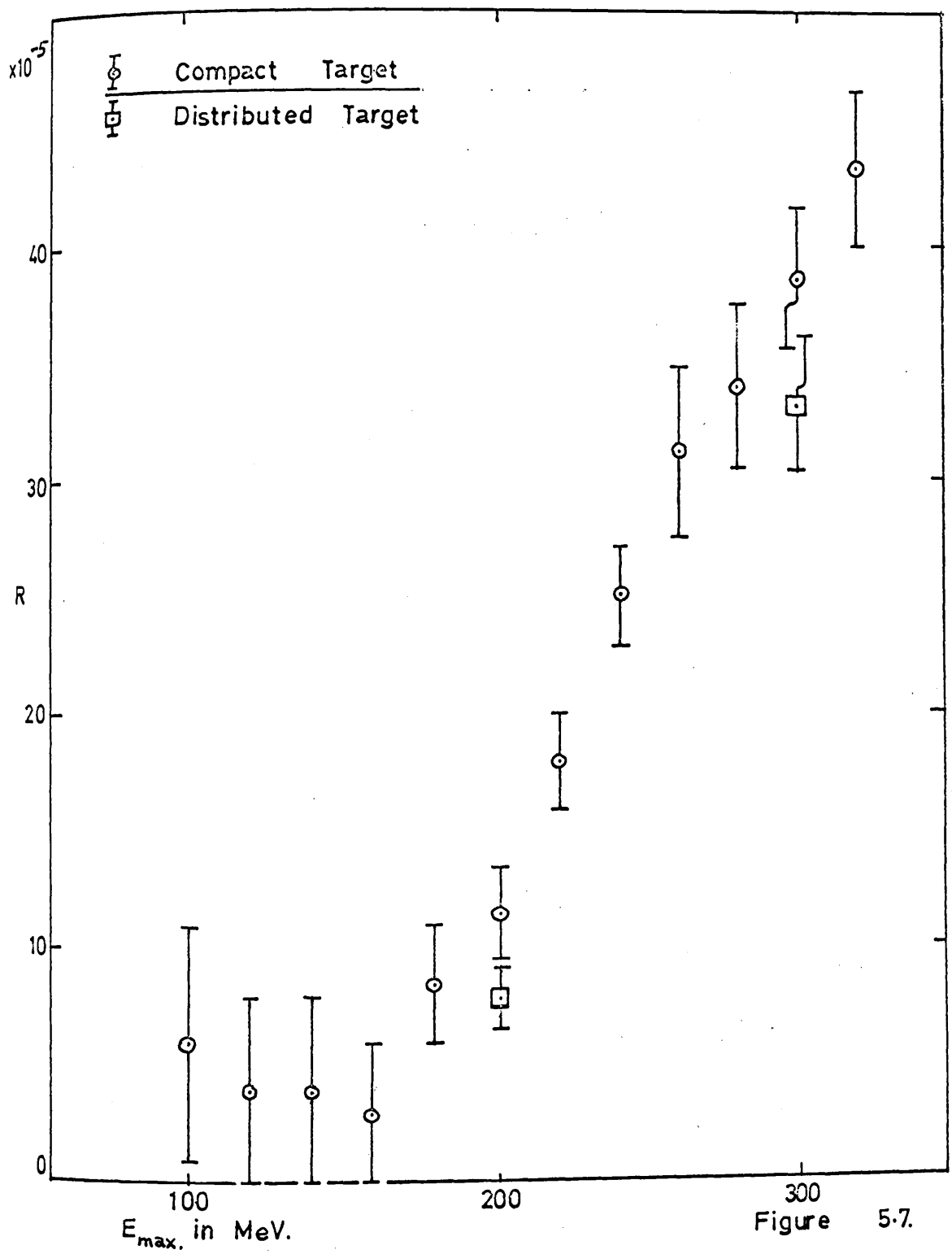
x10^-5
Compact Target
Distributed Target
40
30
R
20
10
0
100
200
300
E max. in MeV.

Figure 5.7.

CHAPTER 6

CROSS SECTION ANALYSIS

The experimental procedure described in the previous chapter involved the use of bremsstrahlung beam from the 320 MeV Glasgow University Electron Synchrotron. Such radiation contains photons of all energies from zero up to the kinetic energy of the initiating electrons. So the desired cross-section must be deduced from an integral (bremsstrahlung) yield curve. Two techniques of analysis used previously were (1) The total spectrum method[6.1], (2) The photon difference method[6.2]. What appears to be a simpler and more accurate method has been described by PENFOLD and LEISS.[6.3] In this chapter, the method of PENFOLD and LEISS, is described in some detail.

Let a sample of a certain material and a suitable monitor with the same area be simultaneously irradiated in the bremsstrahlung beam from an electron accelerator operating at an energy χ. The number of photoreactions of a special type which occur in an arbitrary time divided by the corresponding response of the monitor gives one point on the bremsstrahlung yield curve for the reaction in question. Other points are obtained by repeating the measurement at different values of χ. Eact point is a measurement of the relative response of the sample and monitor to the photon beam. Hence, if the response of the monitor is known, the cross-section for the reaction can be deduced.

The rate of production G_s of (radioactive atoms in the sample

is given by

$$G_s = S\, n_s \int_0^{\chi} \frac{\bar{\phi}(\chi,K)}{K}\, \sigma_s(K)\, dK \quad \ldots\ (1)$$

where:-

S is a constant which contains a factor for the electron beam intensity of the synchrotron and a factor for the proportion of the beam intercepted by the sample

n_s is the relevant number of atoms in the sample and σ_s is the cross-section for the reaction under investigation.

$\frac{\bar{\phi}(\chi,K)}{K}$ is proportional to the cross-section per unit energy interval for the production of photons of energy K by electrons of energy χ. $\frac{\bar{\phi}(\chi,K)}{K}$ is written in this form to make explicit the dominant $\frac{1}{K}$ dependence of the bremsstrahlung. $\bar{\phi}(\chi,K)$ is therefore a function proportional to the intensity spectrum. It varies rather slowly over most of the energy range 0 to χ and falls rapidly to zero near $K = \chi$.

In order to work directly with the convenient function $\bar{\phi}(\chi,K)$ (1) may be rewritten

$$G_s = S\, n_s \int_0^{\chi} \bar{\phi}(\chi,K)\, \Omega_s(K)\, dK \quad \ldots\ (2)$$

where $\Omega_s(K) = \frac{\sigma_s(K)}{K}$ ...(2a) is defined as the "reduced cross-section" for the reaction. A solution is now sought for $\Omega_s(K)$ (from which $\sigma_s(K)$ is easily recovered).

With the same notation, the rate of production of radioactive atoms in the monitor is given by

$$G_m = S\, n_m \int_0^{\chi} \tilde{\phi}\,(\chi,K)\,\Omega_m\,(K)\,dK \quad \ldots\ (3)$$

(with the same "S", absorption of the beam is neglected).

We now define a "reduced yield" $Y\,(\chi)$ given by

$$Y\,(\chi) = \int_0^{\chi} \tilde{\phi}\,(\chi,K)\,\Omega(K)\,dK \quad \ldots\ (4)$$

From (2) and (3) we have

$$Y(\chi) = \frac{G_s}{n_s} \Big/ \frac{G_m}{n_m} \int_0^{\chi} \tilde{\phi}\,(\chi,K)\,\Omega_m\,(K)\,dK \quad \ldots\ (5)$$

$\frac{G_s}{n_s} \Big/ \frac{G_m}{n_m}$ is the "yield point" which is to be calculated from the experimental observations. The expression under the integral sign can be calculated from known values of $\tilde{\phi}\,(\chi,K)$ and σ_m.

From the law of radio-active decay G_s may be expressed in terms of the activity A_s (disintegrations per second) produced in the sample by the reaction under investigation after exposure for time t_o to the synchrotron beam.

$$G_s = A_s/(1 - e^{-\lambda_s t_o}) \quad \ldots\ (6)$$

where λ_s is the decay constant for the radioactive isotope produced. G_m may be expressed similarly.

From (5) and (6) we have

$$Y\,(\chi) = \left(\frac{A_s}{n_s} \Big/ \frac{A_m}{n_m}\right) \left(\frac{1 - e^{-\lambda_m t_o}}{1 - e^{-\lambda_s t_o}}\right) \int_0^{\chi} \tilde{\phi}\,(\chi,K)\,\Omega_m\,(K)\,dK \quad \ldots\ (7)$$

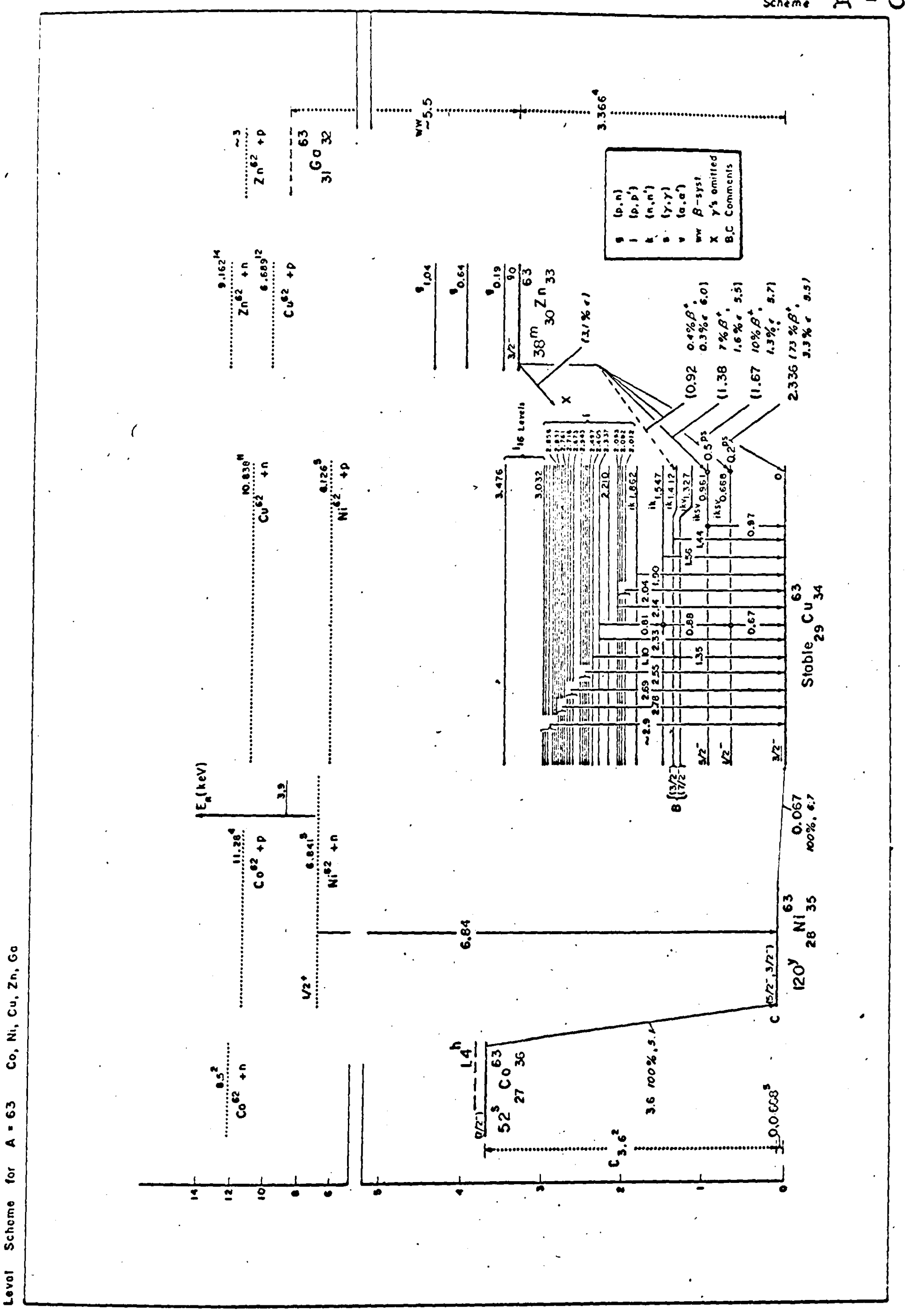

NRC 60-5-58 replacement

Figure 6.1.

The term $(1 - e^{-\lambda_m t_o})/(1 - e^{-\lambda_s t_o})$ is unity when $\lambda_m = \lambda_s$ i.e. if source and monitor reactions result in the same nuclide. In this case the relative activities of source and monitor are independent of variations of beam intensity and the time of irradiation. If $\lambda_m \neq \lambda_s$, this term must be calculated. Calculation of the corresponding factor for a varying beam intensity is very tedious.

n_s and n_m were calculated from the weights of the sample and monitor and the isotopic abundances of the relevant isotopes.

A_s, A_m were obtained from the decay curves plotted from the counting rates of the NaI detector using a channel just wide enough to include the photopeak of 0.511 MeV annihilation quanta. After subtracting background, the decay curves were analysed and the components extrapolated back to t_o. A_s, A_m were calculated from the hypothetical counting rates at t_o using the decay schemes published in the NUCLEAR DATA SHEETS [6.4] (Figs. 6.1 and 6.2). In the case of Zn^{62} for example, there is a γ-ray apart from annihilation radiation which falls in the counting channel and the daughter Cu^{62} makes a contribution to the positron activity. Correction was also made for the different efficiencies of the detector when counting the sample (as liquid) and the monitor (as foil). The experimental determination of the relative efficiencies was described in Chapter 4.

"Yield points" G_s/G_m were calculated for the 38 m Zn^{63} and

NNC 60-5-51 replacement

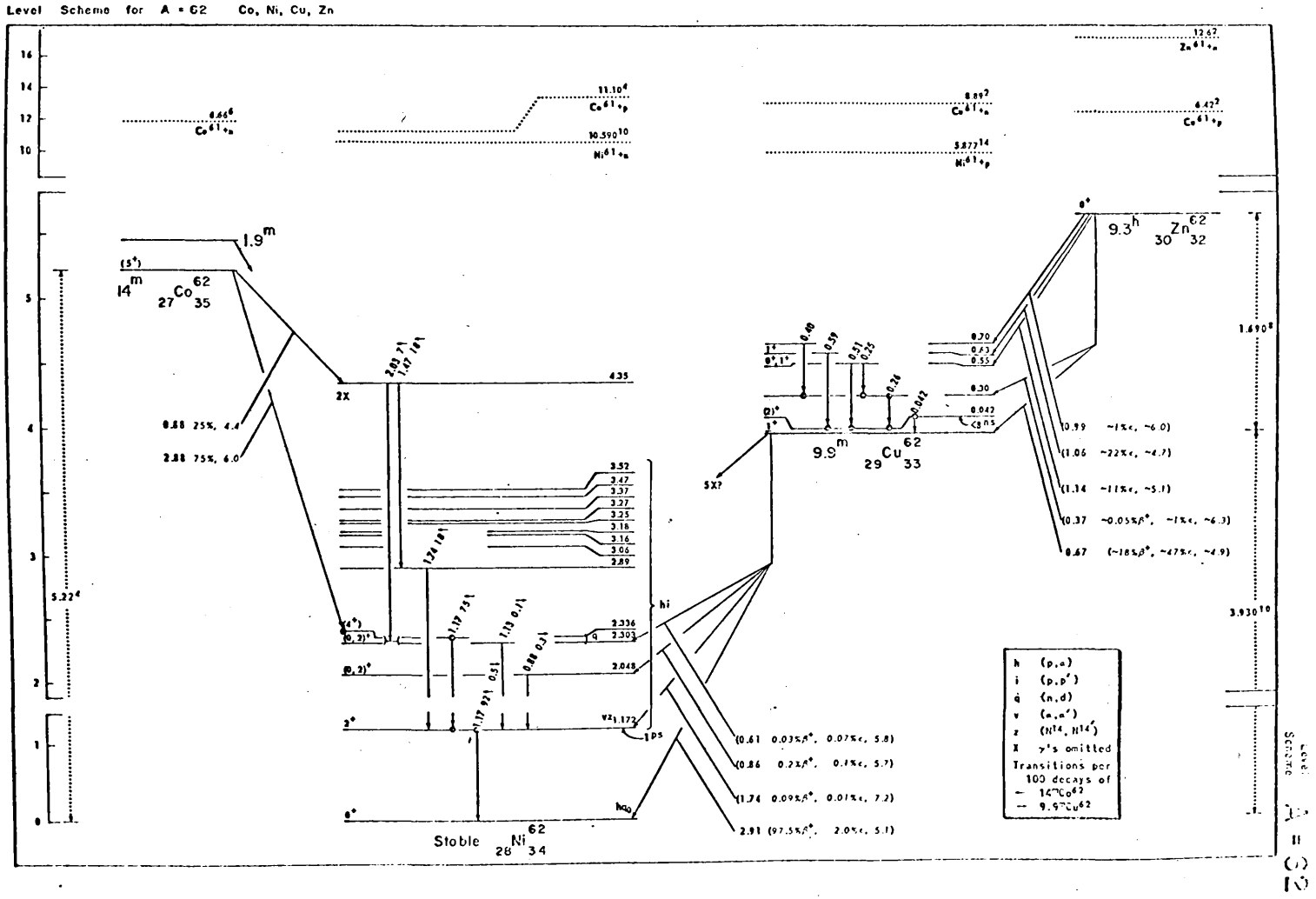

Figure 62.

the 9 h Zn^{62} activities for values of χ between 100 and 320 MeV at 20 MeV intervals (Figs. 4.4 and 4.5). "Corrected" yield points for the $(\gamma,\bar{\pi})$ and $(\gamma,\bar{\pi}n)$ activities were obtained by subtracting the contribution of the interfering two stage process most evident below the meson threshold (Chapter 5). These corrected yield points were then transformed into "reduced yields" $Y(\chi)$ (equation 5).

Once a set of "reduced yields" has been obtained, the problem is to obtain a suitable expression for $\Omega_s(K)$ involving these "reduced yields". Equation (5) can be solved for $\Omega_s(K)$ in principle, by forming combinations of $Y(\chi)$. However, one measures values of $Y(\chi)$ only for a limited number of values of χ and the functional form of $Y(\chi)$ is not known. Hence, even in principle, one can only obtain average values of the cross-section from an experiment. The method of PENFOLD and LEISS accepts this limitation from the beginning but fully sets forth the relationship between the average values of $\Omega_s(k)$ which are obtained and the true values.

Now let it be supposed that the following represents a set of measured values of $Y(\chi)$

$$Y(\chi_m),\ Y(\chi_{m-1}) \ldots\ Y(\chi_i) \ldots\ (8)$$

where $\chi_m > \chi_{m-1}$ .... etc.

The values of χ are chosen at equally spaced intervals Δ (20 MeV in the present experiment). The interval Δ will be referred to as the bin width.

Let us now consider the effect of taking a linear combination

of the measurements represented by equation (8). The linear combination will be specified by a series of numbers $B(\chi_m,\Delta,\chi_i)$ which will be known as B-numbers. As the notation indicates, the B-numbers are functions of χ_m,Δ,χ_i.

We shall now consider the linear combination $C(\chi_m,\Delta)$ where

$$C(\chi_m,\Delta) = \sum_{i=a}^{m} B(\chi_m,\Delta,\chi_i)\, Y(\chi_i) \quad \ldots\ (9)$$

The lower limit on the sum has been arbitrarily set at a and we shall assume that $Y(\chi_i) = 0$ for all $i < a$.

In order to discover the relation between $C(\chi_m,\Delta)$ and the cross-section, we substitute into equation (9) the value of $Y(\chi_i)$ given by equation (5). The result is the following

$$C(\chi_m,\Delta) = \int_0^{\chi} T(\chi_m,\Delta,K)\,\Omega(K)\,dK \quad \ldots\ (10)$$

where

$$T(\chi_m,\Delta,K) = \sum_{i=a}^{m} B(\chi_m,\Delta,\chi_i)\,\Phi(\chi_i,K) \quad \ldots\ (11)$$

The function $T(\chi_m,\Delta,K)$ will be called a <u>weighting function</u> and its determination is crucial to the development of solutions for $\Omega_s(K)$ and to the investigation of the validity of these solutions.

The weighting function is composed of a linear combination of bremsstrahlung spectra, and so it automatically satisfies the following conditions, first, it is identically zero for values of K greater than χ_m, second, over the energy range of the top bin $\chi_m > K > \chi_{m-\Delta}$ it has the same shape as the high energy end of a

bremsstrahlung spectrum, third, it is automatically partitioned into bins of width Δ.

The basic problem is to choose the B-numbers in such a way that the weighting function has a desirable form. That is, so that $C(\chi_m,\Delta)$ is simply related to the cross-section.

The B-numbers were chosen in such a way that the area under the weighting function has a value very close to Δ, and is essentially different from zero only when K is within a bin or two of χ_m. It is mostly contained in the head bin $\chi_m \rangle\!\rangle K \rangle\!\rangle \chi_{m-1}$. In that case, it is meaningful to make use of the centroid energy of $T(\chi_m,\Delta,K)$ which we shall denote by K_m^{Δ}. Consequently it is a good approximation to replace equation (10) by the following

$$C(\chi_m,\Delta) = \Omega_s(K_m^{\Delta})\Delta \quad \ldots\ (12)$$

$$\text{or } \Omega_s(K_m^{\Delta}) = \frac{1}{\Delta} C(\chi_m,\Delta) \quad \ldots\ (13)$$

The method of solution is now complete (except for the choice of B-numbers) since equation (13) combined with (9) yields a value for the cross-section in terms of the measurements which is

$$\Omega_s(K_m^{\Delta}) = \frac{1}{\Delta} \sum_{i=a}^{m} B(\chi_m,\Delta,\chi_i)\, Y(\chi_i) \quad \ldots\ (14)$$

The corresponding value of the real cross-section $\sigma(K_m^{\Delta})$ is obtained by using equation (2a).

Although a table of B-numbers was provided by PENFOLD and LEISS, they were not appropriate for the bin width used in the present

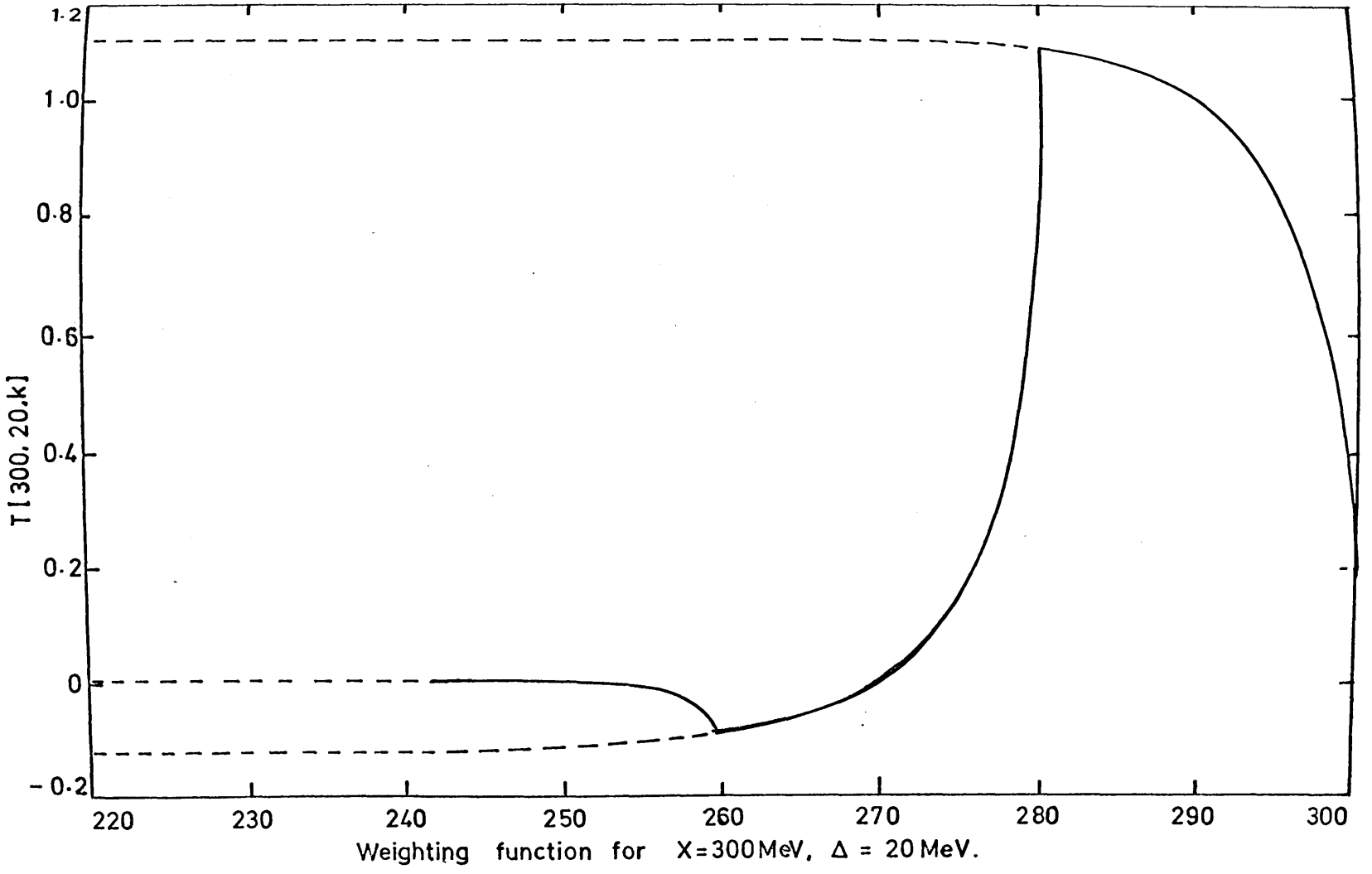
1·2
1·0
0·8
0·6
0·4
0·2
0
−0·2
T[300, 20, k]
220
230
240
250
260
270
280
290
300
Weighting function for X=300MeV, Δ = 20MeV.

Figure 6·3.

experiment. For this experiment B-numbers were worked out by means of equation (11) coupled with the following restrictions,

$$T(\chi_m, \Delta, K) = 1 \text{ for } K = \chi_m - \Delta/2 \quad \ldots\ (15)$$

(the mid-point of the top bin)

$$T(\chi_m, \Delta, K) = 0 \text{ for } K = \chi_i - \Delta/2$$

(the mid point of all lower bins)

$$(i \neq m) \quad \ldots\ (15a)$$

Once a set of B-numbers has been obtained, they may be used in equation (11) to determine the associated weighting function. Typical examples of such weighting functions are shown in Fig. 6.3, and Fig. 6.4. The weighting functions are for χ = 300 MeV and χ = 200 MeV bremsstrahlung respectively. It can be seen that these weighting functions are almost identical. The long tail of the function remains very small down to the lowest energies. The area contained under the function (Fig. 6.3) in the energy range 260- 280 MeV is only 9% of the area contained between 280 - 300 MeV.

The SCHIFF[6.5] "integrated over angles" spectrum for a "thin" radiator was used when calculating the B-numbers. This spectrum shape is appropriate for the target used in the Glasgow synchrotron and values of $\bar{\phi}(\chi, K)$ are tabulated by PENFOLD and LEISS.

There is a set of B-numbers for each energy at which a cross-section is desired. Once these B-numbers are obtained, $\Omega_s(K)$ is worked out by means of equation (14) and is converted into $\sigma_s(K)$ by means of equation (2a). A typical example of how $\Omega_s(K)$ is worked

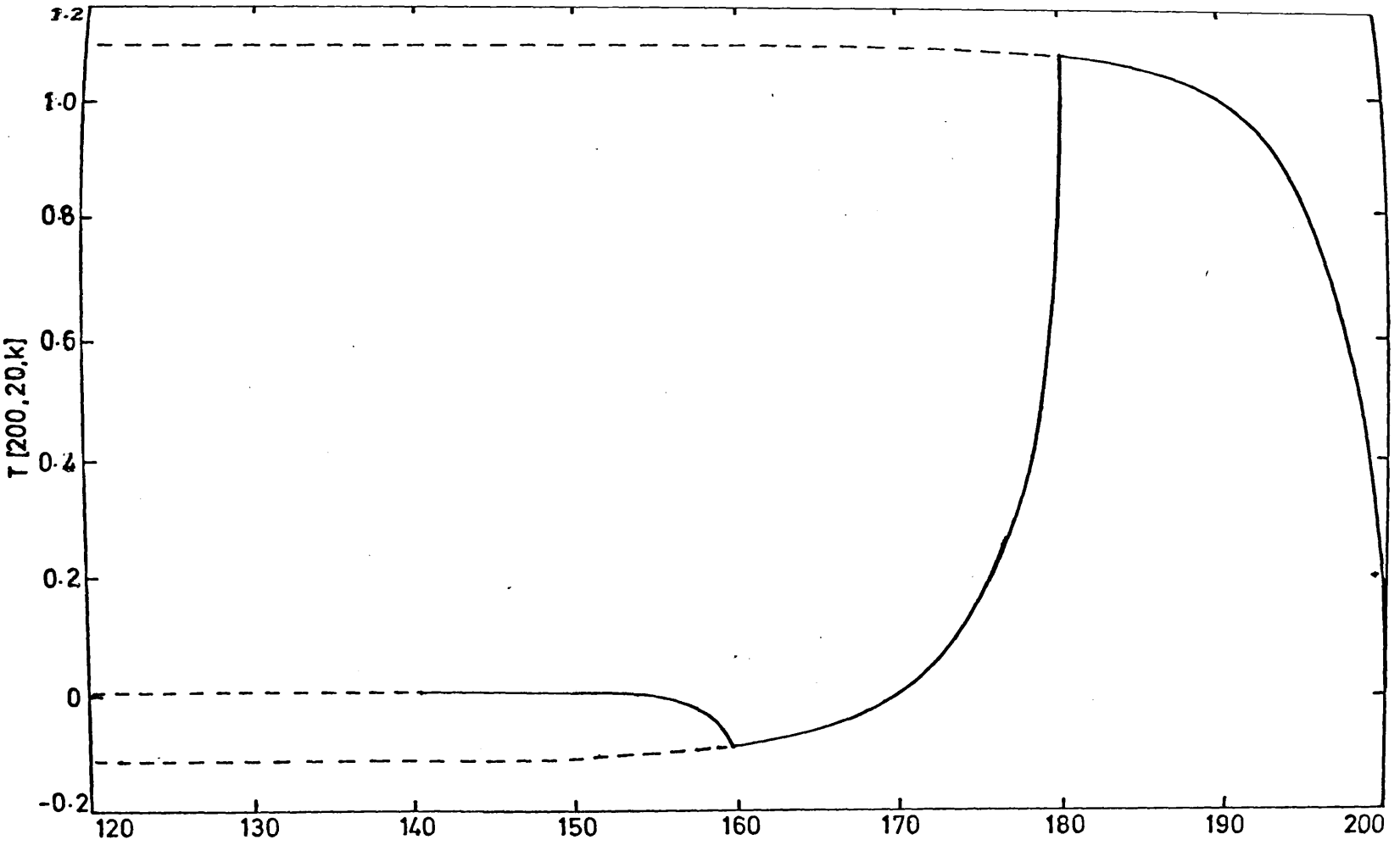

Weighting function for X = 200 MeV, Δ = 20 MeV

Figure 6·4.

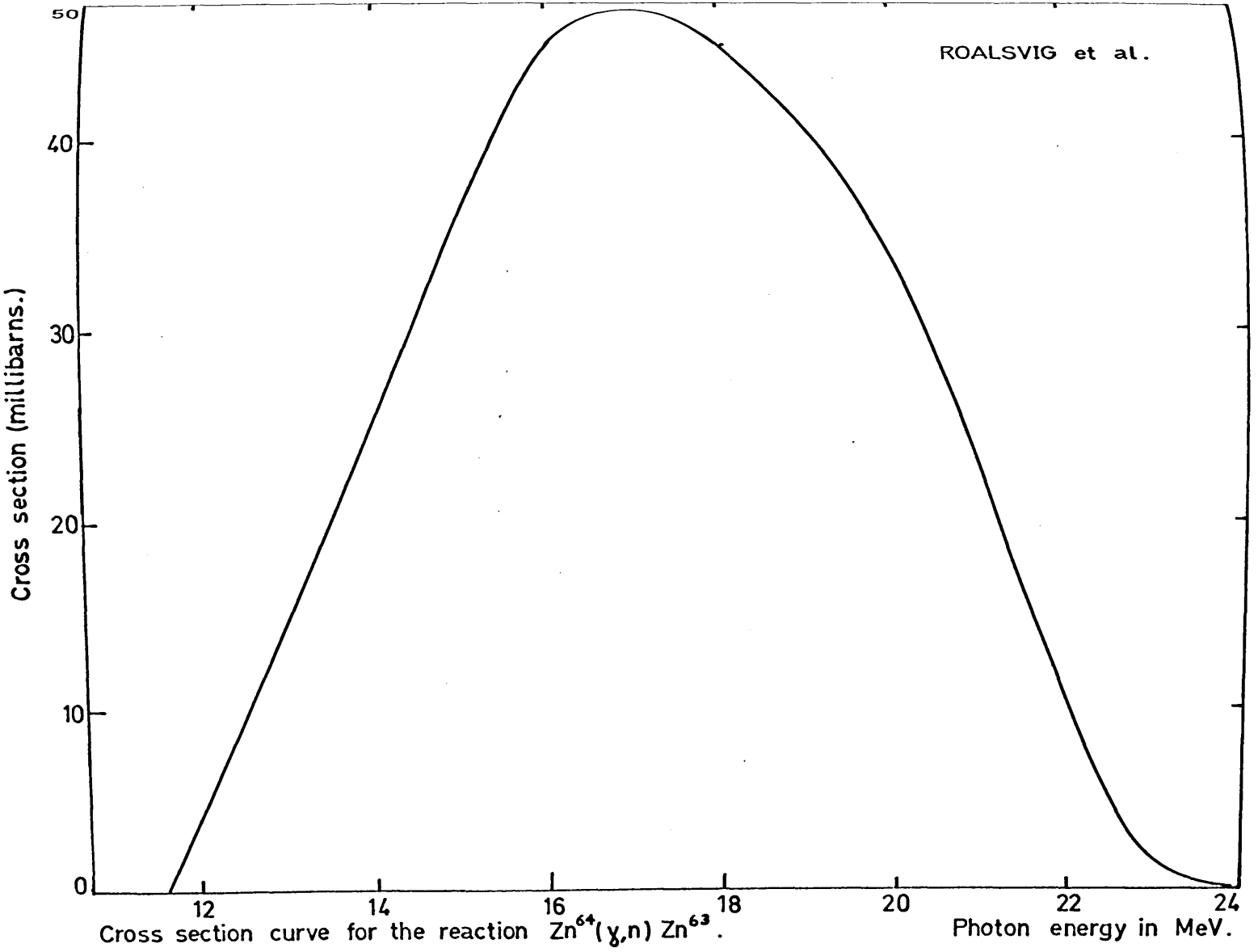

Cross section curve for the reaction $Zn^{64}(\gamma,n)\,Zn^{63}$.

Figure 6·5.

out is given below,

$$\Omega_{290} = \frac{1}{20}\Big\{ 2.7494\ Y_{300} - 3.0950\ Y_{280} + 0.355\ Y_{260} - 0.01\ Y_{240} + 0.01\ Y_{220} \Big\}$$

In the foregoing paragraphs a method of cross-section analysis has been developed. The necessary steps can be summarised as follows:

(1) the "yield points" are transformed into "reduced yields" by means of equation (5),

(2) The "reduced yields" are combined as indicated in equation (14) to obtain values for the reduced cross-section $\Omega_s(\overset{\Delta}{K_m})$

(3) The corresponding values of the real cross-section $\sigma_s(\overset{\Delta}{K_m})$ are obtained by using equation (2a).

Calculation of the $Cu^{63}(\gamma, \pi^-)\ Zn^{63}$ cross section *

The monitoring reaction used for this experiment was Zn^{64} $(\gamma,n)\ Zn^{63}$.

The most recent experimental work on this reaction is that of ROALSVIG et al[6.6]. Their results shown in Fig. 6.5 were used on the evaluation of the integral $\int_0^{\chi} \Phi(\chi,K) \frac{\sigma_m}{K}\, dK$ in equation (5). Integration was performed numerically using the values of $\Phi(\chi,K)$ tabulated by PENFOLD and LEISS. The corrected yield point curve is shown in Fig. 6.6. The "reduced" cross sections averaged over each weighting function were calculated directly from the yield points as described above. These are to be associated with the centroids of the weighting functions which are a little displaced

* The contribution of $Cu^{65}(\gamma, \pi^- 2n)$ to the total yield is discussed in APPENDIX B

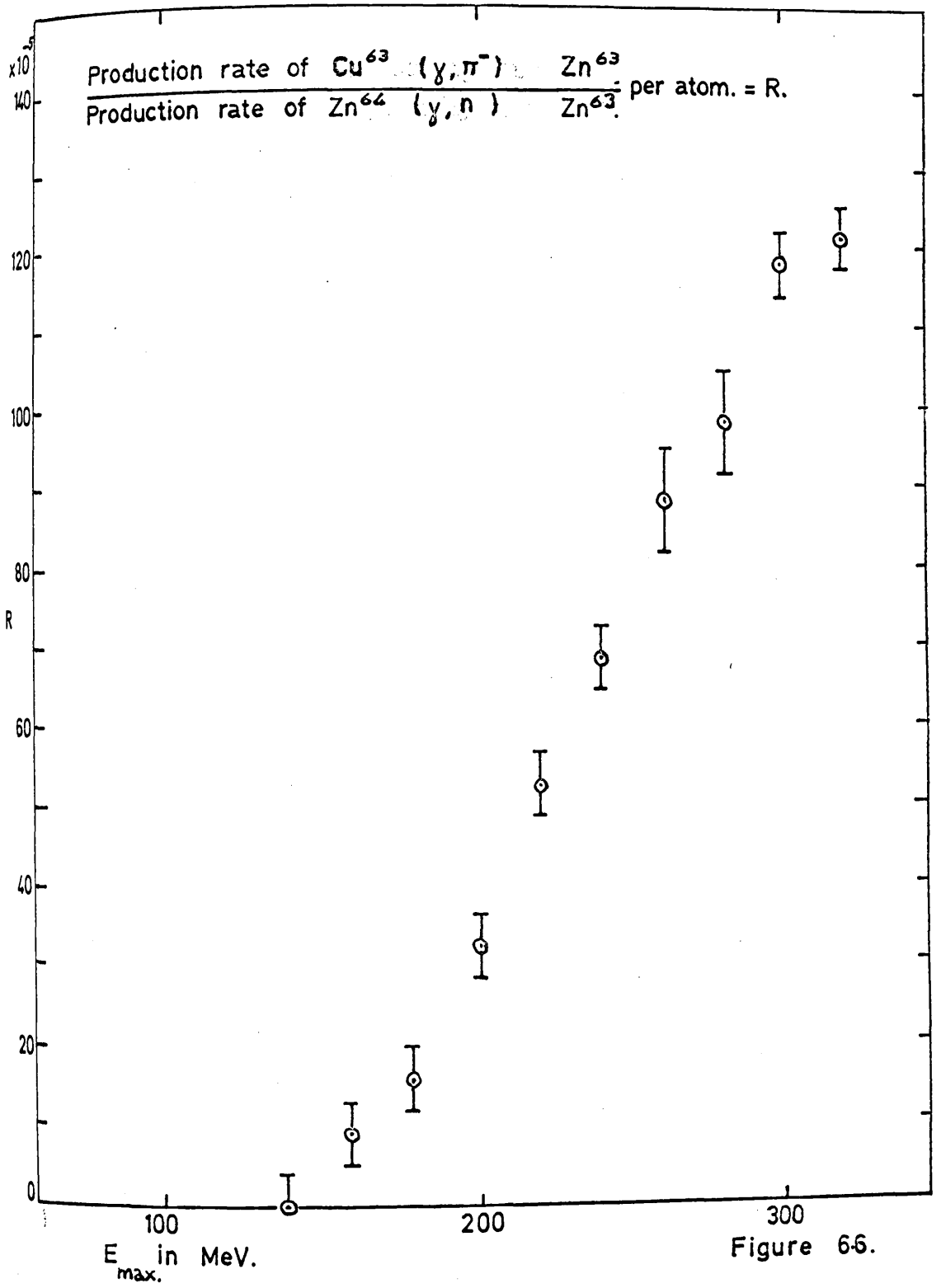
Production rate of Cu^{63} (γ, π^-) Zn^{63} / Production rate of Zn^{64} (γ, n) Zn^{63} per atom. = R.
x10⁻⁵
140
120
100
80
R
60
40
20
0
100
200
300
E max. in MeV.

Figure 6.6.

from the mid point energy of each "bin". The corresponding "real" cross sections were calculated using equation 2a. The procedure used for smoothing these cross sections is described below.

Calculation of the $Cu^{63}(\gamma,\pi^-n)\ Zn^{62}$ cross section *

The ideal monitoring reaction for this experiment would have been $Zn^{64}(\gamma,2n)\ Zn^{62}$. Unfortunately, the absolute cross section for this reaction has not been measured. For this reason the reaction $Cu^{65}(\gamma,n)\ Cu^{64}$ was used.

The half life of Cu^{64} is 12.8 h and that of Zn^{62} is 9 h. The cross section has been measured by FULTZ et al[6.7] and their results were used in the calculation of $\int_0^{\chi} \phi(\chi,K)\frac{\sigma_m}{K}\,dK$ (equation 5). The variation of cross-section with energy for $Cu^{65}(\gamma,n)\ Cu^{64}$ is very similar to that of $Zn^{64}(\gamma,n)\ Zn^{63}$. The factor $(1 - e^{-\lambda_m t_o})/(1 - e^{-\lambda_s t_o})$ was included in equation (7) on the assumption of constant beam intensity during irradiation. Since λ_m and λ_s are of the same order, small variations of beam intensity would not introduce significant error. The "corrected" yield point curve for the $Cu^{63}(\gamma,\pi^-2n)$ reaction is shown in Fig. 6.7. The "reduced" and real cross sections were calculated directly from the yield points.

Data Smoothing

In many experiments it is extremely difficult to achieve sufficient statistical accuracy in the cross-section solution. This forces one to consider the possibility of smoothing. It has

** The contribution of $Cu^{65}(\gamma,\pi^-3n)$ to the yield of Zn^{62} is discussed in APPENDIX B

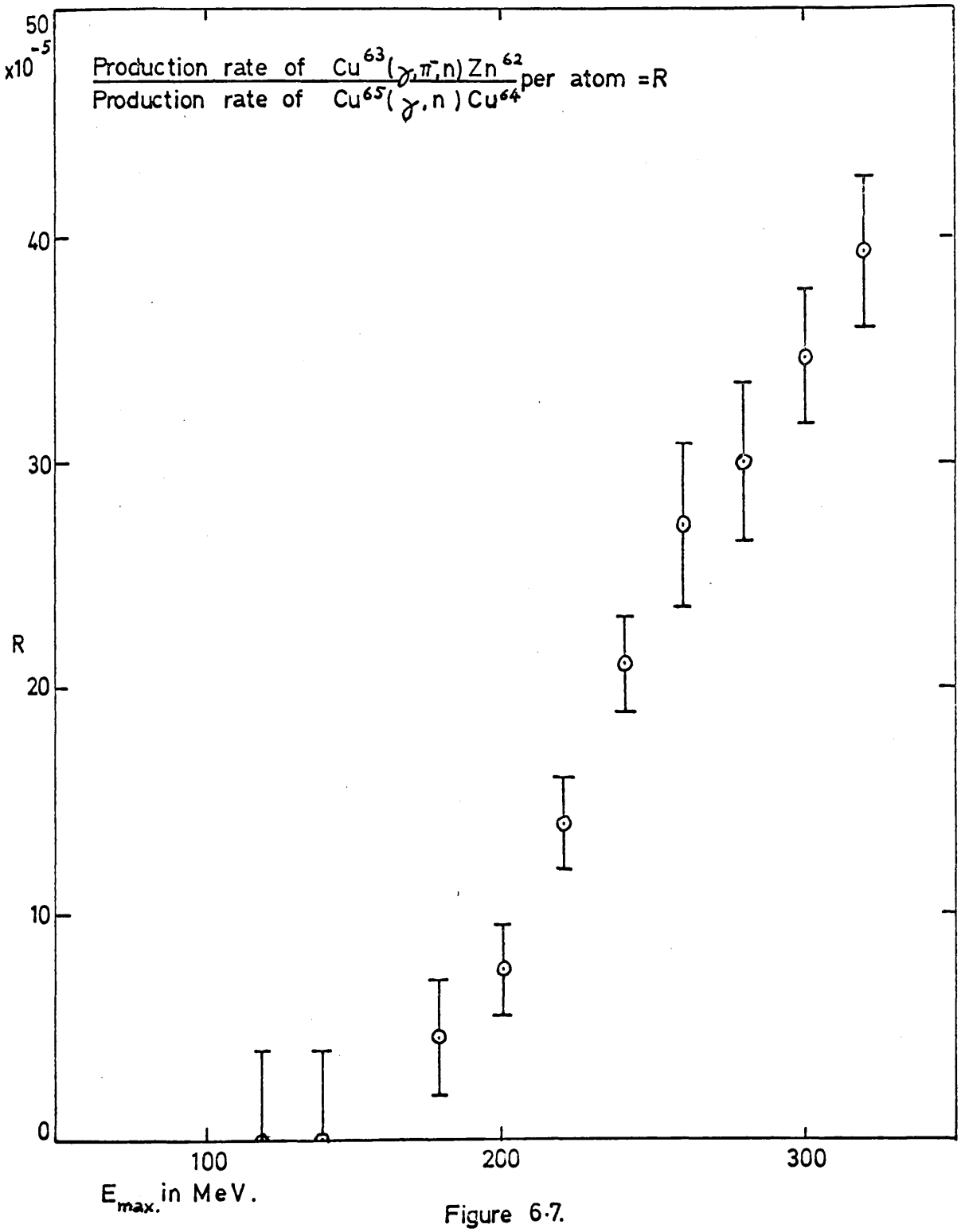
50
x10^-5
Production rate of Cu^63(γ,π⁻,n)Zn^62 per atom =R
Production rate of Cu^65(γ,n)Cu^64
40
30
R
20
10
0
100
200
300
E_max. in MeV.

Figure 6·7.

become common practice to smooth the experimental yield curve in order to obtain a relatively smooth cross-section curve upon analysis. This practice has the limitation that because of the strong dependence of the deduced cross-section upon the higher differences of the "yield curve" any smoothing procedure will introduce errors of a systematic nature. Small systematic errors in the yield values can lead to large errors in the cross-section solutions. What appears to be the most suitable prescription for data processing is to calculate the cross-section and its running integral directly from the measured yield points. A smooth curve can then be drawn through the integral and from this curve smoothed values of the cross-section can be deduced.

In calculating the cross-section for the (γ, π^-) and $(\gamma, \pi^- n)$ reactions above, the real cross-sections (σ_s) were worked out using the actual yield points from Figs. 6.6 and 6.7 respectively. A running integral of the cross-sections was then obtained for each reaction. Smoothed values of the cross-sections were then read off from these integral curves. These smoothed cross sections are tabulated below.

Cu^{63} (γ, π^-) Zn^{63}

Photon energy MeV	140-160	160-180	180-200	200-220	220-240	240-260	260-280	280-300	300-320
Cross-section 10^{-30} cm^2	14	31	43	55	62	68	63	50	26

$Cu^{63}(\gamma, \pi^- n)\ Zn^{62}$

Photon energy MeV	160-180	180-200	200-220	220-240	240-260	260-280	280-300	300-320
Cross-section 10^{-30} cm^2	17	26	30	34	36	36	34	33

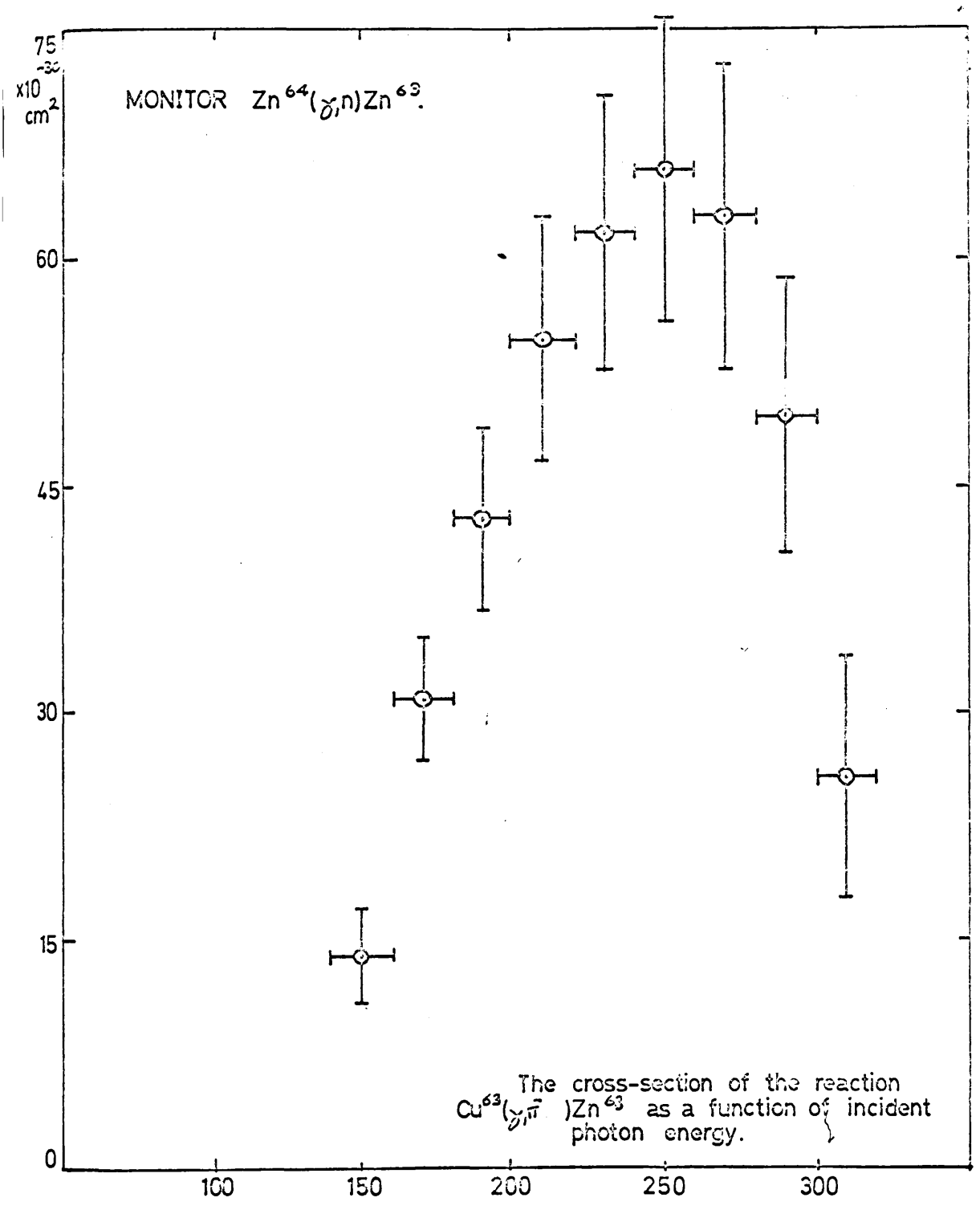

The cross-section of the reaction $Cu^{63}(\gamma,\pi^-)Zn^{63}$ as a function of incident photon energy.

Figure 7.1.

APPENDIX B refers.

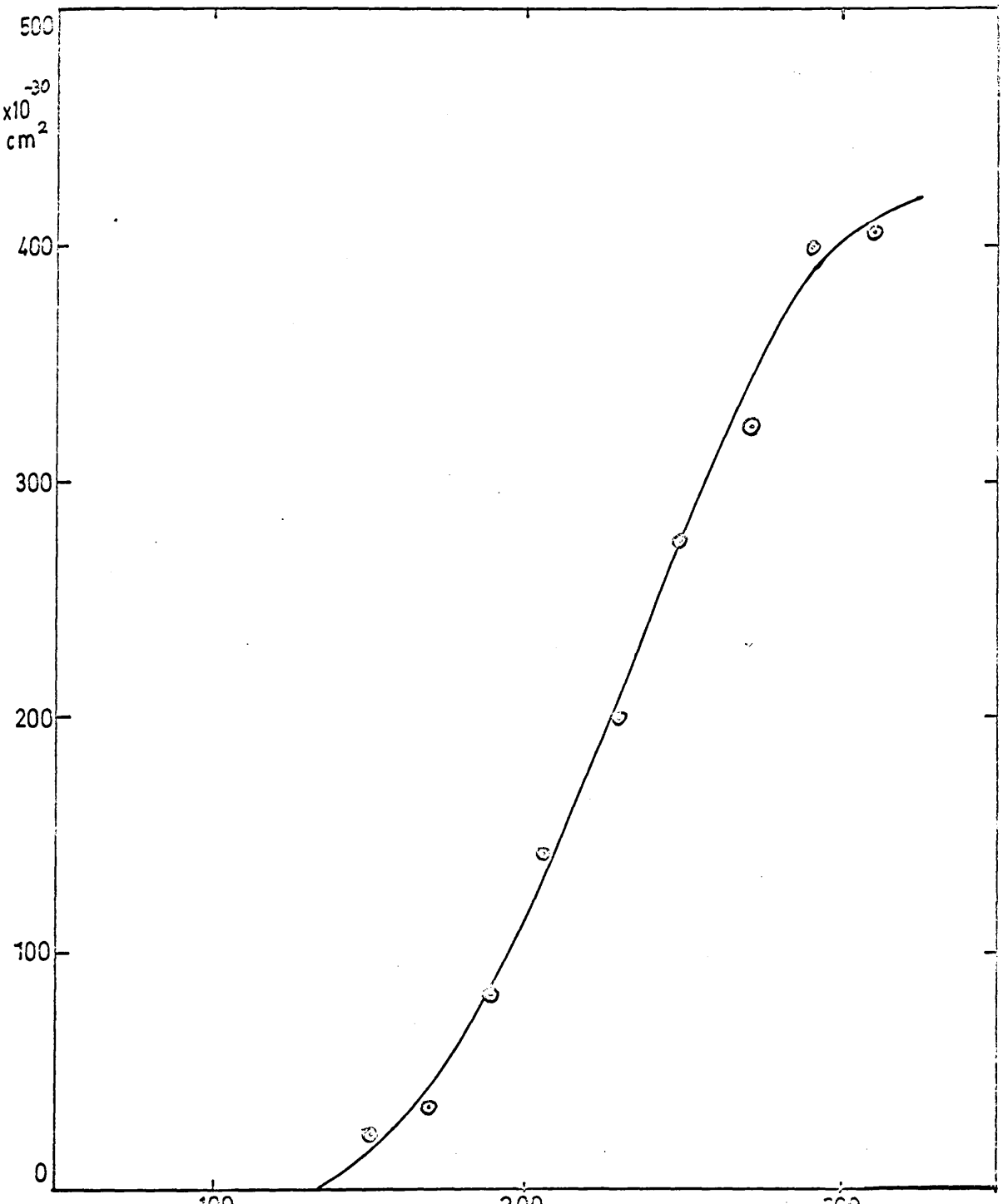

Running integral of cross-section of $Cu^{63}(\gamma,\pi)Zn^{63}$.

Figure 7.2.

CHAPTER 7

DISCUSSION OF PHOTOPION CROSS SECTIONS

The reaction $Cu^{63}(\gamma,\pi^-)Zn^{63}$ (Figs. 7.1 & 7.2)

The curve exhibited in Fig. 7.1 shows that the threshold energy for this reaction is about 140 MeV. It rises rapidly for photon energies above threshold and reaches a maximum value of 70 μbarns at E_γ = 255 MeV. The cross sections shown were averaged over 20 MeV intervals. It is possible that more detailed experiments using smaller energy intervals would show an even steeper rise of the cross section just above threshold. Experiments near threshold are difficult because of the low level of activity produced and are complicated by the contribution of the two stage process discussed in Chapter 5.

For $E_\gamma > 255$ MeV the cross section falls and is probably zero at 320 MeV. This deduction depends rather critically on the observed yields at the two higher beam energies of 300 MeV and 320 MeV (the maximum possible at the time of the experiment).

The reaction $Cu^{63}(\gamma,\pi^-n)Zn^{62}$ (Figs. 7.3 & 7.4)

The threshold for this reaction is about 150 MeV. The cross section rises rather rapidly to 40 μb at about 255 MeV. Between 255 MeV and 320 MeV the cross section may remain constant or fall slowly. One cannot distinguish between these possibilities in view of the large statistical fluctuations.

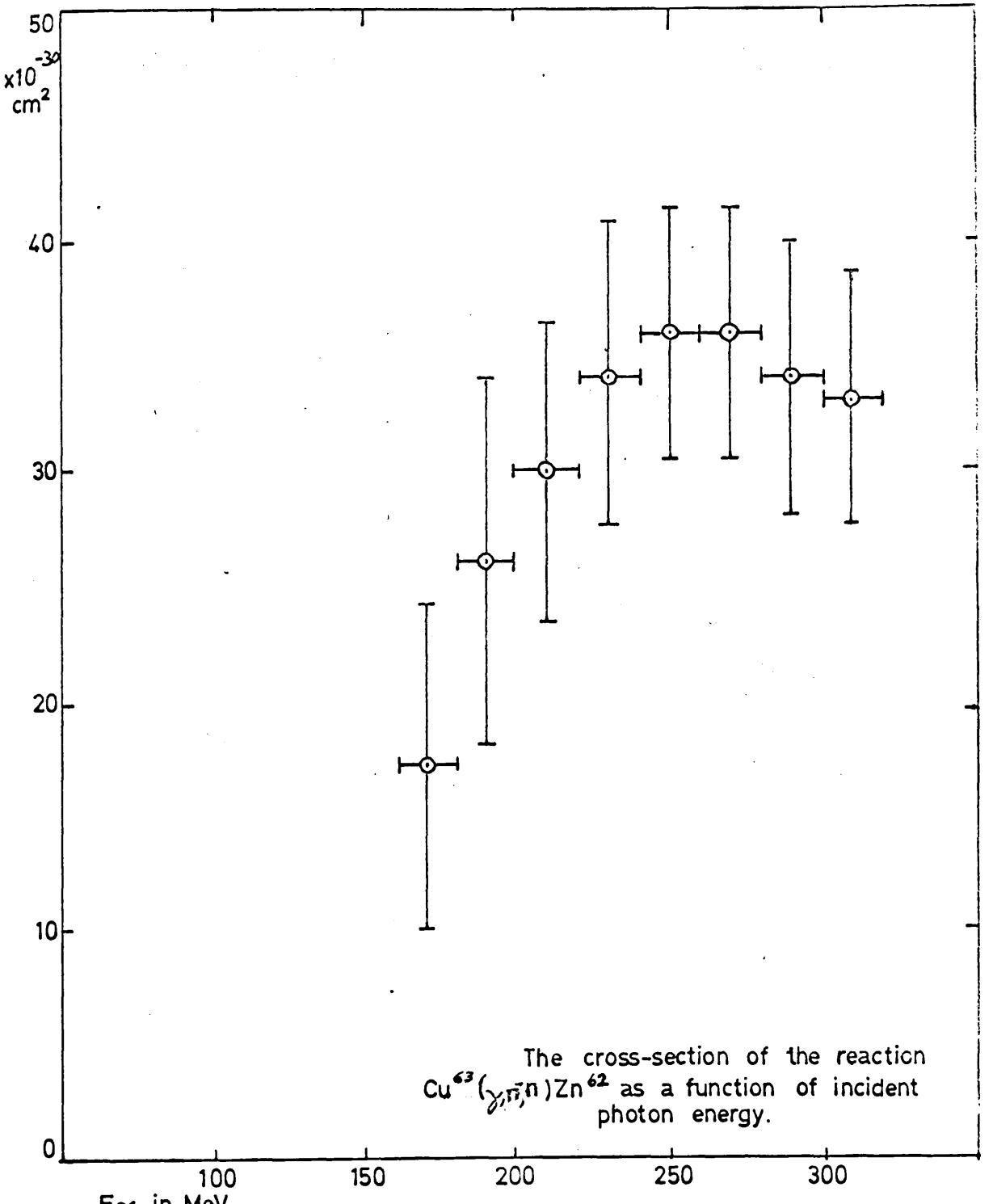

The cross-section of the reaction $Cu^{63}(\gamma,\pi^-n)Zn^{62}$ as a function of incident photon energy.

Figure 7.3.

APPENDIX B refers.

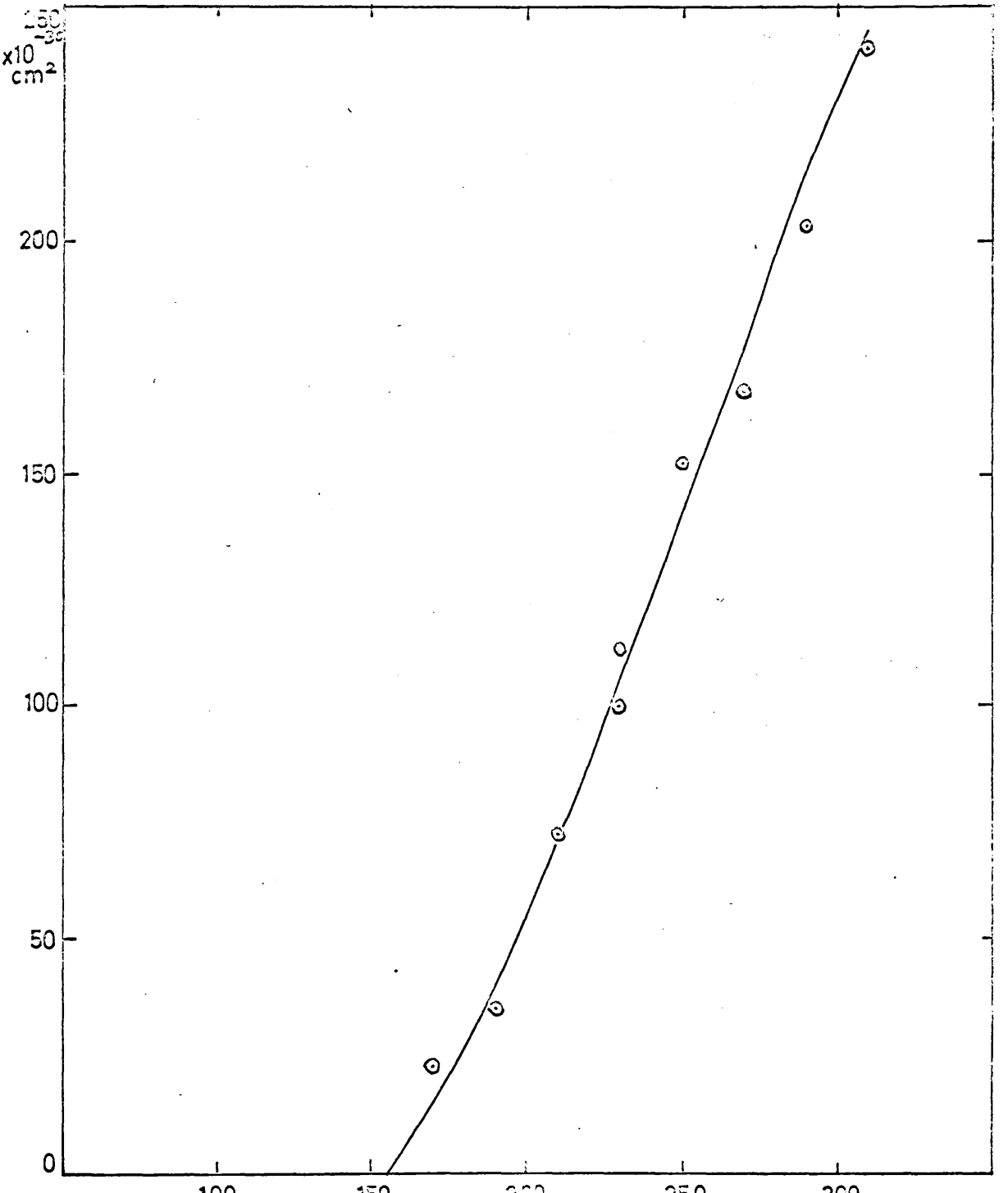

Running integral of cross section of $Cu^{63}(\gamma,\pi^-,n)Zn^{62}$.
Figure 7.4.

INTERPRETATION OF EXPERIMENTAL RESULTS

The significant features of the cross-section curves may now be discussed in relation to the previous experimental and theoretical works reviewed in Chapter 1. The experiments of LITTAUER and WALKER[1.4] showed an $A^{2}/3$ dependence of pion yield with mass number. This relation held most accurately for the total yield of charged pions. The total cross-section for the process as a function of photon energy was not obtained since pions were detected at one angle (135^{o}) in a particular energy range (65 ± 15 MeV). However, other experiments covering a wide range of energy and angle of the emitted pions have also shown a clear $A^{2}/3$ dependence. It is therefore a reasonable assumption that the total cross-section for the production of charged pions by monoenergetic photons does likewise.

LITTAUER and WALKER also measured the $\frac{\pi^{-}}{\pi^{+}}$ ratio which showed variations from 0.6 to 2.2. The yield of pions with a specific sign of charge showed corresponding deviations from the general $A^{2}/3$ trend. The $\frac{\pi^{-}}{\pi^{+}}$ ratio showed a strong correlation with the masses of isobaric nuclei adjacent to the target element (Fig. 1.1), the more stable nucleus being produced with the greater yield.

The $A^{2}/3$ dependence of the pion yield may be explained on the assumption that the pions observed experimentally are those produced at "surface" nucleons. Calculations based on the optical model of the nucleus[1.8] assume that pions are produced uniformly throughout the volume of the nucleus and that absorption in nuclear matter

accounts for the observed "surface" production. The results of experiments involving the detection of high energy mesons can be explained satisfactorily in this way. However, the production of low energy mesons, even in light nuclei, also varies as $A^{2}/3$ which cannot be attributed to an absorption process since the mean free path for absorption of low energy mesons is large compared with the dimensions of the nucleus. It was suggested by WILSON[1.19] that owing to the strong interaction between nucleons, pion production in the core of a nucleus is actually suppressed.

Assuming that pion production in the core of a nucleus is suppressed by some such mechanism as that proposed by WILSON, BUTLER[1.18] was able to account for the main features of the experimental results of LITTAUER and WALKER. It was assumed that pion production takes place at surface nucleons only. Surface nucleons were defined as those outside the nuclear radius r_o where r_o was taken as $1.2 \times A^{1}/3$ fermis. The cross section for the production of positive pions for example was shown to be approximately of the form $\sigma_{\pi^+} = \sigma_f Z\tau$ where σ_f is the production cross section at a free proton, and τ the probability of finding a proton at $r > r_o$. τ is given by

$$\tau = {}^{1}/(1 + {}^{2}/3\ K^{P}_{AV}\ A_o)$$

where K^{P}_{AV} is the average binding energy of a proton (~8 MeV) and varies from nucleus to nucleus. Since $K_{AV} r_o \gg 1$

$$\sigma_{\pi^+} = \frac{\sigma_f}{{}^{2}/3 \times 1.2\ K^{P}_{AV}} \times \frac{Z}{A^{1}/3} \simeq A^{2}/3$$

similarly $\sigma_{\pi^-} = \dfrac{\sigma_f}{2/3 \times 1.2 \times K_{AV}^n} \quad \dfrac{A-Z}{A^{1}/3} \simeq A^{2}/3$

where the production cross sections for π^+ and π^- at a free proton and neutron respectively have been assumed identical. The observed variations in π^-/π^+ ratio are accounted for rather well by this model in terms of Z, (A-Z), K_{AV}^P, K_{AV}^N for specific nuclei.

The simple picture outlined above (and in Chapter 1) may be improved in detail. The surface nucleons are not in fact free and σ_f may be replaced by a modified cross section which takes into account the momentum distribution of nucleons and the intereaction with the core of both nucleons and pions. These considerations have the following effect.

(1) The production threshold is decreased by about the average energy of a surface nucleon (about 8 MeV)

(2) The π^+, π^- ratio is modified since the distribution of nucleon energies alters the effective values of K_{AV}^P and K_{AV}^N above.

For heavy nuclei, particularly when low energy pions are produced by low energy photons, the π^-/π^+ ratio might be expected to show the effect of Coulomb interaction. BUTLER calculated pion yields from bremsstrahlung with a maximum energy corresponding to that used by LITTAUER and WALKER and obtained good agreement with experiment except that the calculated yield was about 60% of that observed. The total cross section for pion production by monochromatic X-rays was not calculated but would of course have the $A^{2}/3$ dependence.

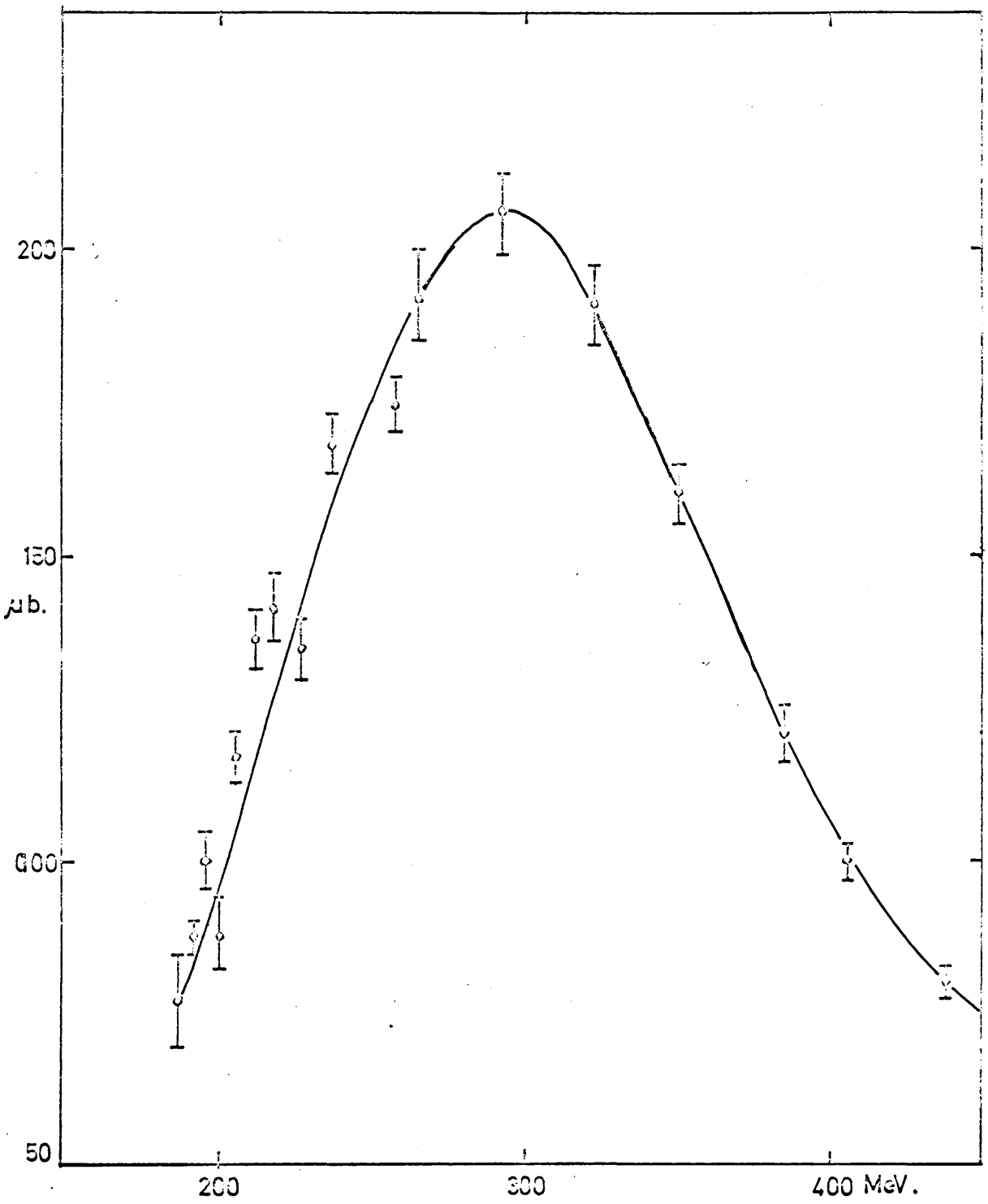

Cross-section for the photoproduction reaction
$\gamma + p \rightarrow n + \pi^+$.

Figure 7.5

There have been very few attempts to measure the total pion production cross section for comparison with the results of the present experiment. By integrating over all angles STEINBERGER and BISHOP[1.3] have derived a value for the total cross-section for π^+ production from carbon at 255 MeV. This is stated to be twice that of the total cross section for π^+ production from hydrogen. The π^-/π^+ ratio for carbon is very nearly unity. If such a light nucleus may be considered representative of nuclear matter, we have, at E_γ = 255 MeV assuming the value 175 μb (Fig. 7.5) for the γ, π^+ cross-section of hydrogen

$$\sigma_{A,\,(\pi^+ + \pi^-)} = \frac{700}{12^{2}/3}\, A^{2}/3\ \mu b$$

$$= 133.6\ A^{2}/3\ \mu b$$

For Cu^{63}, $\sigma_{A\,(\pi^+ + \pi^-)} = 2114\ \mu b$

$$\simeq 2.1\ mb$$

Assuming a ratio of 1.3 for $\frac{\pi^-}{\pi^+}$ ratio in copper[1.4] we have

$$\sigma_{\pi^-} \simeq 1.17\ mb$$

Evidently, for E_γ = 255 MeV the cross-sections for Cu^{63} of γ, π^- ($\simeq 70\ \mu b$) and $\gamma, \pi^- n$ ($\simeq 40\ \mu b$) measured in the present experiment are but a small part of the total cross-section for π^- production (6.5% and 3.5% respectively). It may be mentioned that BUTLER in effect ignored the contribution of the γ, π^- reaction

when calculating yields for comparison with LITTAUER and WALKER's experiment.

Branching ratios of $\gamma, \bar{\pi}$ reactions

The total cross-section for a number of photopion reactions has been studied by activation methods similar in principle to that used in the present experiment. These are listed below for reference:

	$\sigma_{max}(\mu b)$ at $E\gamma$ (MeV)	
$B^{11}(\gamma,\pi^-)C^{11}$ $^{1.28}$	~31	~230
$Ni^{60}(\gamma,\pi^-)Cu^{60}$ $^{1.31}$	~63	~230
$O^{16}(\gamma,\pi^+)N^{16}$ $^{1.33}$	~8	~250
$Al^{27}(\gamma,\pi^+)Mg^{27}$	~13	~220
$V^{51}(\gamma,\pi^-2n)Cr^{49}$ $^{1.38}$	~100	~200
$Bi^{209}(\gamma,\pi^- x\,n)Po^{209-x}$ $^{1.36}$ for x = 0,1,2,3,4,5		
$Cu^{63}(\gamma,\pi^-)Zn^{63}$	~70	~255
$Cu^{63}(\gamma,\pi^-n)Zn^{62}$	~40	~255

* Except in the case of Bi^{209} which is discussed further below, the reactions above are seen to make only a small contribution to the total pion cross section. Reactions of this type may be interpreted in terms of the following simple model.

(1) The incoming photon interacts with an essentially free surface nucleon according to the Butler-Wilson model

$$\gamma + p \rightarrow \pi^+ + n$$

or $$\gamma + n \rightarrow \pi^- + p$$

the yields of neutrons and protons having a dominant $A^2/3$ dependence.

* APPENDIX B refers.

The energy distribution of (for example) protons is given by the differential cross section

$\frac{d\sigma(T_p, E\gamma)}{dT_p}$ for the production of a proton of energy T_p by a photon of energy $E\gamma$ at a surface neutron. $\frac{d\sigma(T_p E\gamma)}{dT_p}$ has approximately the same form as for production at a free nucleon but the maximum cross section occurs at a photon energy of about 250 MeV as compared with 300 MeV.

(2) The pion leaves the nucleus and the recoiling nucleon intereacts with the residual (A-1) nucleus.

The recoiling nucleon may be captured by the residual nucleus which then de-excites by γ-ray emission - in which case we have a π^- or π^+ reaction. This is the only possible outcome if the emission of nucleons is not energetically possible, i.e. for low energy protons produced by photons just above the meson threshold. This outcome however becomes increasingly less probable as other channels are opened.

Higher energy recoil nucleons may escape the residual nucleus or cause the ejection of nucleons either by "evaporation" from the compound nucleus or by direct interaction perhaps followed by an evaporation process.

The total corss-section for pion production by photons of energy E may therefore by expressed as the sum of partial cross-sections

corresponding to the different branching ratios.

$$\sigma_{\pi}^{A}(E\gamma) = \sum \sigma_{\pi,\ xn + yP}$$

where $\sigma_{\pi, xn + yP}$ is the partial cross-section for the emission of a pion accompanied by x neutrons and y protons.

For π^- emission from a nucleus A, Z each partial cross-section has the form

$$\sigma^{A}_{\pi^- + xn + yP}(E\gamma) = (A-Z)\sigma_f \tau \int_0^{T_P^{max}} \frac{d\sigma(T_P, E\gamma)}{dT_P} \sigma^{A-(x+y)}_{x+y}(T_P)dT_P$$

where $\sigma^{A}_{\pi^- + xn + yp}$ is the cross section for the emission of a negative pion accompanied by x neutrons and y protons from the nucleus (A,Z) by photons of energy $E\gamma$, and $\sigma^{A-(x+y)}_{x+y}(T_P)$ is the cross section for the production of x neutrons and y protons from the residual nucleus $\{A - (x + y),\ Z + 1 - y\}$ by protons of energy T_P produced at the surface.

$(A - Z)\sigma_f \tau = \sigma_{\pi^-}(E\gamma)$ is the total cross section for π^-,P production at a surface neutron from the Butler-Wilson theory and contains the "$A^2/3$" dependence (and quite similarly for π^+ production).

The cross sections $\sigma^{A-(x+y)}_{x+y}(T_P)$ are in general not known but are expected to be similar to the cross sections for the same reaction produced by bombardment of $\{A - (x + y),\ Z + 1 - y\}$ by externally produced protons. For instance the reaction $Cu^{63}(\gamma, \pi^-)Zn^{63}$ might be expected to have the same shape of cross section/energy

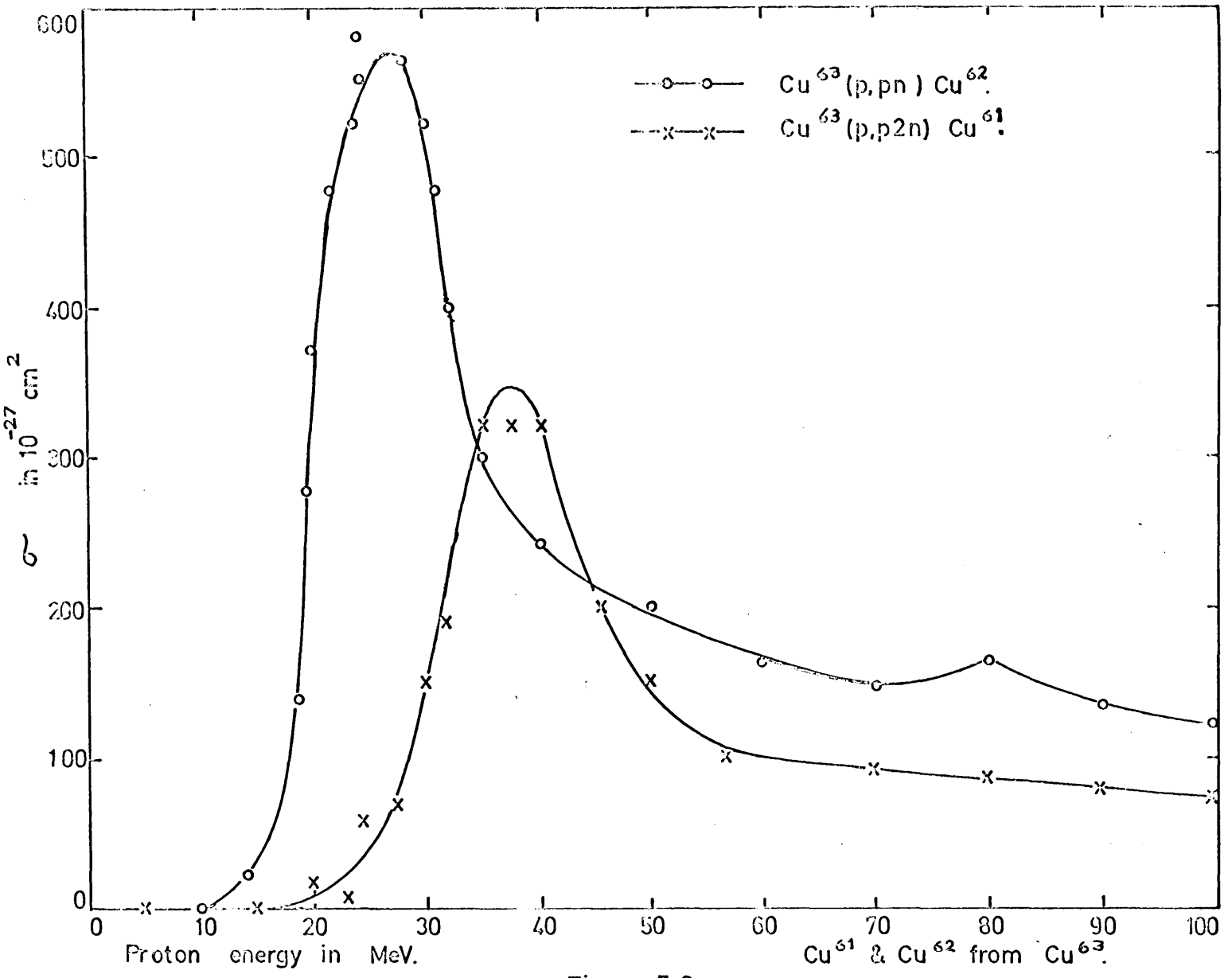
600
500
400
300
200
100
0
σ in 10^{-27} cm^2
$Cu^{63}(p,pn)\ Cu^{62}$.
$Cu^{63}(p,p2n)\ Cu^{61}$.
0
10
20
30
40
50
60
70
80
90
100
Proton energy in MeV.
Cu^{61} & Cu^{62} from Cu^{63}.

Figure 7·6.

curve as $Cu^{62}(p,\gamma)$ - i.e. proton capture. Similarly the cross section for $Cu^{63}(\gamma,\pi^- n)$ might be correlated with $Cu^{62}(p,n)Zn^{62}$.

Using arguments similar to those above YAVIN and PASQUALI have obtained good agreement between the experimentally measured yield of

$$\gamma + Bi^{209} \rightarrow \pi^- + Po^{209-x} + xn$$

where x = 0, 1, 2, 3, 4, 5.

The cross sections for the emission of x neutrons by protons from Bi^{208} were assumed to be similar to those of Bi^{209} computed by JACKSON. The experimental results of BELL and SKARSGARD[7.3] gave an even better fit. The lowest cross section (for an average E_γ = 200 MeV) was found for the (γ,π^-) reaction(0.18 mb)and the highest for $(\gamma,\pi^- 2n)$ (~ 1.6 mb). The errors of this experiment were quite large but the sum of the measured cross sections(2.5 mb) agreed well with the total π^- cross section calculated on the basis of the Butler-Wilson theory.

MEYER and HUMMEL have measured the cross section for $V^{51}(\gamma,\pi^- 2n)$ Cr^{49} and obtained good agreement with the cross section calculated using the above model. Failing proton cross sections for $V^{50}(p,2n)$ Cr^{49} (or other reactions resulting in the same Cr^{51} compound nucleus), the experimental results of MEADOWS for $Cu^{63}(p,2n)$ were used.

The results of MEADOWS, (Figs. 5.2 & 7.6) were used to estimate the relative partial cross sections for reactions of the type Cu^{63} $(\gamma,\pi^- xn)$ and Cu^{63} $(\gamma,\pi^- pxn)$ at an energy E_γ = 255 MeV. The corresponding proton energy spectrum extends from 0 -75 MeV.

Absolute cross sections were then derived using the result of the present experiment (40 μb at 255 MeV) for $Cu^{63}(\gamma,\pi^-n)$. The sum of the cross sections for x = o,1,2,3,4,5 in each of the above reactions amounted to 600 - 700 μb which may be compared with a total cross section of 1200 μb for π^- production calculated according to Butler's theory. It should be noted that a contribution to the total cross section from $Cu^{63}(\gamma,\pi^-\alpha)\ Ni^{59}$ (corresponding to $Cu^{62}(P,\alpha)\ Ni^{59}$) has not been included. Other channels which are energetically possible have also been neglected. It is therefore considered that these results are in good agreement with the Butler-Wilson surface production model.

The contributions of the reactions $Cu^{65}(\gamma,\pi^-2n)\ Zn^{63}$ and $Cu^{65}(\gamma,\pi^-3n)\ Zn^{62}$ to the activities measured in the present experiment have been estimated. The possible errors in the quoted cross sections due to this cause are not believed to exceed 15% which would not affect any previous interpretation of results.

Discussion of the $Cu^{63}(\gamma,\pi^-)\ Zn^{63}$ and the relevant LAING and MOORHOUSE Calculation

LAING and MOORHOUSE[1.27] calculated the cross-sections for $B^{11}(\gamma,\pi^-)C^{11}$ on the basis of both volume and surface production of mesons. They averaged their cross-section over 30 MeV intervals from an energy range of 140 - 320 MeV. HUGHES and MARCH[1.28] determined experimentally the $B^{11}(\gamma,\pi^-)C^{11}$ cross-sections over the same energy range and energy interval. They obtained excellent agreement with

LAING and MOORHOUSE's calculated value for surface production. Later DYAL and HUMMEL[1.32] measured the cross-section for the same reaction and obtained good agreement. MARCH and WALKER[1.31] measured the cross-section for the $Ni^{60}(\gamma, \pi^-)Cu^{60}$ reaction as a function of photon energy. Their total cross-section averaged over the energy range 140 - 320 MeV was about 40 - 50% of what could be expected from extrapolation of the B^{11} cross-section assuming an $A^2/3$ dependence. MEYER et al[1.33] by assuming that the transition probabilities used in LAING and MOORHOUSE's calculation depend more on the total number of states available than on the specific details of the states involved, were able to show excellent agreement with the $O^{16}(\gamma, \pi^+)N^{16}$ cross-section and that expected from extrapolation of the B^{11} result, in spite of the fact that the cross-section observed was only 25% of that expected. By similar arguments WALTER and HUMMEL[7.1] showed that their result for Al^{27} (γ, π^+) Mg^{27} which was 35% of what could be expected from extrapolation of the B^{11} cross-section ($A^2/3$ dependence) could be accounted for. The total cross-section obtained for the $Cu^{63}(\gamma, \pi^-)$ Zn^{63} reaction as a result of the present experiment averaged over 140 - 320 MeV is about 55% of that expected from an $A^2/3$ extrapolation of LAING and MOORHOUSE's value for the B^{11} cross-section.

The experiments involving O^{16} and Al^{27} strongly suggest that the yields of γ, π^- and γ, π^+ reactions depend mainly on the total number of available energy states of the final nuclei. It may be that the cross-section for the (γ, π^-) reaction in B^{11} has a

comparatively large value in any case. It was observed by LITTAUER and WALKER that the production of γ,π^- mesons is greater in the case of nuclei with an extra unpaired neutron such as Li and Be. B^{11} also has an unpaired neutron so that the B^{11} cross-section might be similarly enhanced. However, it is interesting to note that POPOVA et al[1.24] did not find any increase in π^- production in nuclei with excess neutrons.

The Cu^{63} cross-section was worked out on the basis of the $Zn^{64}(\gamma,n)\ Zn^{63}$ cross-section, which was the monitoring reaction. The cross-section used was that of ROALSVIG et al who unfolded their yield curve by the PENFOLD and LEISS method. They compared the result of unfolding their yield curve by the "photon difference" method and found that both methods gave the same cross-section shape and the same energy for the cross-section maximum. The peak and integrated cross-sections given by the PENFOLD and LEISS method were however 40% lower than those given by the photon difference method. It is disturbing that such a large discrepancy should be attributed to different methods of unfolding the yield curve.

Both HUGHES and MARCH and MARCH and WALKER used the reaction $C^{12}(\gamma,n)\ C^{11}$ to monitor their respective γ,π^- reactions and used BARBER et al's [7.2] cross sections for $C^{12}(\gamma,n)C^{11}$. As polythene was used as a second monitor during the present experiment, the cross-section for the $Cu^{63}(\gamma,\pi^-)Zn^{63}$ reaction was worked out on the basis of BARBER et al's carbon cross-section. The result is shown in

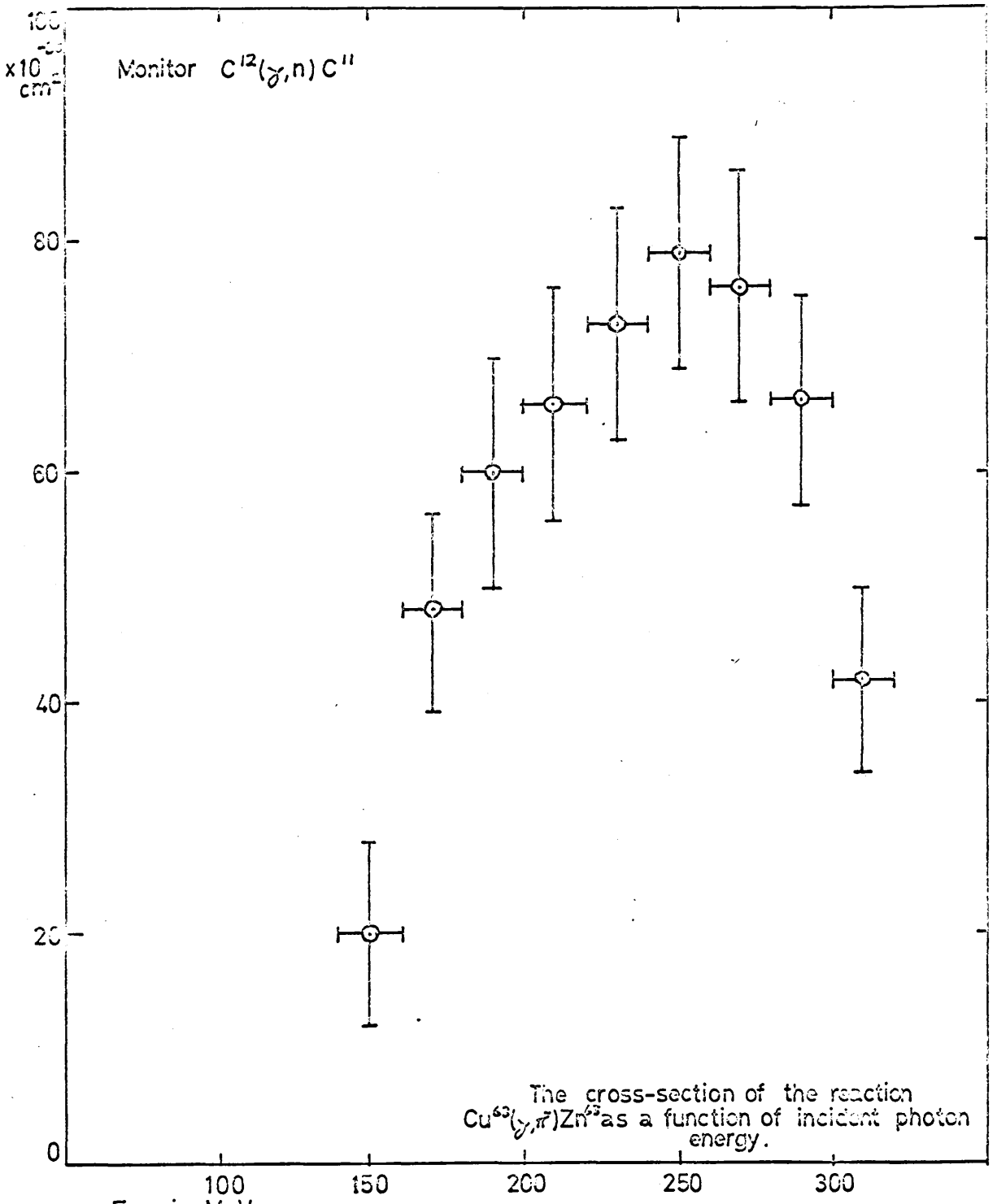

The cross-section of the reaction $Cu^{63}(\gamma,\pi^-)Zn^{63}$ as a function of incident photon energy.

Figure 7·7

Fig. 7.7. The total cross-section for $Cu^{63}(\gamma,\pi^-)Zn^{63}$ averaged over 140-320 MeV using the C^{12} monitor was found to be about 70% of that expected from an $A^2/3$ extrapolation of the LAING and MOORHOUSE result for B^{11} with an uncertainty of 20%. The uncertainty in the first case was about 15%. The increased uncertainty is due to the presence of a tail in the cross-section for the $C^{12}(\gamma,n)C^{11}$ reaction at high energies which introduces an uncertainty in the calculation of $\int \bar{\Phi}(\chi,K)\frac{\sigma_c}{K}dK$.

From the foregoing discussion, it is quite apparent that the $Cu^{63}(\gamma,\pi^-)Cu^{62}$ reaction of the present experiment is quite compatible with LAING and MOORHOUSE's surface production model calculation for a γ,π^- reaction. It should, however, be remembered that as pointed out earlier, a γ,π^- reaction constitutes only a very small portion of the total pion production. Moreover, an estimate of the partial corss-section depends on the detailed structure of the nucleus (the number of energy states available). It is not particularly significant therefore if strict agreement is not obtained for a γ,π^- reaction, since it is for the total pion production that the $A^2/3$ dependence holds most accurately.

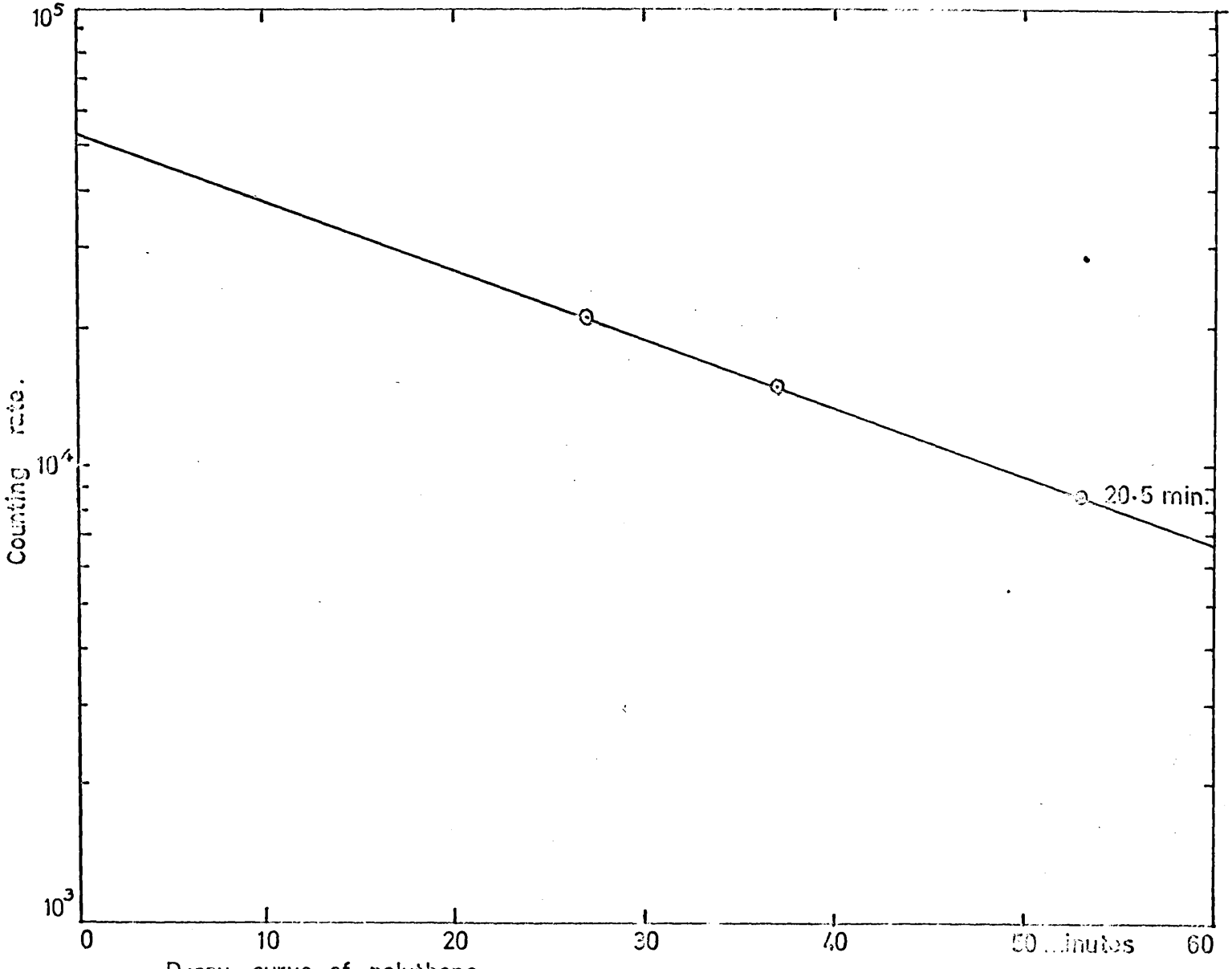

Decay curve of polythene.

Figure 8.1

CHAPTER 8

RELATIVE YIELDS OF VARIOUS PHOTONUCLEON REACTIONS

The RELATIVE YIELDS OF VARIOUS PHOTONUCLEON REACTIONS described in previous chapters was monitored by measuring the activity induced in thin polythene, zinc and copper discs which were exposed during each synchrotron run. The activities induced in zinc by the $Zn^{64}(\gamma,n)Zn^{63}$ reaction and in copper by the $Cu^{65}(\gamma,n)Cu^{64}$ were chosen to monitor the reactions $Cu^{63}(\gamma,\pi^-)Zn^{63}$ and $Cu^{63}(\gamma,\pi^-n)Zn^{62}$ respectively. The reasons for this choice have been explained previously. The polythene disc was included for comparison since cross-section values for the reaction have been published and it has been widely used as a beam monitor by other workers. Several positron activities were induced in the monitor discs in addition to those mentioned above. The relative rates of production of the responsible radioactive isotopes were obtained from the decay curves of annihilation radiation (Figs. 8.1, 8.2 and 8.3). Essentially it is then possible to compare integrals of the form

$$\int_0^{\chi} \tilde{\phi}(\chi,K)\,\frac{\sigma(K)}{K}\,dK$$ for a number of reactions for a series of values of χ the maximum bremsstrahlung energy.

The reactions for which results are presented are as follows:

$Zn^{64}(\gamma,n)Zn^{63}$

$Zn^{64}(\gamma,2n)Zn^{62}$

$Zn^{64}(\gamma,P2n)Cu^{61}$

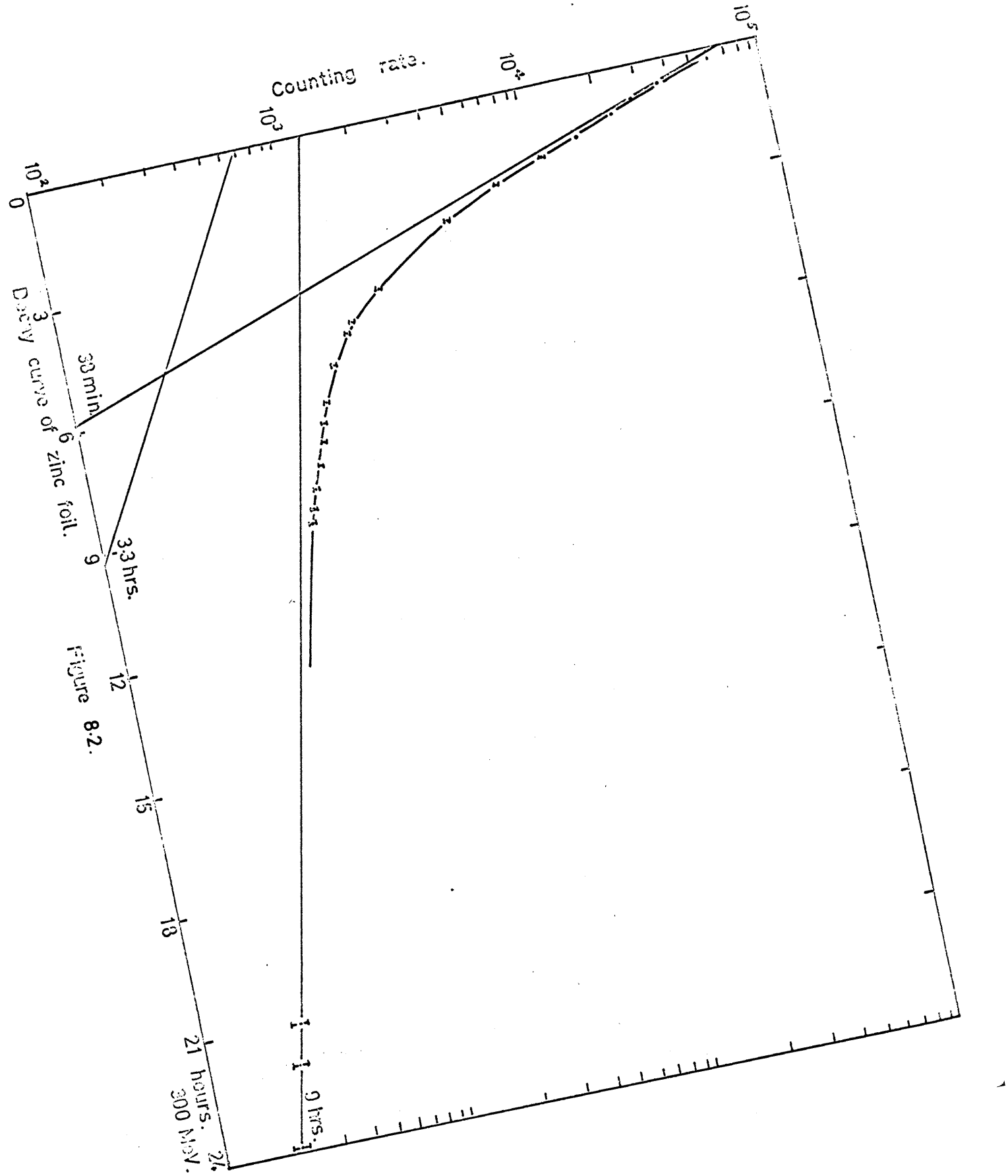
Counting rate.
10^5
10^4
10^3
10^2
0
3
6
9
12
15
18
21
Decay curve of zinc foil.
33 min.
3.3 hrs.
2½ hours.
300 MeV.
0 hrs.

Figure 8.2.

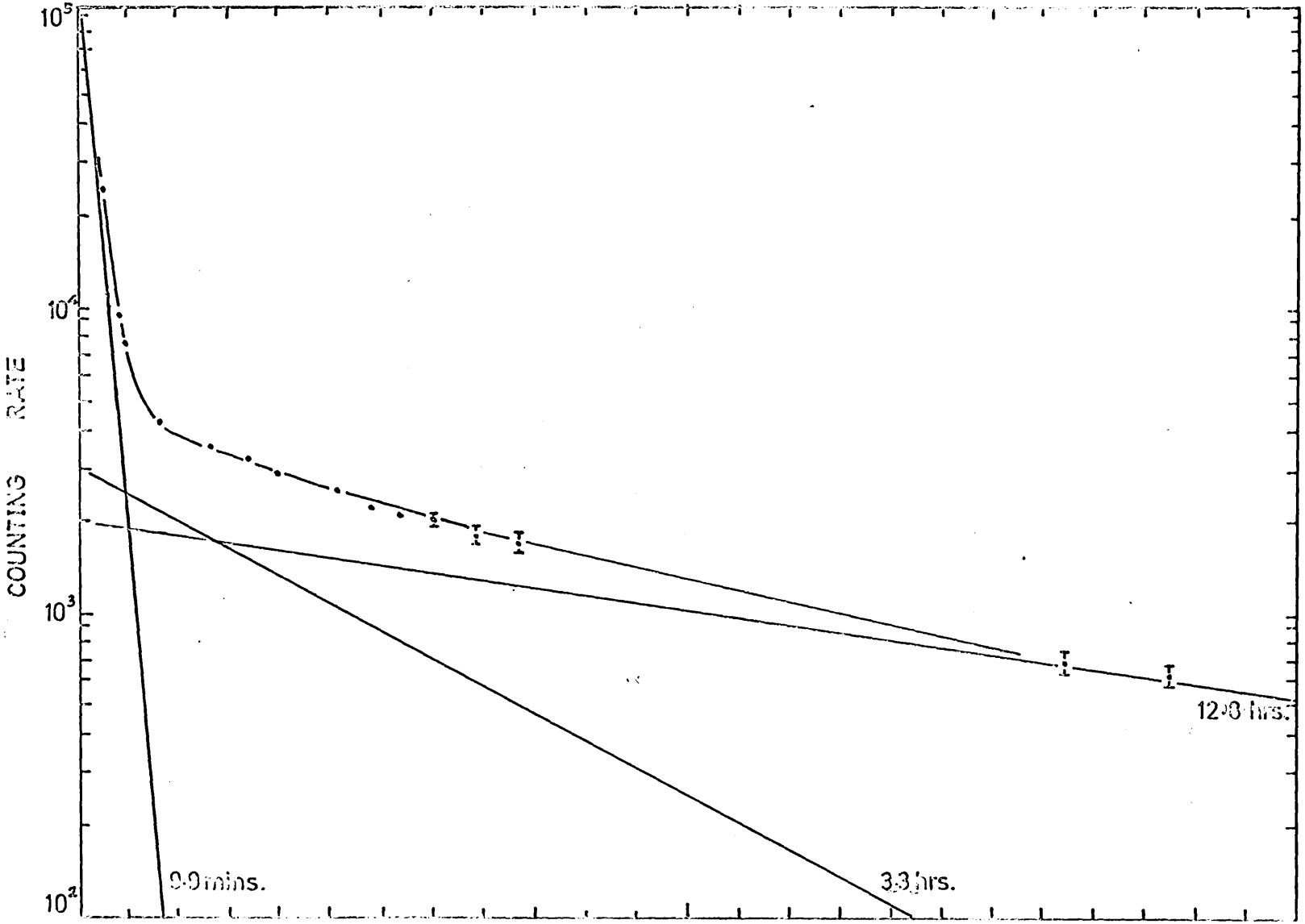

Figure 8.3. Decay Curve of Copper Foil.

$Cu^{63}(\gamma,n)Cu^{62}$

$Cu^{63}(\gamma,2n)Cu^{61}$

$Cu^{65}(\gamma,n)Cu^{64}$

$C^{12}(\gamma,n)C^{11}$

The cross-section for such photo nucleon reactions typically increases with X-ray energy to a maximum at about 20 -30 MeV and falls to zero below 50 MeV (The "Giant Resonance").

The value of χ was varied between 100 MeV and 320 MeV and the function $\bar{\phi}(\chi,K)$ was therefore always approximately constant over the energy range at which each reaction had a significant cross-section. The ratios of integrals of the type $\int_0^{\chi} \bar{\phi}(\chi,K) \frac{\sigma(K)}{K} dK$ would not be expected to vary appreciably with χ. One is in effect comparing the values of the total integral of the reduced cross-section defined in a previous chapter (6)

The results are presented in Figs. 8.4, 8.5 and 8.6 and the table following.

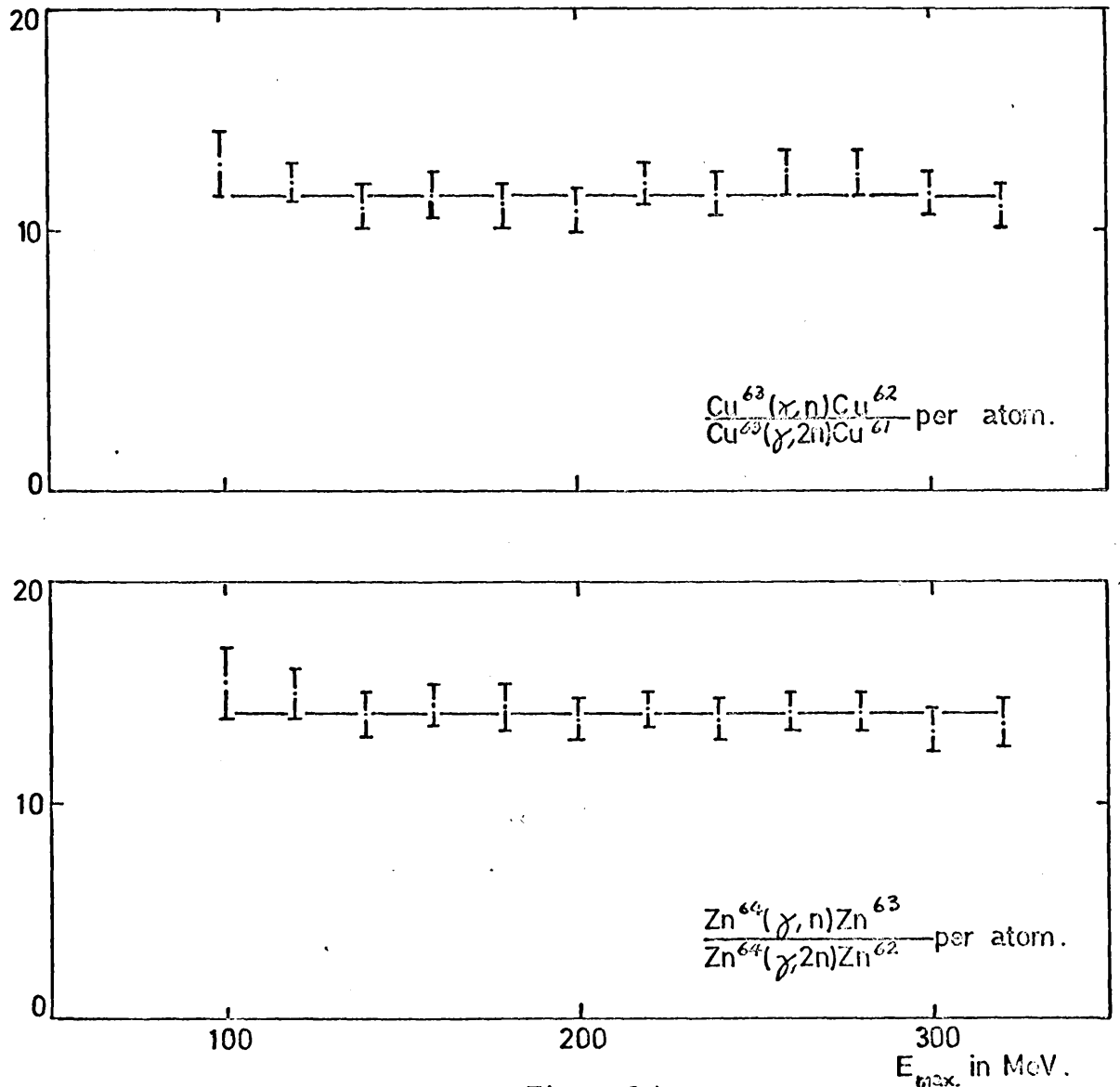
20
10
0
$\frac{Cu^{63}(\gamma,n)Cu^{62}}{Cu^{63}(\gamma,2n)Cu^{61}}$ per atom.
20
10
0
$\frac{Zn^{64}(\gamma,n)Zn^{63}}{Zn^{64}(\gamma,2n)Zn^{62}}$ per atom.
100
200
300
$E_{max.}$ in MeV.

Figure 8.4.

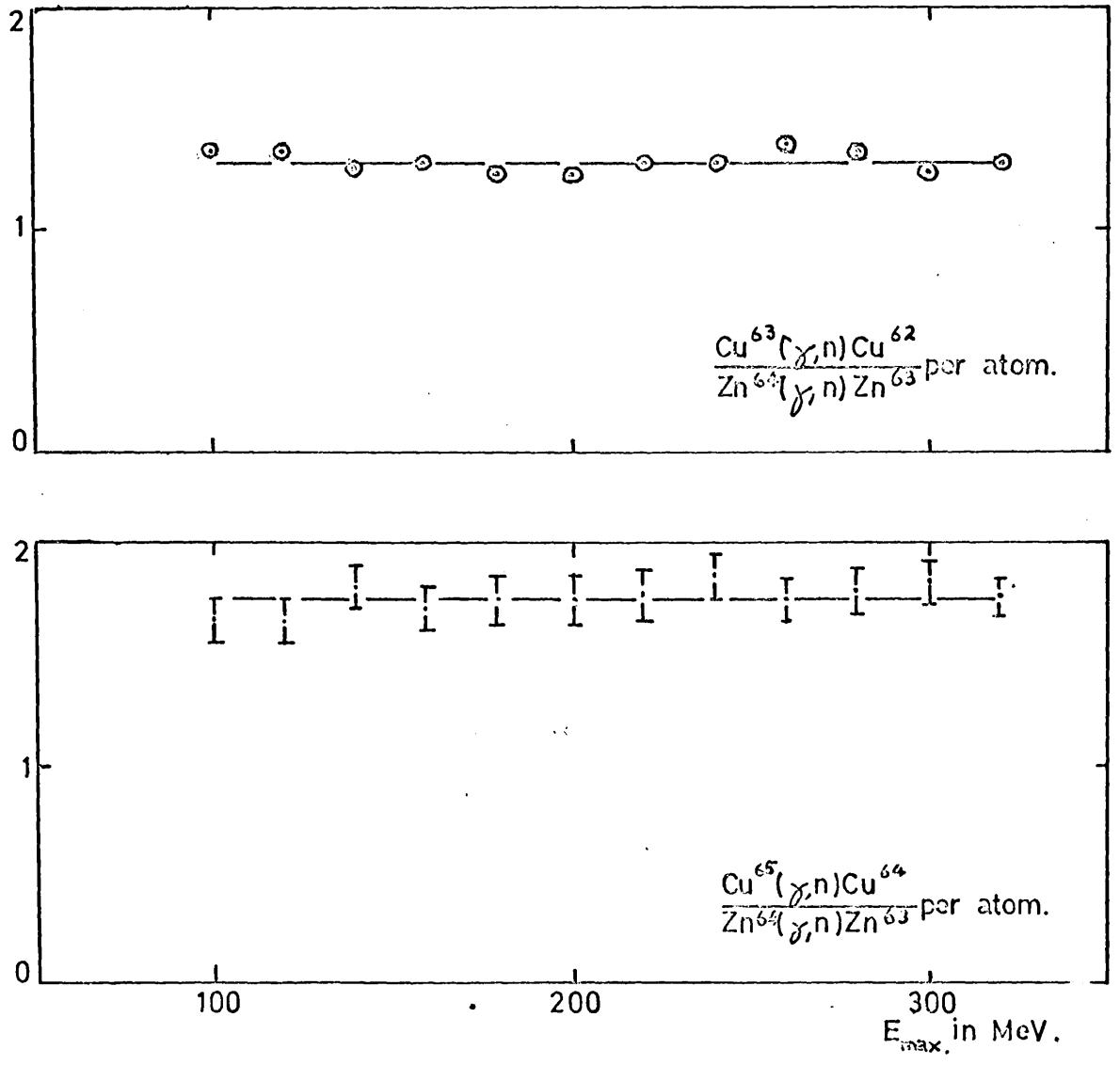
2
1
0
$\frac{Cu^{63}(\gamma,n)Cu^{62}}{Zn^{64}(\gamma,n)Zn^{63}}$ per atom.
2
1
0
$\frac{Cu^{65}(\gamma,n)Cu^{64}}{Zn^{64}(\gamma,n)Zn^{63}}$ per atom.
100
200
300
$E_{max.}$ in MeV.

Figure 8·5.

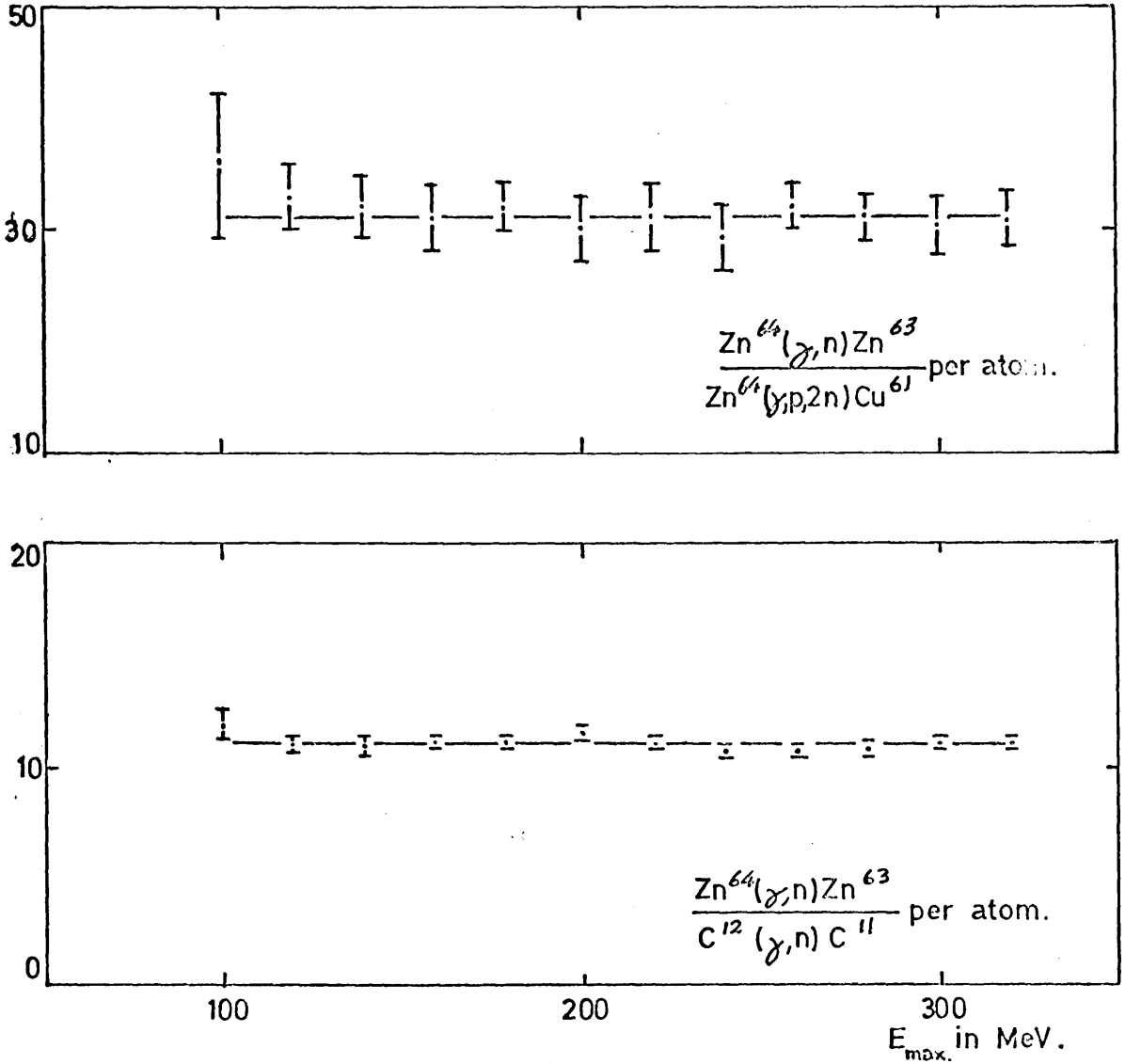
50
30
10
$\frac{Zn^{64}(\gamma,n)Zn^{63}}{Zn^{64}(\gamma,p,2n)Cu^{61}}$ per atom.
20
10
0
$\frac{Zn^{64}(\gamma,n)Zn^{63}}{C^{12}(\gamma,n)C^{11}}$ per atom.
100
200
300
$E_{max.}$ in MeV.

Figure 8·6.

TABLE

Reaction	Yield relative to $Zn^{64}(\gamma,n)Zn^{63}$ ($Zn^{64}(\gamma,n)Zn^{63}$ = 1.00)
$Zn^{64}(\gamma,n)Zn^{63}$	1.0
$Zn^{64}(\gamma,2n)Zn^{62}$	0.0714
$Zn^{64}(\gamma,p2n)Cu^{61}$	0.032
$Cu^{63}(\gamma,n)Cu^{62}$	1.3
$Cu^{63}(\gamma,2n)Cu^{61}$	0.113
$Cu^{65}(\gamma,n)Cu^{64}$	1.75
$C^{12}(\gamma,n)C^{11}$	0.091

The fact that the ratios shown are independent of χ encourages one to believe that there is no significant rise in the cross-section for these reactions for high energy photons. It also becomes possible to use any one reaction as an absolute beam monitor ($\chi > 100$ MeV) once the integral $\int \tilde{\phi}(\chi,K) \frac{\sigma(K)}{K} dK$ is known relative to that for a reaction for which a measurement of the absolute cross-section as a function of energy is available.

HELMHOLZ and STRAUCH[8.1] and DEBS[8.2] et al. have published relative yields for the same reactions produced by 335 MeV and 320 MeV bremsstrahlung respectively. These workers measured the induced activities by β-counting The results presented here are in good agreement with these earlier works.

Level Scheme for A = 64 Co, Ni, Cu, Zn, and Ga

NRC 59-2-13

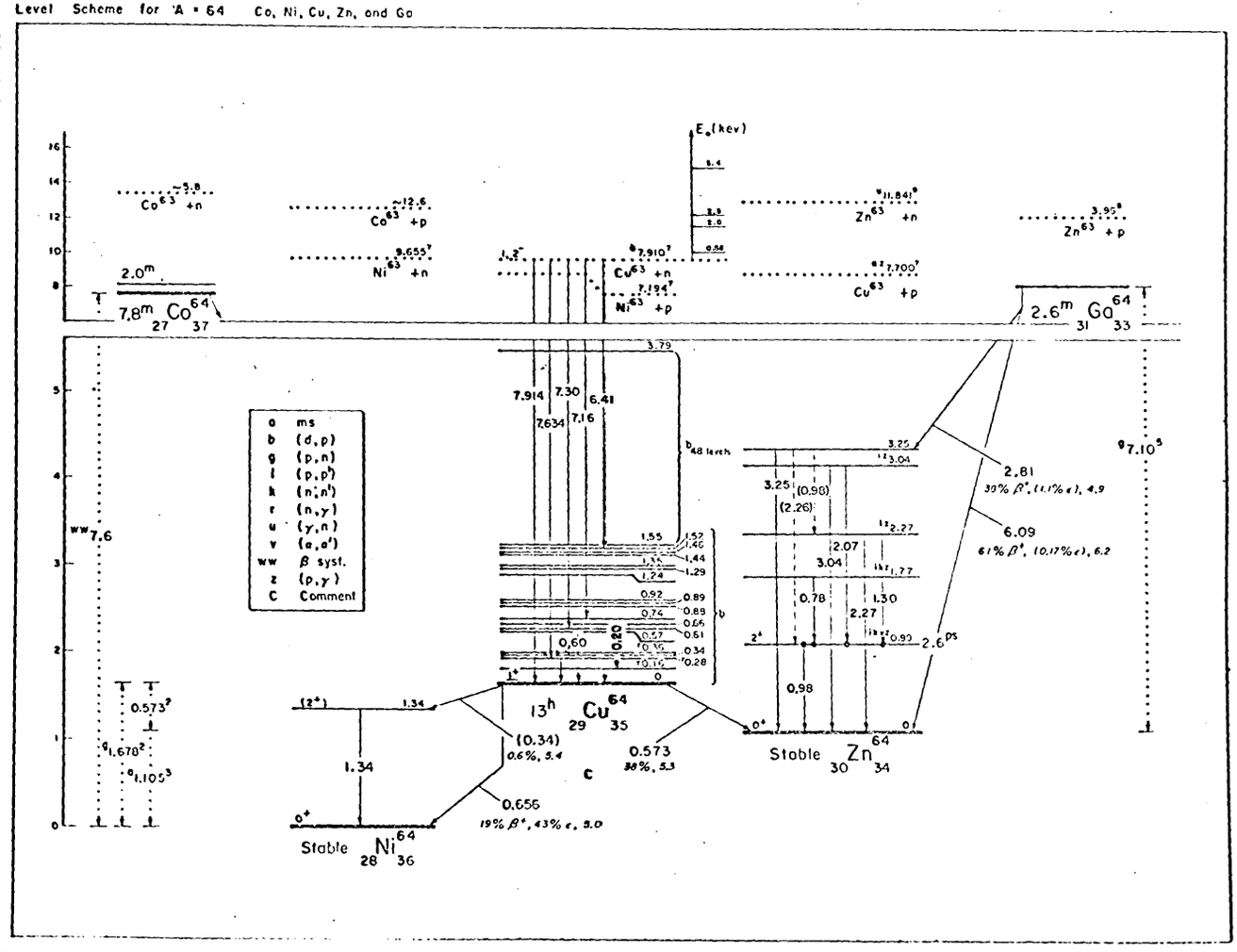

Figure 8.7.

Level Scheme A = 64

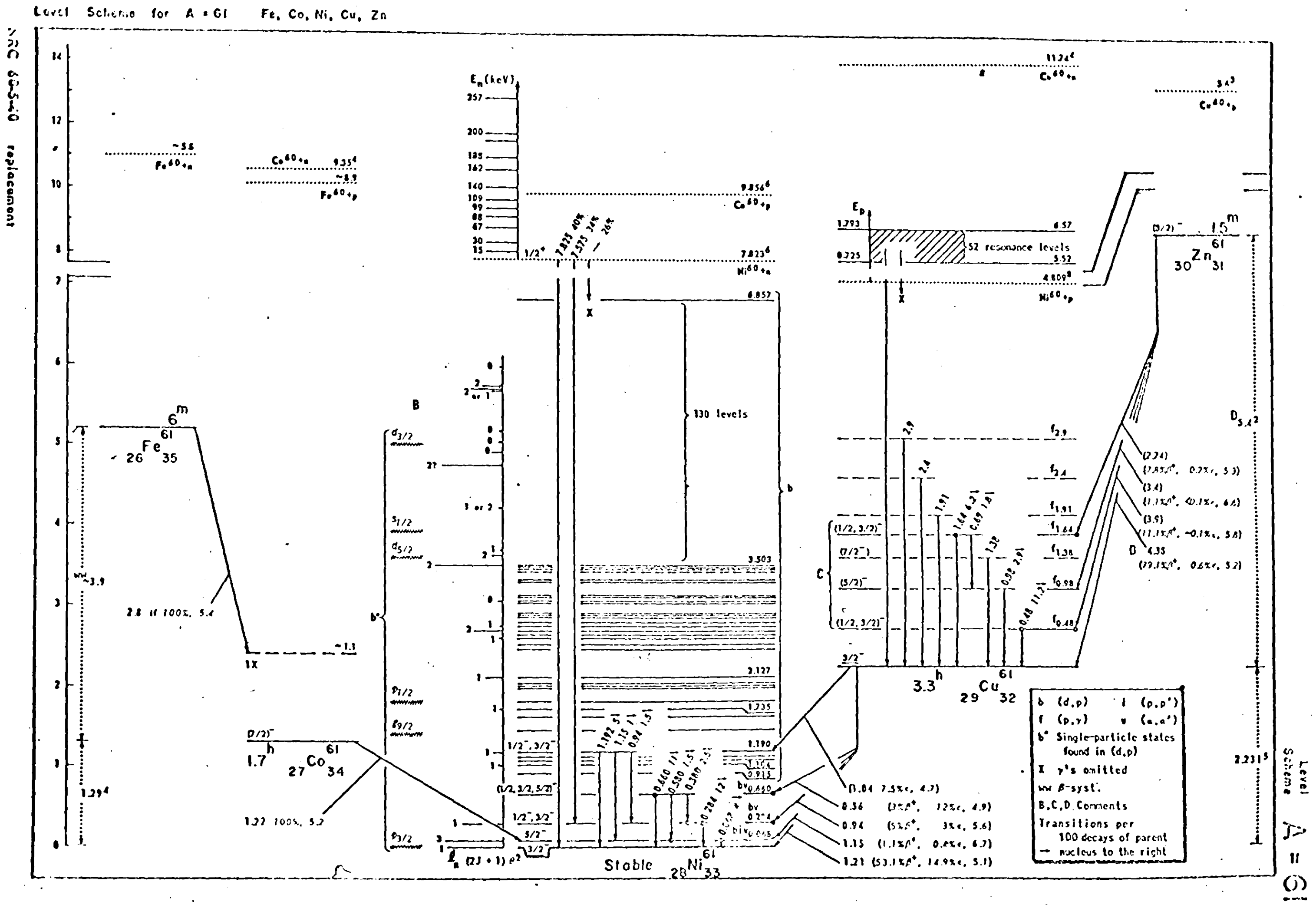

Level Scheme for A = 61 Fe, Co, Ni, Cu, Zn
NRC 60-5-40 replacement
Level Scheme A = 61
130 levels
52 resonance levels
Stable
b (d,p)
f (p,γ)
b* Single-particle states found in (d,p)
X γ's omitted
B,C,D Comments
Transitions per 100 decays of parent nucleus to the right

Figure 8.8.

REFERENCES

1.1 McMillan, E.M., Peterson, J.M., White, R.S., Science 110, 579 (1949)

1.2 Mozley, R. F., Phys. Rev. 80, 493 (1950)

1.3 Steinberger, J. and Bishop, A. S., Phys. Rev. 86, 171 (1952)

1.4 Littauer, R. M. and Walker, D., Phys. Rev. 86, 838 (1952)

1.5 Lax, M. and Feshbach, H., Phys. Rev. 81, 189 (1951)

1.6 Chew, G. F. and Goldberger, M. L., Phys. Rev. 77, 470 (1950)

1.7 Palfrey, T. R., Nefkens, B. M. K., Mortara, L. and Loeffler, F. J., Phys. Rev., 1323, 122 (1961)

1.8 Brueckner, K. A., Serber, R. and Watson, K. M., Phys. Rev. 84, 258 (1951)

1.9 Chedester, C., Isaacs, P., Sachs, A. and Steinberger, J., Phys. Rev. 82, 958 (1951)

1.10 Byfield, H., Kessler, J, and Lederman, L. M., Phys Rev. 86, 17 (1952)

1.11 Francis, N. C. and Watson, K. M., Phys. Rev. 89, 328 (1953)

1.12 Imhof, W., Knapp, E. A., Easterday, H. and Perez-Mendez, V., Phys. Rev. 108, 1041 (1957)

1.13 Williams, W. S. C., Crowe, K. M. and Friedman, R. M., Phys. Rev. 105, 1840 (1957)

1.14 Frank, R. M., Gammel, J. L. and Watson, K. M., Phys. Rev. 101, 891 (1956)

1.15 Waters, J. R., Phys. Rev. 113, 1133 (1959)

1.16 McClelland, W. M., Phys. Rev. 123, 1423 (1961)

1.17 Kabe, S., Kato, S., Kifune, T., Kimura, Y., Kobayashi, M., Kondo, K., Nagashima, Y. and Nishikawa, T., J. Phys. Soc. Japan 19, 1800 (1964)

1.18 Butler, S. T., Phys. Rev. 87, 1117 (1952)

1.19 Wilson, R. R., Phys. Rev. 86, 125 (1952)

1.20 Rosengren, J. W. and Dudley, J. M., Phys. Rev. 89, 603 (1953)

1.21 George, E. P., Proc. Phys. Soc. 69A, 110 (1956)

1.22 Stork, D. H., Phys. Rev. 93, 868 (1954)

1.23 Belousov, A. S., Rusakov, S. V. and Tamm, E. I., J E T P, 8, 247 (1959)

1.24 Popova, V. M., Semarko, N. G. and Yagudina, F. R., J E T P, 9, 965 (1959)

1.25 Baldin, A. M. and Lebedev, A. I., J E T P, 6, 940 (1958)

1.26 Belousov, A. S., Govorkov, B. B. and Goldanskii, V. I., J E T P, 9, 164 (1959)

1.27 Laing, E. W. and Moorhouse, R. G., Proc. Phys. Soc., 70B, 629 (1957)

1.28 Hughes, I. S. and March, P. V., Proc. Phys. Soc. 72, 259 (1958)

1.29 Hogg, W. R. and Sinclair, D., Phil. Mag. 1, 466 (1956)

1.30 Bellamy, E. H. and Hogg, W. R., Proc. Phys. Soc., 79, 1197 (1962)

1.31 March, P. V. and Walker, T. G., Proc. Phys. Soc., 77, 293 (1961)

1.32 Dyal, P. and Hummel, J. P., Phys. Rev. 127, 2217 (1962)

1.33 Meyer, R. A., Wallers, W. B. and Hummel, J. P., Phys. Rev. 138, B 1421 (1965)

1.34 Ramchandran, G. and Devanathan, V., Nucl. Phys., 66, 595 (1965)

1.35. Chew, G. F., Goldberger, M. L., Low, F. E. and Nambu, Y., Phys. Rev. 106, 1345 (1957)

1.36 Yavin, A. I., and Pasquali, G. D., Phys. Rev. 132, 431 (1963)

1.37 Jackson, J. D., Can. J. Phys. 34, 767 (1956)

1.38 Meyer, R. A. and Hummel, J. P., Phys. Rev. 140, B 48 (1965)

2.1 Same as 1.31

2.2 Hofstadter, R., Phys. Rev. 74, 100 (1948)

2.3 Miller, W. F. and Snow, W. J., Nucleonics, 19 (11), 174 (1961)

2.4 Fairstein, E., Rev. Sci. Instr., 27, 475 (1956)

2.5 Gustafson, P. F., Marinelli, L. D. and Brar, S. S., A N L - 5967, p. 154 (1958)

2.6 Brown, T., Phys. Rev. 96, 754 (1954)

2.7 Sternheimer, R. M., Phys. Rev. 88, 851 (1952)

2.8 Rossi, B., Rev. Mod. Phys. 20, 537 (1948)

2.9 Puppi, G. and Dallaporta, N., Progress in Cosmic-Ray Physics, Vol. I, Ch. IV (North Holland Publishing Co.)

2.10 Heath, R. L. A E C - Report I D O - 16408

2.11 Bosch, H. E. and Caracoche, M. C., Nucl. Inst. Meth. 22, 77 (1963)

3.1 Cholak, J., Hubbard, D. M. and Burkey, R. E., Ind. Engg. Chemistry (Anal. Edn.) 15, 754 (1943)

5.1 Meadows, J. W., Phys. Rev. 91, 885 (1953)

5.2 Byerley, P. R. (Jr.) and Stephens, W. E., Phys. Rev. 83, 54 (1951)

5.3 Bonner, N. A., Freidlander, G., Pepkowitz, L. P. and Perlman, M. L. Phys. Rev. 71, 511 (1947)

6.1 Diven, B. C. and Almy, G. M., Phys. Rev. 80, 407 (1950)

6.2 Katz, L. and Cameron, A. G. W., Can. J. Phys. 29, 518 (1951)

6.3 Penfold, A. S. and Leiss, J. E. Phys. Rev. 114, 1332 (1959)
University of Illinois Report, 1958

6.4 Nuclear Data Sheets Published by the National Academy of Sciences - National Research Council for The Nuclear Data Group - Oak Ridge National Laboratory

6.5 Schiff, I. L., Phys. Rev. 82, 252 (1951)

6.6 Roalsoig, J. P., Haslam, R. N. H. and Bergsteinsson, J. L., Can. J. Phys. 38, 320 (1960)

6.7 Fultz, S. C., Bramblett, R. L., Caldwell, J. T. and Harvey, R. R., Phys. Rev. 133, B1149 (1964)

7.1 Walters, W. B. and Hummel, J. P., Phys. Rev. 143, 833 (1966)

7.2 Barber, W. C., George, W. D. and Reagan, D. D. Phys. Rev. 98, 73 (1955)

7.3 Bell, R. E. and Skarsgard, H. M. Can. J. Phys. 34, 745 (1956)

8.1 Helmholz, A. C. and Stranch, K. Phys. Rev. 86, 78 (1950)

8.2 Debs, R. J., Eisinger, J. T., Fairhall, A. W., Halpern, I. and Richter, H. G. Phys. Rev. 97, 1325 (1955)

APPENDIX "A"

TABLE I

B.D.H. COPPER ANALAR

(0.005" FOILS)

Maximum Limits of Impurities

Acid Insoluble Matter	nil
Tin (Sn)	0.001 per cent
Silver (Ag)	0.001 " "
Iron (Fe)	0.01 " "
Bismuth (Bi)	0.0005 " "
Lead (Pb)	0.002 " "
Arsenic (As)	0.0002 " "

TABLE II

H. & W. COPPER ANALAR

(0.004" FOILS)

Maximum Limits of Impurities

Acid Insoluble Matter	0.01 per cent
Arsenic (As)	0.0001 " "
Bismuth & Lead	0.002 " "
Iron (Fe)	0.005 " "
Manganese (Mn)	0.002 " "
Nickel (Ni)	0.01 " "
Silver (Ag)	0.0008 " "
Tin (Sn)	0.001 " "

ELECTROLYTIC ZINC

(99.9%)

Impurities

TABLE III

Lead (Pb)	0.0026 Per Cent
Cadmium (Cd)	0.0012 " "
Iron (Fe)	0.0009 " "
Copper (Cu)	0.0003 " "